

**PERFORMANCE ANALYSIS OF ENERGY  
HARVESTED NOMA-ENABLED  
HETEROGENEOUS NETWORKS**

**Ph.D. Thesis**

*by*

**ABHINAV SINGH PARIHAR**



**DEPARTMENT OF ELECTRICAL ENGINEERING  
INDIAN INSTITUTE OF TECHNOLOGY  
INDORE  
OCTOBER, 2023**



**PERFORMANCE ANALYSIS OF ENERGY  
HARVESTED NOMA-ENABLED  
HETEROGENEOUS NETWORKS**

**Ph.D. THESIS**

*Submitted in partial fulfillment of the  
requirements for the award of the degree*

*of*

**DOCTOR OF PHILOSOPHY**

*by*

**Abhinav Singh Parihar**



**DEPARTMENT OF ELECTRICAL ENGINEERING  
INDIAN INSTITUTE OF TECHNOLOGY**

**INDORE**

**OCTOBER, 2023**





## INDIAN INSTITUTE OF TECHNOLOGY INDORE

### CANDIDATE'S DECLARATION

I hereby certify that the work which is being presented in the thesis entitled "**PERFORMANCE ANALYSIS OF ENERGY HARVESTED NOMA-ENABLED HETEROGENEOUS NETWORKS**" in the partial fulfillment of the requirements for the award of the degree of DOCTOR OF PHILOSOPHY and submitted in the DEPARTMENT OF ELECTRICAL ENGINEERING, Indian Institute of Technology Indore, is an authentic record of my own work carried out during the time period from June 2019 to October 2023 under the supervision of Prof. Vimal Bhatia, Professor, Indian Institute of Technology Indore, India.

The matter presented in this thesis has not been submitted for the award of any other degree of this or any other institute.

17 October 2023

Signature of the student with date  
(**ABHINAV SINGH PARIHAR**)

-----

This is to certify that the above statement made by the candidate is correct to the best of my knowledge.

17.10.2023

Signature of Thesis Supervisor with date  
(**Prof. VIMAL BHATIA**)

-----

**Abhinav Singh Parihar** has successfully given his Ph.D. Oral Examination held on **March 20, 2024**.

20.03.2024

Signature of Thesis Supervisor with date  
(**Prof. VIMAL BHATIA**)

-----



## ACKNOWLEDGEMENTS

There is always a sense of gratitude with which one expresses an offer for the helpful and needy services someone renders during all the phases of life. First of all, I would like to thank the almighty God because he choose this esteemed institute for me, without whose blessings I could never achieve this milestone.

I express my sincere gratitude to my Ph.D. supervisor Prof. Vimal Bhatia for his motivation, guidance, and continuous support throughout my thesis work. I am thankful for all the freedom he gave me to explore various research topics and was always available for discussion despite his busy schedule. I would also like to thank my PSPC committee members Prof. Mukesh Kumar and Prof. Shaibal Mukherjee for their fruitful discussions and suggestions towards my research.

I would like to thank the Visvesvaraya Ph.D. Scheme of Ministry of Electronics & Information Technology, Government of India, being implemented by Digital India Corporation for providing financial assistance. I would also like to thank the Finnish national agency TFK program, Finland for the financial assistance for the research visit at Oulu University, Finland. This research visit helped me meet new people and experts who have helped shape my Ph.D. thesis.

I am truly thankful to all the faculty members and the staff of IIT Indore for their invaluable cooperation throughout my thesis work. I would also like to thank all the members of the Signal and Software group (SaSg) for their encouragement and support that helped me to face the hard phase of my life and never let me feel lonely along this long journey. Specially, I would like to extend my appreciation to my seniors Dr. Pragya Swami, Dr. Mahendra Singh Thakur, Dr. Shaik Parvez, Dr. Sandesh Jain, Dr. Praveen Kumar Singya, Dr. Anuj Agrawal, and Purva Sharma who helped me every time wherever I required. I would like to thank my friends Amit Baghel, Deepak Kumar, Justin Jose, Vidya Bhaskar Shukla, Vaishali Sharma, Shubham Bisen, Anupma Sharma, and other colleagues who helped me in several ways during my thesis work.

Moreover, whatever little I have achieved in my life, the credit goes to my parents whom I take great pride in dedicating this thesis. They have always been a source of inspiration for me and have kept trust and faith in whatever I did. I must express my appreciation to my in-laws for their best wishes for my Ph.D. studies. A sincere thanks to my best friend and wife Dr. Swati Rajput, for standing by me through the thick and thin of the research journey. It would be impossible for me to complete my PhD without her support. Her constant encouragement and emphasis on hard work has brought a positive transformation in my life. Finally, I would like to acknowledge my late grandmother, whose unconditional love and care I can never forget. Her constant inquiries about my well-being during our phone conversations served as a reminder of the importance of family, love, and connection. Though she is no longer with us, her presence and love continue to inspire me, and I dedicate this thesis to her memory.

ABHINAV SINGH PARIHAR



*Dedicated to my parents, my grandmother and  
my wife*



## ABSTRACT

The 5G wireless network, which has been introduced in the market in recent times, offers the potential to enhance network performance and establish seamless connectivity across various locations. Nevertheless, the advent of numerous emerging applications such as extended reality, telepresence, telesurgery, and autonomous driving demands high connectivity while also upholding the associated reliability standards. Paired with a significant increase in the quantity of smart devices and the Internet of Things (IoT), these demands are projected to saturate the 5G network in the future. As a result, the research community has been spurred to explore advancements beyond the scope of 5G wireless technology.

In order to facilitate high data speeds and accommodate extensive connectivity within restricted spectrum resources, it is imperative to explore sophisticated multiple access technologies designed for the forthcoming generation of wireless systems. The concept of non-orthogonal multiple access (NOMA) has captured substantial attention and exhibited immense potential in bolstering connectivity and augmenting capacity. By exploiting the signal superposition at transmitters and the successive interference cancellation (SIC) at receivers, NOMA enables users served by the same time/frequency/space/code resource block to be further multiplexed and distinguished in the power domain. Hence, it can dramatically enhance the network capacity and user connections, as well as reducing the outage probability. Furthermore, rapidly increased users and huge data demands has lead to the conventional network comprising of only macro base station (MBS) tier to shift toward more practical heterogeneous cellular networks (HetNets). The HetNets comprises of the MBS tier deployed with small BSs, e.g., femto base station (FBS) tier, to aid the MBS tier, especially in the overcrowded areas such as shopping malls, sports venues, airports, and others. In parallel, to achieve the vision of a green communication system, simultaneous wireless information and power transfer (SWIPT) is a new paradigm in wireless networks that provides simultaneous energy harvesting and information transmission. This thesis provides a systematic treatment of this newly emerging technology, from the basic principles of NOMA, to its combination with SWIPT and HetNets, to achieve improved spectral efficiency, energy efficiency and reliability.

In this thesis, initially, application of SWIPT in networks employing cooperative NOMA is investigated with imperfect channel state information (CSI). The performance is investigated in a multi-tier downlink scenario with MBSs and FBSs. The distribution of MBSs and FBSs follow Poisson point process (PPP) model. Unlike solutions in the existing literature, instead of using only the superimposed signal for energy harvesting (EH), in this chapter, the cooperating node/user employs EH using interference from the adjacent base stations. The harvested energy is utilized for cooperative transmission to the far user. Expressions for outage probability and throughput are derived at the user pair (comprising a cell-center user and a cell-edge user) served using NOMA. Comparison of the proposed EH system with the existing solutions is highlighted.

Second, this thesis investigates the application of SWIPT in HetNets employing cooperative NOMA and carrier sensing. The HetNets consists of MBS under-laid by small-base stations (SBS). The distribution of MBSs follow PPP model, while the SBS tier supports NOMA and carrier sensing for its transmission. It is challenging to manage interference due to the SBSs' random placement. So, at the SBS

---

tier, carrier sensing becomes crucial. Since the PPP model is unable to accurately simulate correlated base stations, advanced stochastic geometry methods are used to model the SBS tier with carrier sensing. Carrier sensing helps in reducing interference by blocking the base stations within a specific range from transmitting. The analysis at SBS tier is carried out in two phases. In the direct phase transmission, the SBS transmits the superimposed signal to a user pair, comprising of a cell-centre user (CCU) and a cell-edge user (CEU), using NOMA principle. The CCU acts as a cooperative relay to forward information to the CEU in the cooperative phase. Unlike existing literature, instead of using only the superimposed signal for EH, in this thesis, the cooperating user (i.e. CCU) employs EH using interference from the adjacent base stations along with the EH from the superimposed signal. Expressions for outage probability and throughput are derived at the user pair served using NOMA. Comparison of the proposed EH system with existing solutions are highlighted and useful insights are drawn.

Third, for the purpose of both EH and information decoding, a receiver can either employ two distinct sets of independent antennas or opt for a configuration where it shares the same antenna. The latter approach requires less hardware complexity compared to the former and can even be realized with a single antenna. In the case of shared antenna, the time switching (TS) architecture can be utilized. TS architecture involves the use of a straightforward switch that toggles between EH and information decoding at different time intervals. Hence this thesis explores a NOMA enabled HetNet with a TS protocol at the cooperating user for EH. The cooperative user employs EH utilizing neighbouring base stations (BS) interference and the transmitted NOMA signal. Closed-form expressions of outage probability and energy efficiency are derived, and comparisons with useful insights are drawn for EH-enabled and without EH-enabled systems. To ensure the users' fairness, the proportional fairness (PF) index is also evaluated.

Fourth, most works are based upon the simple linear energy harvester model where the output power is linearly proportional to the input power. However, as most rectennas include non-linear components (e.g., diodes and capacitors), the input/output relationship is non-linear, hence it is necessary to perform analysis with nonlinear harvester models. Hence this thesis studies the performance of EH assisted cooperative NOMA in a two-tier HetNet with a realistic non-linear EH model. The thesis proposes an analytical methodology for improving the performance of NOMA user with poor channel conditions by employing EH and cooperative NOMA at the user with good channel conditions. The analysis is considered at the NOMA pair served by the SBS. Cooperation is carried out by one of the users in a NOMA pair which acts as decode and forward relay node assisted with EH. The outage probability at the NOMA users is derived in closed form using tools of stochastic geometry. The performance of the proposed system is compared with the system without EH and the system with linear EH. It is shown that the proposed system attains higher throughput than orthogonal multiple access (OMA) without EH in the considered scenario.

Fifth and in the last, the SWIPT based systems are appropriate for the short distance communication. To overcome this limitation, power beacon (PB) is used to supply power for wireless devices. PBs are low-cost stations for recharging wireless IoT devices as they do not require any computational capabilities and backhaul links. Therefore, they can be deployed in large numbers at locations with connec-

---

tions to the electrical grid. Hence, this thesis studies the performance of PB assisted downlink cooperative NOMA in a wireless powered communication network (WPCN) with realistic non-linear EH model. This thesis proposes an analytical methodology for improving performance at blocked user (BU) at the edge of network via an intermediate node (IN). IN deployed in the coverage area of the BS, acts as decode-and-forward relay to perform cooperative transmission. IN assists the BS in communicating with the blocked IoT device after harvesting energy from PB mounted on the BS. IN employs NOMA to serve IoT devices with heterogeneous quality of service requirements in order to achieve higher spectral and energy efficiency. A practical non-linear EH model is employed at IN to power the cooperative transmission to the IoT devices. The performance of the proposed scheme is compared with the system employing OMA and it is shown that the proposed scheme attains improved performance in terms of outage probability, system throughput, and energy efficiency.

Lastly, numerical results are compared with Monte-Carlo simulations to verify the correctness of the derived expressions.



# Contents

<b>ABSTRACT</b>	<b>i</b>
<b>LIST OF FIGURES</b>	<b>ix</b>
<b>LIST OF TABLES</b>	<b>xi</b>
<b>LIST OF ABBREVIATIONS/ACRONYMS</b>	<b>xii</b>
<b>List of Symbols</b>	<b>xvii</b>
<b>1 Introduction</b>	<b>1</b>
1.1 Overview . . . . .	1
1.2 Non-orthogonal Multiple Access . . . . .	2
1.2.1 Basic Principles . . . . .	4
1.2.2 Key Technologies of NOMA . . . . .	4
1.2.3 Mathematical Description of NOMA . . . . .	7
1.2.4 Downlink and Uplink NOMA Transmission . . . . .	7
1.2.5 Cooperative NOMA . . . . .	8
1.3 Heterogeneous Networks . . . . .	9
1.3.1 Stochastic Geometry for Heterogeneous Networks . . . . .	9
1.3.2 NOMA Enabled Heterogeneous Networks . . . . .	11
1.4 Point Process . . . . .	12
1.5 Simultaneous Wireless Information and Power Transfer . . . . .	13
1.5.1 Time Switching . . . . .	14
1.5.2 Power Splitting . . . . .	14
1.6 Wireless Communication Channel Model . . . . .	15
1.7 Performance Metrics . . . . .	16
1.8 Motivation . . . . .	18
1.8.1 Related Works . . . . .	19
1.8.2 NOMA and cooperative transmission . . . . .	20
1.8.3 Wireless Energy Harvesting and NOMA . . . . .	21
1.9 Thesis Flowchart, Outline, and Contributions . . . . .	22
<b>2 SWIPT Enabled Cooperative NOMA Heterogeneous Network</b>	<b>27</b>
2.1 Motivation and Contribution . . . . .	28
2.2 System Model . . . . .	29
2.2.1 SINR at CCU and CEU . . . . .	31
2.3 Performance Analysis . . . . .	33
2.3.1 Outage Probability at CCU . . . . .	33

2.3.2	Outage Probability at CEU . . . . .	34
2.3.3	System Throughput . . . . .	37
2.3.4	Proportional Fairness Index . . . . .	37
2.4	Results and Discussions . . . . .	38
2.5	Summary . . . . .	42
<b>3</b>	<b>SWIPT Enabled Heterogeneous Networks with NOMA and Carrier Sensing</b>	<b>43</b>
3.1	Motivation and Contribution . . . . .	44
3.2	System Model . . . . .	45
3.2.1	SINR at CCU and CEU . . . . .	46
3.3	Modeling SBS Tier . . . . .	49
3.4	Performance Analysis . . . . .	51
3.4.1	Outage probability at CCU . . . . .	51
3.4.2	Outage Probability at CEU . . . . .	54
3.4.3	System Throughput . . . . .	57
3.4.4	System Energy Efficiency . . . . .	58
3.5	Results and Discussions . . . . .	58
3.6	Summary . . . . .	66
<b>4</b>	<b>Time Switching based Energy Harvesting Enabled Cooperative NOMA HetNets</b>	<b>69</b>
4.1	System and Channel Model . . . . .	71
4.1.1	SINR at SU and WU . . . . .	74
4.2	Performance Analysis . . . . .	76
4.2.1	Outage probability at SU . . . . .	76
4.2.2	Outage probability at WU . . . . .	77
4.2.3	System Throughput . . . . .	77
4.2.4	System Energy Efficiency . . . . .	78
4.2.5	PF Index . . . . .	78
4.3	Results and Discussions . . . . .	79
4.4	Summary . . . . .	86
<b>5</b>	<b>SWIPT and NOMA Enabled Heterogeneous Networks with Non-linear Energy Harvesting</b>	<b>87</b>
5.1	System and Channel Model . . . . .	89
5.2	Performance Analysis . . . . .	91
5.2.1	Outage Probability at SU . . . . .	91
5.2.2	Outage Probability at WU . . . . .	93
5.2.3	System Throughput . . . . .	95
5.3	Results and Discussions . . . . .	96
5.4	Summary . . . . .	99
<b>6</b>	<b>Power Beacons Assisted NOMA Based Wireless Powered Communication Networks</b>	<b>101</b>
6.1	Communication scenarios and contribution . . . . .	102
6.2	System Model . . . . .	103
6.2.1	Energy Harvesting Phase . . . . .	105
6.2.2	Information Transmission Phase . . . . .	106

6.3	Performance Analysis . . . . .	107
6.3.1	Outage Performance . . . . .	107
6.3.2	System Throughput . . . . .	109
6.3.3	System Energy Efficiency . . . . .	109
6.4	Results and Discussions . . . . .	110
6.5	Summary . . . . .	114
<b>7</b>	<b>Conclusions and Future Works</b>	<b>115</b>
7.1	Conclusions . . . . .	115
7.2	Future Works . . . . .	118
	<b>REFERENCES</b>	<b>121</b>
	<b>LIST OF PUBLICATIONS</b>	<b>139</b>



# List of Figures

1.1	Basic principles of NOMA. . . . .	5
1.2	Time switching receiver architecture. $\alpha$ is the time switching coefficient which describes the portion of the time to be dedicated for energy harvester and the information decoder. . . . .	14
1.3	Power splitting receiver architecture. $\beta$ is the power splitting coefficient, such that $\beta$ times the received power is used for information decoding and the rest i.e., $1 - \beta$ times received power is used for EH. . . . .	15
1.4	Flowchart of the thesis. . . . .	22
2.1	Illustration of a downlink cooperative NOMA-SWIPT system model with a tagged FBS and a NOMA user pair in a multi-tier scenario. The spatial distributions of the MBS and the FBS follow PPP assumption. . . . .	30
2.2	Variation of outage probability at the CCU with transmit SNR. . . . .	38
2.3	Variation of outage probability at the CEU with transmit SNR. . . . .	39
2.4	Comparison of proposed EHSI-PPP system with EHS-PPP system. . . . .	40
2.5	System throughput versus transmit SNR for the target rates $R_1=0.5$ and $R_2=0.5$ . . . . .	41
2.6	Proportional fairness (PF) index versus transmit SNR. . . . .	42
3.1	Illustration of a downlink cooperative NOMA-SWIPT system model with a tagged SBS and a NOMA user pair in a multi-tier scenario. The spatial distributions of the SBS follow marked PPP assumption. . . . .	45
3.2	Variation of outage probability at the CCU with transmit SNR. . . . .	59
3.3	Variation of outage probability at the CEU with transmit SNR. . . . .	60
3.4	Variation of outage probability at the CCU with transmit SNR for different values of $\lambda_s$ . . . . .	61
3.5	Variation of outage probability at the CEU with transmit SNR for different values of $\lambda_s$ . . . . .	62
3.6	Comparison of proposed EHSI-RPP system with EHSI-PPP system. . . . .	62
3.7	System throughput versus transmit SNR for the target rates $R_1=0.5$ and $R_2=0.5$ . . . . .	63
3.8	System Energy Efficiency versus transmit SNR . . . . .	64
3.9	Outage Probability versus PS factor $\beta$ at transmit SNR of 36dB. . . . .	65
4.1	A downlink EH enabled cooperative NOMA system model in a two-tier situation with a tagged SBS broadcasting to NOMA user pair. The MBS and SBS spatial distributions are consistent with the PPP assumption. . . . .	72

4.2	Total transmission time block $T$ . . . . .	72
4.3	Outage probability at SU versus transmit SNR . . . . .	80
4.4	Outage probability at WU versus transmit SNR . . . . .	81
4.5	Outage probability at SU versus transmit SNR for different values of TS factor $\alpha$ . . . . .	82
4.6	Outage probability at WU versus transmit SNR for different values of TS factor $\alpha$ . . . . .	83
4.7	System throughput versus transmit SNR for the target rates $R_1 = 0.5$ and $R_2 = 0.5$ . . . . .	84
4.8	Energy efficiency versus transmit SNR . . . . .	85
4.9	PF index versus transmit SNR . . . . .	85
5.1	Illustration of a downlink NOMA assisted HetNet scenario. . . . .	88
5.2	Variation of outage probability at the SU with transmit SNR. . . . .	96
5.3	Variation of outage probability at the WU with transmit SNR. . . . .	97
5.4	System throughput versus transmit SNR for the target rates $R_1=0.5$ and $R_2=0.5$ . . . . .	98
6.1	Illustration of a downlink PB assisted WPCN scenario and total transmission time block with time splitting protocol. . . . .	104
6.2	Outage probability comparison of NOMA and OMA . . . . .	110
6.3	Variation of outage probability with transmit SNR for different values of $\beta$ . . . . .	111
6.4	Variation of outage probability with transmit SNR for different values of $\alpha$ . . . . .	111
6.5	System throughput versus transmit SNR . . . . .	112
6.6	System energy efficiency versus transmit SNR . . . . .	113
6.7	System throughput versus TS factor $\beta$ for different values of transmit SNR . . . . .	113

# List of Tables

4.1	Parameters used for obtaining the mathematical and simulation results [1], [2]. . . . .	79
4.2	Outage probability comparison between the proposed system with the existing solutions at the transmit SNR of 36dB . . . . .	80



# List of Abbreviations/Acronyms

**5G** fifth generation.

**6G** sixth generation.

**AF** amplify-and-forward.

**AWGN** additive white Gaussian noise.

**BER** bit error rate.

**BS** base station.

**BU** blocked user.

**CCU** cell-center user.

**CDF** cumulative distribution function.

**CEE** channel estimation error.

**CEU** cell-edge user.

**CoMP** coordinate multi-point.

**CR** contention radius.

**CSI** channel state information.

**DF** decode-and-forward.

**DT** delay-tolerant.

**EH** energy harvesting.

**FBS** femto base station.

**FD** full-duplex.

**FU** femto user.

**HCP** hard core parameter.

**HCPP** hard core point process.

- HD** half-duplex.
- i.i.d.** independent and identically distributed.
- IN** intermediate node.
- IoT** internet of things.
- IP** information processing.
- IRS** intelligent reflecting surface.
- IT** information transmission.
- LANs** local area networks.
- LoS** line-of-sight.
- LTE** long term evolution.
- MAC** medium access channel.
- MBS** macro base station.
- MIMO** multiple-input and multiple-output.
- MRC** maximal ratio combining.
- NGMA** next generation multiple access.
- NLD** non-linear distortion.
- NLoS** non-line-of-sight.
- NOMA** non-orthogonal multiple access.
- OFDM** orthogonal frequency division multiplexing.
- OMA** orthogonal multiple access.
- PA** power amplifier.
- PDF** probability density function.
- PF** proportional fairness.
- PPP** Poisson point process.
- PS** power splitting.
- QoS** quality of service.
- RF** radio frequency.

**RIS** reconfigurable intelligent surface.

**RPP** repulsive point process.

**RV** random variable.

**SBS** small base station.

**SC** selection combining.

**SINR** signal-to-interference and noise ratio.

**SNR** signal-to-noise ratio.

**SU** strong user.

**SWIPT** simultaneous wireless information and power transfer.

**TS** time switching.

**UE** user equipment.

**VLC** visible light communication.

**WPCN** wireless powered communication network.

**WPT** wireless power transfer.

**WU** weak user.



## List of Symbols

- Basic arithmetic and calculus notations with their definitions.

## Elementary & Special Functions

Notation	Definition
$\Gamma(x)$	$= \int_0^{\infty} t^{x-1} e^{-t} dt$ is the Gamma function.
$\Gamma(x, y)$	$= \int_y^{\infty} t^{x-1} e^{-t} dt$ is the upper incomplete Gamma function.
$\Upsilon(x, y)$	$= \int_0^y t^{x-1} e^{-t} dt$ is the lower incomplete Gamma function.
$\mathcal{K}_\nu(x)$	$= \frac{1}{2} \left(\frac{x}{2}\right)^\nu \int_0^{\infty} \frac{e^{-t-\frac{x^2}{4t}}}{t^{\nu+1}} dt$ represents the modified Bessel function of the second kind of order $\nu$ .
$Q(x)$	$= \frac{1}{\sqrt{2\pi}} \int_x^{\infty} e^{-\frac{t^2}{2}} dt$ is the Gaussian $Q$ -function.

## Probability & Statistics

Let  $X$  be a random variable (RV).

Notation	Definition
$\mathbb{E}[\cdot]$	statistical expectation operator
$\mathcal{P}(\cdot)$	statistical probability operator
$f_X(\cdot)$	probability density function (PDF) of a RV $X$
$F_X(\cdot)$	cumulative distribution function (CDF) of a RV $X$
$\mathcal{CN}(\mu, \sigma^2)$	complex normal distribution with mean $\mu$ and variance $\sigma^2$



# Chapter 1

## Introduction

### 1.1 Overview

In wireless communication, ultra-high data rates, energy efficiency, ultra-reliable and low-latency communication (URLLC), enhanced mobile broadband (eMBB), global coverage and connectivity, and massive machine-type communication (mMTC) are stringent requirements for beyond fifth generation (5G) networks [3]. At the physical layer, the speed of the cellular links has increased manifold from 50 kbps in 2G systems, 144 kbps in 2.5G systems, approximately 2 Mbps in 3G systems to around 100 Mbps in 4G systems (3GPP-LTE and WiMAX), around 1 Gbps in 5G and around 1 Tbps in sixth generation (6G) systems. Similarly, the speed of indoor wireless local area networks (LANs) has increased from 11 Mbps in IEEE 802.11b to 300 Mbps in IEEE 802.11n within the last 20 years [4]. Although 4G systems provide many services with high data rates, there is still a gap between customers' requirements and the services provided by 4G systems. The 5G network aims to connect the entire world in a seamless manner with ubiquitous communications between anybody, anything, everywhere, and at any time. Achieving an idealistic 5G network would require pioneering research and innovative methods to be implemented in the conventional approaches to deal with the spectrum crunch. In this regard, the research has shifted to develop advanced methods and groundbreaking wireless technologies to manage massively connected devices. So far, some potential candidates have been proposed to address challenges of 5G, such as, massive multiple input multiple output, millimeter-wave (mmWave) communications, ultra dense network,

visible light communication, cognitive communication, cooperative communication, non-orthogonal multiple access (NOMA), etc. NOMA is highly expected to increase system throughput and accommodate massive connectivity, therefore, is studied under the third generation partnership project (3GPP) framework, from Release 14 in 2015 to Release 16 in 2019, where NOMA was formally adopted for downlink transmission in Release 15, also termed Evolved Universal Terrestrial Radio Access [5–7]. With the current unveiling of the 5G wireless systems, significant efforts are being made towards the full inclusion of NOMA in beyond 5G systems. NOMA breaks the orthogonality rule for the multiple access and is able to provide service to multiple users simultaneously on the same resource block (i.e., same frequency, and the same time). Such an multiple access scheme is capable of addressing both, the spectrum scarcity and the need for increased simultaneous connected devices.

## 1.2 Non-orthogonal Multiple Access

The multiple access scheme is defined as a technique of serving multiple users over the same channel by applying rules to cancel or limit the interference between the users, e.g., by providing orthogonality in frequency, or time, or space, etc. The use of a suitable multiple access technology is fundamental to the physical layer and has evolved with different generations of wireless communication. The type of multiple access schemes have shown significant improvements with the advancement of wireless networks. For instance, the first generation operated on frequency division multiple access, which is an analog frequency modulation scheme. The multiple access schemes were transformed into digital modulation from the second generation. The second generation utilized digital modulation and performed multiplexing in time, also known as time division multiple access (TDMA). After TDMA, Qualcomm [8] proposed another useful MA scheme, known as code division multiple access (CDMA). The use of CDMA was prominent in the third generation networks. However, CDMA was not capable of supporting data rates with high speeds, hence the 4G network adopted yet another advanced technique, the orthogonal frequency division multiple access (OFDMA) [9]. The orthogonal multiple access (OMA) techniques are widely accepted in the 4G networks [10].

NOMA has been contemplated as a potential candidate in providing superior spectral efficiency and massive connectivity. Recently, NOMA has been proposed for the 3GPP long term evolution (LTE) [11], [12]. It is worth pointing out that in long term evolution-Advanced (LTE-A), NOMA is implemented as a two-user case [6]. Broadly, NOMA is categorized as power domain (PD)-NOMA and code domain (CD)-NOMA (generally referred as sparse code multiple access). CD-NOMA includes multiple access solutions relying on low-density spreading [13], sparse code multiple access [14], multi-user shared access [15], successive interference cancellation amenable multiple access [16], etc. PD-NOMA and CD-NOMA differ in their basic principle of application. As the names suggest, while PD-NOMA exploits the power domain, CD-NOMA exploits the code domain for non-orthogonal resource allocation. However, due to simpler implementation, PD-NOMA has gained more popularity [17], since no big changes are required at the transmitter as compared to the current 4G technology. This work focuses on the application and analysis of PD-NOMA. PD-NOMA exploits a new dimension of power domain. Therefore, it is capable of serving multiple users simultaneously on a given resource block (RB) by applying successive interference cancellation (SIC). The messages/signals of multiple users with different channel conditions are superimposed and transmitted, as shown in Fig. 1.1(b). Application of NOMA considering two user equipment (UE), termed as cell-center user (CCU) and cell-edge user (CEU), is illustrated in Fig. 1.1(b). Based on the order of users' channel gain conditions, SIC is applied to decode their signal [18]. Assume that the base station (BS) allocates more power to the CEU, owing to its weak channel with respect to the BS due to larger distance from the BS as compared to CCU. After receiving the superimposed signal, CEU decodes its own signal by treating CCU's signal as interference. Whereas, CCU performs SIC, i.e., it decodes CEU's signal first and cancels it from the received signal. After SIC, CCU decodes its own signal. Fundamentally, the implementation of PD-NOMA (referred as NOMA hereafter) is different from the conventional approach used in OMA technologies, e.g., in frequency division multiple access, TDMA, CDMA, and OFDMA. By exploiting the power domain, NOMA is able to serve multiple users by assigning different power based on the user's channel condition, thereby is capable of utilizing the spectrum more efficiently, which is essential for the future genera-

tion networks. A theoretical comparison between the conventional OMA technique namely OFDMA and NOMA is depicted in [18]. The comparison shows that theoretically, users served using NOMA achieves improvement in their rate as compared to OFDMA. The improvement is credited to the increased bandwidth (BW) allocated to the users served using NOMA, which otherwise is distributed between the users due to the orthogonal allocation of resources under OMA. Moreover, by exploring the users' channel condition opportunistically, NOMA can serve multiple users with different requirements [19].

The major advantages of NOMA, which make it popular are, improved spectral efficiency, massive connectivity, and compatibility. The improved spectral efficiency is attributed to the fact that NOMA serves multiple users on the same resource block, i.e., the same frequency and time, which indicates efficient utilization of the spectrum and also leads to enhanced sum throughput of the system [18]. Furthermore, users are served simultaneously, which implies a larger number of active devices leading to massive connectivity. NOMA can support a larger number of users on a given resource block as compared to OMA, which dedicate an entire resource block for one user only. Moreover, the application of NOMA requires only minimal changes in the current 4G network [17]. The development of the superposition coding and SIC technologies both in theory and practice guarantees compatibility and easier implementation of NOMA.

### **1.2.1 Basic Principles**

The fundamental concept of NOMA is to realize the multiple access technologies from the power domain (as shown in Fig. 1.1(a)). Unlike the conventional multiple access technologies, NOMA is capable of bringing a new power dimension to perform multiplexing in the existing time/frequency/code domain. In other words, NOMA can be regarded as an add-on" technique, which provides the very promising potential to be well integrated with the existing MA paradigms.

### **1.2.2 Key Technologies of NOMA**

The key enabling technologies for NOMA is based on two principles, namely, superposition coding and SIC. In fact, these two technologies are not new and the roots

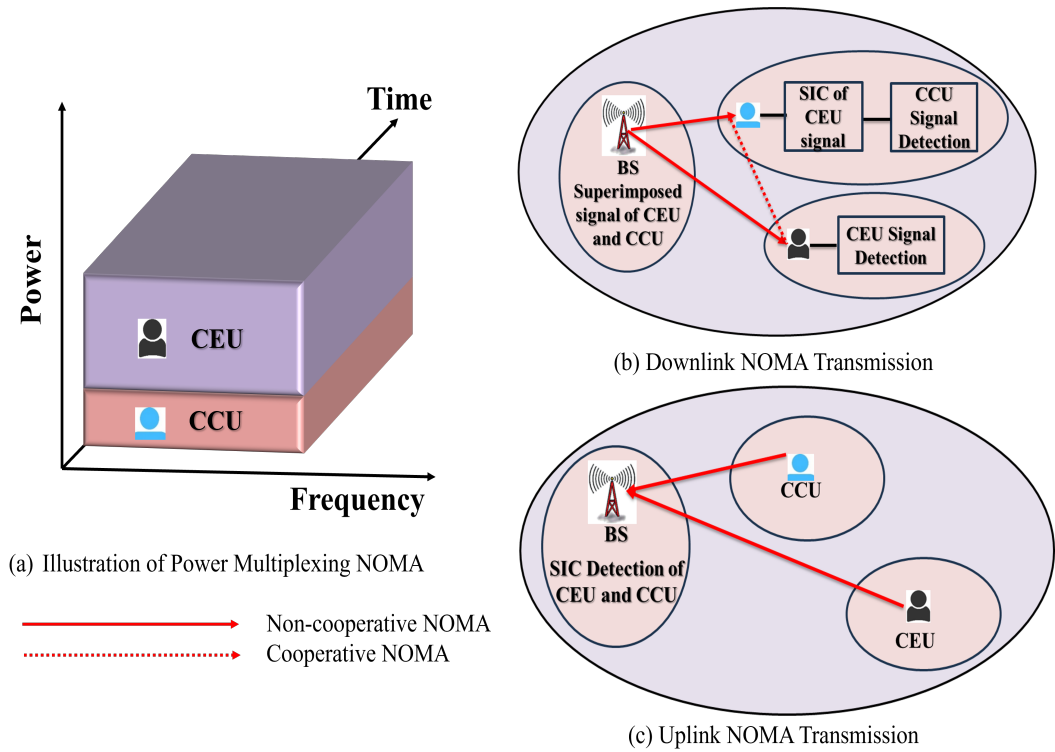


Figure 1.1: Basic principles of NOMA.

of them can be found in many existing literature. As the two main technologies superposition coding and SIC continue to mature both in theoretical and practical aspects, NOMA is able to be applied in the next generation networks without considering the implementation issues. By invoking superposition coding technique, the BS transmits the combination of superposition coded signals of all users' messages. Without loss of generality, the channel gains of users are with respect to a particular ordering (e.g., increasing order or decreasing order). In the traditional OMA schemes, one of the popular power allocation policy is water filling policy. However, in NOMA, users with poor channel conditions are supposed to allocate more power. By doing so, it can ensure that the users with poor channel condition can decode the message of themselves by treating other users' messages as noise. For those users which are in good channel conditions, SIC technologies can be applied to enable subtract the interference from other users with poorer channel conditions.

### Superposition Coding

As first proposed by Cover as early as in 1972 [20], the elegant idea of superposition coding is regarded as one of the fundamental building blocks of coding schemes to

achieve the capacity on a scalar Gaussian broadcast channel [21]. More particularly, it was theoretically demonstrated that superposition coding is capable of achieving the capacities of Gaussian broadcasting channel capacity [22] and of achieving the capacities of the general degraded broadcast channel capacity. The fundamental concept of superposition coding is that it is able to encode a user with poor channel condition at a lower rate and then superimpose the signal of a user with better channel condition on it. Due to the solid foundation laid on the information perspective, researchers begin to apply superposition coding technologies to enormous channels, such as interference channels [23], relay channels [24], multiple access channels [25], and wiretap channels [26]. While the aforementioned contributions sufficiently motivate the use of superposition coding from theoretic perspective, another breakthrough which have been made on superposition coding is to bring this technique from theory to practice [27, 28]. Specifically, [27] designed an experimental platform using a software-radio system to investigate the performance of superposition coding. The set of achievable rate pairs under a packet-error constraint was determined.

### **Successive Interference Cancellation**

Aiming to improve the network capacity with efficient managing interference, SIC is regarded as a promising technology for performing interference cancellation in wireless networks. SIC technique achieves interference cancellation with the following procedure: it enables the user with stronger link to decode the user with weaker link first. Then, it regenerates the signal of weaker user at the stronger user side and subtract the interference. At last the stronger user decodes its information without suffering the interference from the weaker user. It is demonstrated that SIC is capable of reaching the region boundaries of Shannon capacity, both in terms of the broadcast channel and multiple access networks. Additionally, one main advantage of SIC is that it requires low hardware complexity design at the receiver side [29]. As such, SIC has been widely studied and various version was been employed in practical systems such as CDMA [30] and vertical-bell laboratories layered space-time (V-BLAST) [31]. Furthermore, SIC has been exploited in several practical scenarios, such as multi-user multiple input multiple output (MIMO) networks [32],

multi-hop networks [33], random access systems [34], and stochastic geometry modeled large-scale networks [35]. Another important development on SIC is that it has been implemented in some commercial systems, e.g., IEEE 802.15.4.

### 1.2.3 Mathematical Description of NOMA

For better illustrating the relationship between NOMA and OMA from the information theoretic aspect, an analytical demonstration is provided with examining the high signal noise ratio (SNR) performance. Consider a two user case of downlink NOMA transmission, first  $h_1$  and  $h_2$  are denoted as the channel coefficients of the user 1 and user 2,  $\rho$  as the transmit SNR at the BS and assume that  $|h_1|^2 \leq |h_2|^2$  without loss of generality. According to the Shannon Capacity theorem, the obtaining throughput in the context of OMA can be expressed as  $\frac{1}{2} \log_2(1 + \rho|h_1|^2)$  and  $\frac{1}{2} \log_2(1 + \rho|h_2|^2)$ , respectively. Regarding to NOMA, the obtaining throughput are given by  $\log_2\left(1 + \frac{\rho\alpha_1|h_1|^2}{1+\rho\alpha_2|h_1|^2}\right)$  and  $\log_2(1 + \rho\alpha_2|h_2|^2)$ , where  $\alpha_1$  and  $\alpha_2$  are the power allocation coefficients which satisfies  $\alpha_1 \geq \alpha_2$  and  $\alpha_1 + \alpha_2 = 1$ . At high SNR approximation, the sum throughput of OMA and NOMA are  $\frac{1}{2} \log_2(\rho|h_1|^2) + \frac{1}{2} \log_2(\rho|h_2|^2) = \log_2\left(\rho\sqrt{|h_1|^2|h_2|^2}\right)$ , and  $\log_2(\rho|h_2|^2)$ , respectively. As such, it is noted that in high SNR region, the sum throughput of NOMA significantly outperform OMA, especially for the scenarios when the channel conditions of two users are largely different. On the stand point of mathematically thinking, the performance improvements brought by NOMA is mainly due to the fact that the resource (e.g., time/frequency) splitting factor  $\frac{1}{2}$  that outside of the logarithm, is more damaging than the power allocation inside of the logarithm.

### 1.2.4 Downlink and Uplink NOMA Transmission

Downlink NOMA transmission employees the superposition coding technique at the BS for sending combination signals and the SIC technique at users for interference cancellation. More specifically, as shown in Fig. 1.1(b), at the side of cell center user (CCU), the interference of the superimposed signal can be cancelled with employing SIC technique. While at the side of cell edge user (CEU), it will decode the message by treating CCU as interference. This thesis focuses on the downlink NOMA transmission scenarios. This is attributes to the fact that a downlink version of NOMA

transmission, namely, multi-user superposition transmission (MUST), has been already included in the long term evolution advanced (LTE-A) standards, which is more promising as a candidate for 5G.

Unlike the downlink NOMA transmission, the uplink NOMA transmission requires that the BS should send controlling signals to multiple users for power allocation first. Then multiple users transmit their own information to the BS in the same orthogonal resource block resource (as shown in Fig. 1.1(c)). With the aid of SIC technique, the BS decodes all the messages of users following increasing/decreasing decoding order.

### 1.2.5 Cooperative NOMA

The core idea of cooperative NOMA is to regard strong NOMA users as several decode-and-forward (DF) relays to help weak NOMA users. Still taking the two user downlink transmission in Fig. 1.1(b) as an example. The cooperative NOMA requires two time slots for transmission. The first slot, namely, direct transmission phase, is the same as the non-cooperative NOMA (as shown in Fig. 1.1(b) with solid line). During the second time slot which is called cooperative phase, CCU will forward the decoded message to CEU with invoking DF relaying protocol (as shown in Fig. 1.1(b) with dash line). [10] proposed this novel concept sparked that interests to researchers since the cooperative NOMA fully exploits the penitential benefits of SIC and DF decoding. In this thesis, the design.

Compared with the conventional NOMA, the key advantages of the cooperative NOMA transmission can be summarized as follows. 1) Technique integration: with applying SIC technology in NOMA, the message of the weak user has already been decoded at the side of strong user. As such, it is natural to consider the use of DF relay protocol; 2) Better fairness: one key feature of cooperative NOMA is that the reliability of the weak user is significantly improved. As a consequence, the fairness of the NOMA transmission can be guaranteed; and 3) High diversity gain: cooperative NOMA is capable of achieving higher diversity gain for the weak NOMA user, which is an effective approach to overcome the multi-path fading.

## 1.3 Heterogeneous Networks

With increasing data demands in cellular networks and with link efficiency approaching its fundamental limits, there emerges a need to improve spectral efficiency. A possible way of doing this is increasing the number of macro base station (MBS). However, more MBSs in an already dense network would imply higher inter-cell interference [36]. Also, deploying additional MBSs can cost immense expense due to site acquisition in dense areas. An alternate strategy to deal with the ongoing issue is deploying smaller base stations, i.e., BS with lower power (250mW to approximately 2W) and smaller transmission range, which also poses lower deployment cost. Such small base stations include pico base stations, femto base station (FBS), etc. The small base stations can be overlaid with the MBS, creating a HetNet, which is an accepted design for the LTE-A wireless networks. HetNet comprising of MBS, with transmit power of up to 40W, overlaid with FBSs, which transmit at substantially lower power and are typically deployed in an unplanned manner. Installing small base stations improve coverage and provide capacity gain via higher spatial reuse. Unlike the pico base stations, which are meant for outdoor use, the FBSs are designed for indoor users. Since the FBSs are particularly user-installed, thereby, they can select the mode of their operation, i.e., which users in the network can access the FBSs. The FBSs can work in two access modes, open access and closed access [37, 38]. Under closed access, only a closed/fixed group of subscribers (users) have access to the service. However, in open access, any user can connect to the FBS, i.e., a user is allowed to connect to any tier without any restrictions.

### 1.3.1 Stochastic Geometry for Heterogeneous Networks

Stochastic geometry deals with the probability distributions related to the random spatial models or random topology [39–42]. In a wireless network setting, the main theme of the stochastic geometry-based model is to endow probability distributions on the locations of transmitters and receivers in a network. In other words, the transmitter and receiver locations are assumed to be the realizations of point processes or random processes in Euclidean space (such as  $\mathbb{R}^2$ ). The point process based models of wireless nodes have been a standard approach for the performance anal-

ysis of wireless ad hoc networks for a long time (see [43–46] for a rich history of the random spatial modeling of wireless networks). In the context of cellular networks, in [47, 48] Poisson point process (PPP) is used as the spatial distribution of BSs for the traffic and economic models of the networks. [49] characterized the fundamental performance metrics like coverage and rate of a single tier cellular network with PPP-distributed BSs. [37] formulated a PPP-based analytical model for a general multi-tier cellular network consisting of macro and small cell BSs (SBSs).

In a stochastic geometry based cellular network model, the BSs and user locations are treated as realizations of some random point pattern, also known as a point processes. Then the performance metrics of the network (such as the coverage and rate of an arbitrary user) are evaluated as functionals of these point processes. The key role of stochastic geometry is to transform these point process functionals (which are sum, product or the combination of sum and product over the points) to easy-to-compute expressions which are often times integrals over  $\mathbb{R}^2$ . The most common practice is to use the homogeneous PPP as the spatial model for the BSs and users. This assumption is equivalent to saying that the users and BSs are placed independently and uniformly at random over a plane. The PPP-based models have gained significant popularity in cellular network modeling because of the following reasons.

**Tractability:** It is possible to obtain easy-to-compute expressions (which often times reduces to closed forms) of the key performance metrics like the coverage and rate [49]. It is also possible to generalize the network models to a K-tier HetNet model with different types of BSs (such as macro, pico and femto cells) [37]. As a result, a wide set of network deployment scenarios can be studied using this model [50, 51].

**Flexibility:** These models are very flexible to be used for the performance evaluation of different technologies, such as self-powered energy harvesting BSs [52], MIMO enabled networks [53], localization [54] and millimeter wave (mm-wave) communication [55], and many more. The PPP-based modeling and analysis of cellular networks is quite mature by now. Referring to [50, 56, 57] for more pedagogical treatment of the topic as well as extensive surveys of the prior art. Over the last decade PPP has remained the foundation of the stochastic geometry based cellular

network models.

### 1.3.2 NOMA Enabled Heterogeneous Networks

NOMA and HetNets have achieved immense popularity individually. However, the two technologies combined pose more promising advantages due to the reasons mentioned below [58].

- Increased transmit signal-to-interference-and-noise-ratio (SINR): Apart from its several benefits, higher density of BSs in a HetNet results in increased interference, thereby reducing SINR at the user. Using NOMA enabled BSs enables intelligent tracking of different categories of interference, e.g., inter/intra-tier interference and intra-group interference. This effectively increases the SINR at the users.
- Improved fairness: Fairness among the users is very important for the HetNets, especially while investigating efficient resource allocation in multi-tier networks. NOMA provides an efficient way to address fairness by allocating more power to the user with poorer channel condition. Hence, NOMA plays a role of high significance in the HetNets.

MBS usually serves similar types of users where power is equally distributed amongst the users. However, FBS is a device like a wireless local area network router where it supports dense users with far varying needs like Internet of Things (IoT) devices and high definition video transmissions at the same time [59]. Such differences in requirements need a proportionate power splitting. NOMA techniques enable such power splitting for multiple users with different data needs. Hence, NOMA at FBS tier is more likely than at the MBS tier for dense networks. Furthermore, NOMA has a significant role in HetNets in situation where users are offloaded to the open access FBS tier, and the FBS happens to be fully-loaded [60] with its registered subscribers. Since a fully-loaded FBS cannot allocate orthogonal resource to the incoming offloaded user, NOMA plays a vital role in serving the offloaded user by pairing it with the appropriate pairing user.

## 1.4 Point Process

The conventional design adopted for the traditional cellular network is grid based. The grid based model places the BSs (specifically the MBS) on a grid. Although the grid based models are popular and are used extensively, however, they are highly idealized and are not easily tractable. Due to the intractability, complex system-level simulations are used to calculate the outage probability and rate of the network. Furthermore, interference modeling is a challenging task, even while considering single-tier cellular networks. The characterization of interference in a single-tier network, assuming the conventional hexagonal grid based model, requires massive Monte-Carlo simulations [8] due to intractability or inaccurate results due to unrealistic assumptions [61]. Thus, a more realistic model with tractable analysis is required, especially for modeling the multi-tier BSs of the HetNets. Practically, due to varied capacity demands across the service area (e.g., residential areas, parks, suburban, and rural areas), the BSs are far from following a grid-based model. If snapshots of BSs at various location is checked, the position of the BSs with respect to each other will be random. This makes the grid based model very idealistic, and its assumptions violate realistic characteristics of a network. Such topological randomness is true for single-tier and multi-tier networks. The design of HetNet requires interference avoidance. Therefore, rigorous yet simple interference models are necessary. Stochastic geometry provides the necessary tools to model the multitier networks. Besides, capturing the topological randomness of the BSs, stochastic geometry tools are competent in providing tractable analysis [56, 62, 63]. In stochastic geometry, the randomness of the BSs is captured using various point processes, appropriate for the given practical scenario. This makes the point process an essential object in stochastic geometry. A point process is defined as a random collection of points in space. The locations of BSs (or users/devices) are the points that are generated using spatial point processes. Detailed discussion on different point processes are given in [63], [56], [42]. Some of the popular point processes considered in the existing literature to analyze the cellular networks are Poisson point process [37], [60], [64], hard core point process [65], [66], [67], and Poisson cluster process [68–70]. A brief introduction to the common point processes is given below:

- Poisson point process: A point process  $\Omega = \{x_i, i = 1, 2, 3, \dots\} \subset \mathbb{R}^d$  is called a PPP if and only if the number of points inside any compact set  $B \subset \mathbb{R}^d$  is a Poisson random variable, and the numbers of points in disjoint sets are independent, where  $d$  represents number of dimensions.
- Hard core point process (HCPP): An HCPP is a repulsive point process where the distance between two co-existing points is always greater than a predefined hard core parameter  $r$ . A point process  $\Omega = \{x_i, i = 1, 2, 3, \dots\} \subset \mathbb{R}^d$  is an HCPP if and only if  $\|x_i - x_j\| \geq r \forall x_i, x_j \in \omega, i \neq j$ , where  $r > 0$  is a predefined hard core parameter.
- Poisson cluster process (PCP): The PCP is used to model random patterns produced by random clusters. The PCP is constructed from a parent PPP  $\Omega = \{x_i, i = 1, 2, 3, \dots\} \subset \mathbb{R}^d$  by replacing each point  $x_i \in \Omega$  with a cluster of points  $\mathcal{C}_i, \forall x_i \in \omega$ , where the points in  $\mathcal{C}_i$  are independently and identically distributed in the spatial domain.

For more formal and detailed definitions of the point processes, readers can refer to [56, 63].

## 1.5 Simultaneous Wireless Information and Power Transfer

In wireless communication networks, energy harvesting (EH) is a new paradigm that enables terminals to recharge their batteries using the received radio-frequency (RF) signal [71]. The energy constraint issue in wireless networks can be resolved by RF-EH. EH is the process of transforming RF energy into electrical energy. In contrast to traditional battery or grid-powered communications, the EH offers several unique advantages and promising benefits for future wireless communications, such as self-sustaining functionality, reduction of carbon footprint, wireless nodes that don't require battery replacement, and many more [72]. As a result, EH in wireless networks is becoming increasingly popular in a variety of applications, such as medicinal implants, remote environmental monitoring, etc. Particularly in the RF-EH, simultaneous wireless information and power transfer (SWIPT) provides

simultaneous transfer of information and power. SWIPT-enabled receiver architectures such as time switching (TS) and power splitting (PS) are commonly used.

### 1.5.1 Time Switching

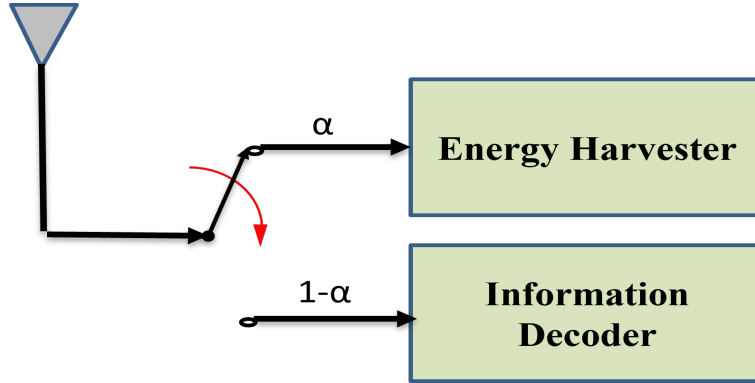


Figure 1.2: Time switching receiver architecture.  $\alpha$  is the time switching coefficient which describes the portion of the time to be dedicated for energy harvester and the information decoder.

TS architecture, also known as co-located receiver architecture, shares the same antenna for EH and information reception [73]. As illustrated in Figure 1.2, the receiver employed in this architecture includes an RF energy harvester, an information decoder, and a switch that alters the system's receiving antenna. Based on a TS sequence, the receiver antenna switches between the energy harvester and information decoder circuit periodically. Further, the TS receiver also requires accurate information/energy scheduling and time synchronization. The TS factor can be optimized to achieve optimum performance.

### 1.5.2 Power Splitting

The PS receiver divides the received signal into two power streams of different power levels with a certain PS ratio before signal processing is performed at the receiver [73]. To enable simultaneous EH and information decoding, both power streams are then delivered to an information decoder and energy harvester as depicted in Figure 1.3. Further, by varying PS ratios, the information rate and the harvested energy can be balanced according to the system requirements. Furthermore, the overall performance can also be improved by optimizing the PS ratio.

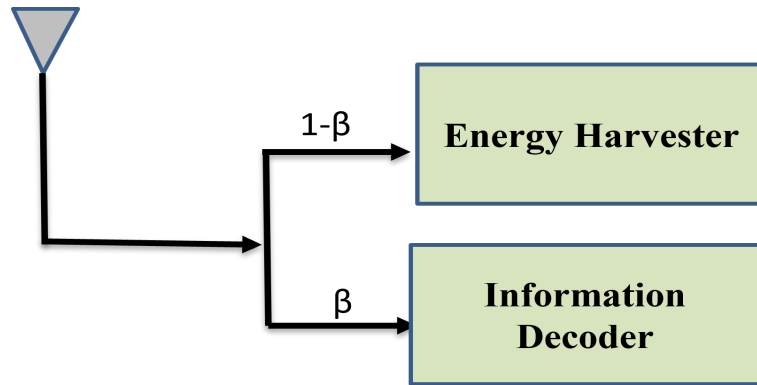


Figure 1.3: Power splitting receiver architecture.  $\beta$  is the power splitting coefficient, such that  $\beta$  times the received power is used for information decoding and the rest i.e.,  $1 - \beta$  times received power is used for EH.

## 1.6 Wireless Communication Channel Model

The radio-wave propagation through the wireless channel can be primarily characterized by two phenomena, multi-path propagation, and shadowing. Mathematically, finding the exact analysis of the fading phenomenon is a complex task. However, through researchers' constant efforts, statistical models have been developed to characterize the channel under fading. The radio environment between the transmitter and receiver tends to fluctuate during transmission of the signal. Based on the fluctuations, there exist various fading models that statistically describe the nature of the multi-path propagation. Few of the commonly used fading models include Rayleigh fading, Nakagami-m fading, Ricean fading, and Weibull fading [74], [75]. This thesis utilizes Rayleigh distribution for the small scale fading as discussed below:

- **Rayleigh distribution:** The Rayleigh distribution is the most popular method for describing the radio channel's statistical behavior. It is operated in the case where multipath propagation exists without a dominant line-of-sight (LoS) path between the end users. Due to the constructive or destructive interference of the multipath components, the in-phase and quadrature-phase components of the received signal are modeled with a zero mean complex Gaussian random process. Thus, the amplitude of the received signal is Rayleigh distributed.

The PDF of the Rayleigh distributed signal can be expressed as

$$f_{\gamma}(x) = \frac{1}{\Omega} \exp\left(-\frac{x}{\Omega}\right), \quad x \geq 0 \quad (1.1)$$

where  $\Omega$  represents the average SNR.

## 1.7 Performance Metrics

To examine the performance of SWIPT-enabled cooperative NOMA based HetNets, several performance metrics are used for different modulation schemes. To fix various design issues of wireless communication systems, these performance measures are used. Commonly used performance metrics are instantaneous signal-to-noise ratio (SNR), outage probability, system throughput, energy efficiency, ergodic capacity, and average symbol error rate (ASER) [75].

1. **Instantaneous SNR:** The instantaneous SNR is a basic performance metric that is used to quantify the signal corruption due to noise. Instantaneous SNR is related to data detection as it is measured at the output of the receiver and is an excellent indicator of the overall fidelity of the communication system. Instantaneous SNR can be expressed as

$$\gamma = \frac{\text{Received signal power at the receiver}}{\text{Received noise power at the receiver}} = \frac{P|h|^2}{\sigma^2}, \quad (1.2)$$

where  $P$ ,  $h$ , and  $\sigma^2$  represent the transmit power, channel parameter, and noise variance, respectively. Due to the multipath fading in wireless communication, average SNR is a more appropriate performance metric than instantaneous SNR. Average SNR is the statistical averaging over the probability distribution of the fading and is given as  $\Omega = \mathbb{E}[\gamma]$ , where  $\mathbb{E}[\cdot]$  represents the statistical expectation operator.

2. **Outage Probability:** Outage probability is one of the important performance metric that depicts link failure probability and is mainly used in the case of a slow-fading scenario. It is defined as the probability that the received end-to-end instantaneous SNR ( $\gamma$ ) of the considered system lies below

a predefined threshold ( $\gamma_{\text{th}}$ ), which can be given as

$$\begin{aligned}\mathcal{P}_{\text{out}}(\gamma_{\text{th}}) &= \Pr[\gamma < \gamma_{\text{th}}] \\ &= \int_0^{\gamma_{\text{th}}} f_{\gamma}(x) dx,\end{aligned}\tag{1.3}$$

where  $f_{\gamma}(\cdot)$  represents the PDF of  $\gamma$ ,  $\gamma_{\text{th}} = 2^{r_{\text{th}}} - 1$ , and  $r_{\text{th}}$  represents the threshold data rate.

3. **System throughput:** The system throughput is one of the important performance metrics to characterize spectrum utilization. It can also be referred to as mean spectral efficiency. Based on the derived expression of outage probability, the system throughput can be formulated as

$$\tau = [1 - \mathcal{P}_{\text{out}}(\gamma_{\text{th}})] r_{\text{th}}.\tag{1.4}$$

4. **Energy efficiency:** Energy efficiency is an important performance metric in the wireless communication system to achieve the vision of green communication systems. It is defined as the overall data transferred to the overall consumed energy. The overall data transferred is referred to as system throughput. Energy efficiency can be expressed as

$$\eta_{\text{EE}} = \frac{\tau}{P}.\tag{1.5}$$

5. **Ergodic capacity:** Ergodic capacity quantifies the ultimate reliable communication limit over fading channels. Instantaneous capacity (measured in bps/Hz) is defined as the maximum rate achieved by the communication channel and can be determined as  $C = \log_2(1 + \gamma)$ . Hence, ergodic capacity is obtained by averaging the instantaneous capacity over the PDF of the instantaneous SNR ( $\gamma$ ), which is defined as

$$\begin{aligned}\mathcal{C}_e &= \mathbb{E}[\log_2(1 + \gamma)] \\ &= \int_0^{\infty} \log_2(1 + x) f_{\gamma}(x) dx.\end{aligned}\tag{1.6}$$

6. **Average symbol error rate (ASER):** ASER is an important performance metric for wireless communication systems that can be determined by averaging the symbols with error at the receiver. For any digital modulation technique, the generalized ASER expression by using the CDF-based approach can be given as

$$\mathcal{P}_e = - \int_0^\infty \mathcal{P}'_s(e|x)\mathcal{P}_{out}(x)dx, \quad (1.7)$$

where  $\mathcal{P}'_s(e|x)$  represents the first order derivative of the conditional symbol error probability ( $\mathcal{P}_s(e|x)$ ) for the received SNR.

## 1.8 Motivation

As a promising candidate for future fifth generation (5G) and beyond systems, NOMA transmission offers a multitude of advantages. One of its standout features is its high spectrum efficiency, a vital performance metric in wireless networks. NOMA achieves exceptional spectrum efficiency by allowing multiple users to share a single resource block, be it time, frequency, or code. Unlike traditional power allocation policies, NOMA allocates more power to weaker users, striking a crucial balance between fairness and system throughput. Moreover, NOMA's ultra-high connectivity capabilities align perfectly with the 5G vision of connecting billions of smart devices, such as those in the IoT. By capitalizing on its non-orthogonal characteristic, NOMA efficiently supports numerous devices with fewer RBs compared to conventional OMA methods. In addition, NOMA exhibits excellent compatibility as it can complement existing OMA techniques like TDMA, FDMA, CDMA, or OFDMA by introducing a new power dimension. With the maturation of superposition coding and SIC technologies in both theory and practice, NOMA holds the promise of seamless integration into existing wireless systems.

Motivated by the flexibility and compatibility of NOMA, this thesis aims at investigating the application of NOMA with recent advanced technologies, e.g., HetNets, and SWIPT. Various stochastic tools are utilized to evaluate the performance of the proposed system models. The application of SWIPT in networks employing cooperative NOMA is investigated in a multi-tier downlink scenario with MBSs and FBSs. The NOMA is applied at the FBS tier and performance analysis is performed at

the femto users distributed uniformly in the coverage area of FBS. The near user employs SWIPT using superimposed NOMA signal and the interference from the adjacent base stations. The harvested energy is utilized for cooperative transmission to the far user. Besides, the outage probability and system throughput is evaluated at the user pair served by the FBS using NOMA. Moreover, for interference management at the small base station tier, medium access channel (MAC) protocol is applied by utilizing carrier sensing. The performance of the resulting network is investigated using repulsive point process. Moreover, since the TS architecture require less hardware complexity compared to the PS architecture. This motivates to explore a NOMA enabled HetNet with a TS protocol at the cooperating user for EH. Furthermore, the application of NOMA involves pairing of users with varying channel conditions, consideration of user fairness is also crucial. This motivates to ensure the users' fairness, and evaluate the proportional fairness index. Moreover, the rectennas in the energy harvester include non-linear components (e.g., diodes and capacitors), hence the input/output relationship is non-linear. Therefore, this thesis studies the performance of EH assisted cooperative NOMA in a two-tier HetNet with a realistic non-linear EH model. Furthermore, the SWIPT based systems are appropriate for the short distance communication. To overcome this limitation, PB is used to supply power for wireless devices. Hence, this thesis studies the performance of power beacon (PB) assisted downlink cooperative NOMA in a wireless powered communication network (WPCN) with realistic non-linear EH model.

### 1.8.1 Related Works

The concept and practical consideration on NOMA is investigated in [18]. Performance of downlink NOMA with randomly deployed users is studied in [76], which proves the superior ergodic rate achieved by NOMA over OMA. Sub-channel assignment, power allocation, and user scheduling in NOMA is studied in [77]. In [19], impact of user pairing in NOMA is studied and [78] studies a low complexity user pairing algorithm. In [79], cooperation techniques are studied from NOMA perspective. Authors in [80] analyze NOMA in a cognitive underlay network wherein the interference from primary network to secondary users is considered. A joint fractional time allocation and beamforming in NOMA network is investigated in

[81]. A fair power allocation scheme for NOMA is discussed in [82]. The authors in [19] prove that in a NOMA group, a user with better channel condition, i.e., a strong user achieves higher throughput in comparison to a user with poorer channel condition, i.e., a weak user. In [83], a coordinated superposition coding scheme is presented, which can improve the CEU's rate, without sacrificing the rate of the users, which are close to the BS. In this direction, cell boundary user's performance is also analyzed in [84], and user fairness in NOMA is dealt in [85], where a dynamic user clustering problem is formulated from a fairness perspective, and power allocation coefficients for the users in each cluster is optimized. Furthermore, to eliminate unfairness in NOMA networks, cooperative NOMA is used wherein a nearby user (i.e., a strong user) is treated as a relay to assist a distant user (i.e., a weak user) as studied in [79]. The authors in [86] use energy harvesting at the strong user to assist the weak user using cooperative NOMA. As a further advance, the fairness issue of NOMA has been addressed in [87], by examining appropriate power allocation policies among the NOMA users. In [88], the sum rate and outage probability of NOMA with partial CSI is investigated. The work in [89] investigate NOMA using stochastic geometry.

### 1.8.2 NOMA and cooperative transmission

The recent research works associated to NOMA with cooperative relaying systems are based on two common relay protocols, namely, amplify-and-forward (AF) relay protocol and DF relay protocol. For AF relaying, [90] and [91], investigated the outage performance of the systems in single antenna AF relay aided NOMA down-link transmission scenarios, while both the BS and the users were equipped with single antenna and multiple antenna, respectively. It also illustrated the potential gains of NOMA over OMA in both two scenarios. Regarding the DF relaying protocol, apart from the well integration with the cooperative NOMA protocol which is proposed in [79], a DF based two-stage relaying protocol was proposed in [92]. Apart from extending the transmission coverage of wireless networks, another key aspect of cooperative communication is to generate spatial diversity for combating the deleterious fading. Coordinate multi-point (CoMP) transmission, as an effective approach to mitigate the interference, is particularly capable of improving the

performance of the users at the edge of the cell. [83] first attempted to employ NOMA into CoMP transmission system for spectral efficiency improvement. A new coordinated superposition coding scheme with the aid of Alamouti code was proposed. In an effort to explore more efficient design approach, [93] proposed a novel opportunistic NOMA transmission scheme in CoMP system and showed the effectiveness compared with the conventional joint-transmission NOMA. [94] considered a coordinated direct and relay transmission scheme, where the BS communicated with a near user and a relay simultaneously with invoking NOMA technique during the first phase, while communicated with a far user with the aid of the relay. [95] proposed a NOMA based power allocation for a downlink CRAN scenario, which can be also regarded as a coordinated transmission scenario where all the BSs are controlled by a cloud.

### 1.8.3 Wireless Energy Harvesting and NOMA

Recently, harvesting energy from ambient RF signals has received increasing attention due to its convenience in providing energy self-sufficiency to a low power communication system [96]. With recent advances in the technology of low power devices both in industry [97] and academia [98], it is expected that harvesting energy from RF signals will provide a practically realizable solution for future applications, especially for networks with low power devices such as wireless sensor network nodes [99, 100]. SWIPT, which was initially proposed in [101], has rekindled the interest of researchers to explore more energy efficient networks. In [101], it was assumed that both information and energy could be extracted from the same RF signals at the same time, which does not hold in practice. Motivated by this issue, two practical receiver architectures, namely TS receiver and PS receiver, were proposed in a MIMO system in [102]. Since point-to-point communication systems with SWIPT are well established in the existing literature, recent research on SWIPT has focused on two common cooperative relaying systems: AF and DF. On one hand, for AF relaying, a TS-based relaying protocol and a PS-based relaying protocol were proposed in [103]. On the other hand, for DF relaying, a new antenna switching SWIPT protocol was proposed in [104] to lower the implementation complexity. Additionally, a novel wireless energy harvesting DF relaying protocol was proposed in

[105] for underlay CR networks to enable secondary users can harvest energy from the primary users. In [106], the application of SWIPT to DF cooperative networks with randomly deployed relays was investigated using stochastic geometry in a cooperative scenario with multiple source nodes and a single destination. A scenario in which multiple source-destination pairs are randomly deployed and communicate with each other via a single energy harvesting relay was considered in [79]. Regarding NOMA systems related with SWIPT, in [107], the uplink NOMA transmission considering energy constrained users which can harvest energy from the BS with adopting "harvest-then-transmit" protocol. The results demonstrate that NOMA can provide considerable improvements in terms of system throughput, fairness and energy efficiency.

## 1.9 Thesis Flowchart, Outline, and Contributions

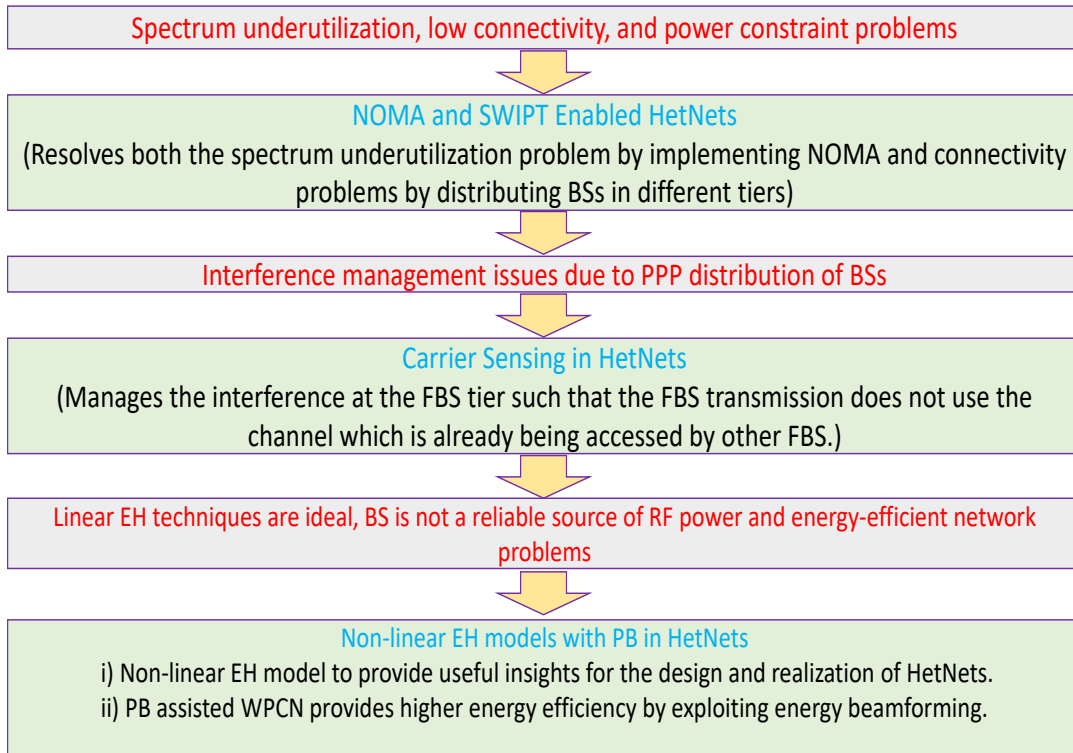


Figure 1.4: Flowchart of the thesis.

The flowchart of the thesis is shown in Figure 1.4. The thesis is organized into 7 chapters, which are briefly described with their contributions as follows:

**Chapter 1. Introduction :** In chapter 1, a brief introduction to the NOMA, cooperative NOMA, various performance metrics, simultaneous wireless information and power transfer, HetNets, and finally, the motivation and major contributions of the work presented in the thesis are provided.

**Chapter 2. SWIPT Enabled Cooperative NOMA Heterogeneous Network:** In this chapter, an analytical framework is proposed for a SWIPT-enabled cooperative NOMA based heterogeneous downlink network. The model aimed to improve the performance at the CEU using cooperation from the CCU. The CCU is enabled with SWIPT to prevent their battery from draining while performing cooperation. The CCU utilizes the RF energy from the superimposed signal and the aggregate interference of the HetNets. The analytical expressions of outage probability for both the CCU and the CEU are derived. Further, analytical expressions of system throughput, and user fairness is also investigated. The chapter also investigates a practical case of imperfect CSI, and its impact on the system. The proposed system model is compared with commonly used EH models where EH is performed using only the superimposed signal, and new insights from the proposed system model are drawn.

**Chapter 3. SWIPT Enabled Heterogeneous Networks with NOMA and Carrier Sensing:** In this chapter, application of SWIPT in HetNets employing cooperative NOMA is investigated. The HetNets consists of MBS under-laid by SBS. The distribution of MBSs follow Poisson point process model, while the SBS tier supports NOMA and carrier sensing for its transmission. Carrier sensing helps in reducing interference by blocking the base stations within a specific range from transmitting. In this work, the analysis at SBS tier is carried out in two phases. In the direct phase transmission, the SBS transmits the superimposed signal to a user pair, comprising of a CCU and a CEU, using NOMA principle. The CCU acts as a cooperative relay to forward information to the CEU in the cooperative phase. The CCU is enabled with SWIPT to prevent their battery from draining while performing cooperation. The CCU utilizes the RF energy from the superimposed signal and the aggregate interference of the HetNets. The analytical expressions of outage probability for both the CCU and the CEU are derived. Further, analytical expressions of system throughput, and user fairness is also investigated. The chapter also

investigates a practical case of imperfect CSI, and its impact on the system. The proposed system model is compared with commonly used EH models where EH is performed using only the superimposed signal, and new insights from the proposed system model are drawn.

**Chapter 4. Time Switching based Energy Harvesting Enabled Cooperative NOMA HetNets:** This chapter studies the performance of EH assisted cooperative NOMA two-tier HetNets for self-sustaining beyond 5G communication systems. The chapter proposes an analytical methodology for examining the use of EH in HetNets with cooperative NOMA. The study is performed at the NOMA pair served by the SBS. Cooperation is carried out by one of the users in a NOMA pair which acts as an EH decode and forward relay node. TS protocol is employed at the cooperating user for EH. Closed-form expressions of outage probability and energy efficiency are derived, and comparisons with useful insights are drawn for EH-enabled and without EH-enabled systems. To ensure the users' fairness, the proportional fairness (PF) index is also evaluated.

**Chapter 5. SWIPT and NOMA Enabled Heterogeneous Networks with Non-linear Energy Harvesting:** This chapter studies the performance of EH assisted cooperative NOMA in a two-tier HetNet with a realistic non-linear EH model. The chapter proposes an analytical methodology for improving the performance of NOMA user with poor channel conditions by employing EH and cooperative NOMA at the user with good channel conditions. The analysis is considered at the NOMA pair served by the SBS. Cooperation is carried out by one of the users in a NOMA pair which acts as decode and forward relay node assisted with EH. The outage probability at the NOMA users is derived in closed form using stochastic geometry. The performance of the proposed system is compared with the system without EH and the system with linear EH. It is shown that the proposed system attains higher throughput than OMA without EH in the considered scenario.

**Chapter 6. Power Beacons Assisted NOMA Based Wireless Powered Communication Networks:** In this chapter, the performance of power beacon (PB) assisted downlink cooperative NOMA in a wireless powered communication network (WPCN) with realistic non-linear EH model is studied. This chapter proposes an analytical methodology for improving performance at blocked user at the

edge of network via an intermediate node (IN). IN deployed in the coverage area of the BS, acts as decode-and-forward relay to perform cooperative transmission. IN assists the BS in communicating with the blocked IoT device after harvesting energy from PB mounted on the BS. IN employs NOMA to serve IoT devices with heterogeneous quality of service (QoS) requirements in order to achieve higher spectral and energy efficiency. A practical non-linear EH model is employed at IN to power the cooperative transmission to the IoT devices. The performance of the proposed scheme is compared with the system employing OMA and it is shown that the proposed scheme attains improved performance in terms of outage probability, system throughput, and energy efficiency.

**Chapter 7. Conclusions and Future Works:** All the contributions of the thesis have been summarized in this chapter, and important insights and conclusions have been presented. Further, the scope for future works is also discussed.



## Chapter 2

# SWIPT Enabled Cooperative NOMA Heterogeneous Network

Spectrally efficient and sustainable techniques with minimum hardware cost are critical for realizing feasible and green beyond 5G wireless networks. NOMA has been considered as a viable multiple access technique for supporting massive number of devices with high spectral efficiency [108]. The underlying concept of NOMA is to have multiple users sharing orthogonal resource block thereby efficiently utilizing the given spectrum/resources [109]. Also, SWIPT draws considerable attention for deployment of energy efficient networks. In SWIPT, both energy, as well as information, is extracted at the same time from the transmitted RF signal. The concept was initially given in [101] for point-to-point link which was extended to parallel links in [110]. Two practical receiver designs, i.e., TS and PS are planned in a relay assisted system in [103]. SWIPT targets two important cooperative relaying systems, namely, DF and AF. For cooperative DF relaying, a novel low complexity antenna switching SWIPT protocol was proposed in [104]. In [106], SWIPT applications to cooperative DF networks with spatially deployed random relays were studied applying stochastic geometry with multiple transmitters and a single receiver. For AF cooperative networks, relaying protocols based on TS and PS was proposed in [103]. In [111], resource allocation algorithm design for SWIPT in orthogonal frequency division multiple access systems was studied, whereas [112] studied resource allocation in energy cooperation enabled two-tier HetNets with NOMA. Secrecy performance in a downlink NOMA system in the presence of eavesdropper is investigated in

[113]. In [114] security enhancement in a two slot cooperative NOMA scheme is proposed. Optimization for energy efficiency in SWIPT-enabled NOMA scheme is addressed in [115]. A resource allocation problem regarding the imperfect SIC case in a cooperative NOMA HetNet was investigated in [116].

## 2.1 Motivation and Contribution

In the existing literature, only limited work exists on outage performance in SWIPT enabled with multi-tier interferences. In [76], the performance of the NOMA scheme in a single BS is studied in terms of the outage and ergodic rate and it is found that NOMA can achieve a higher sum rate as compared to OMA. In [2], a SWIPT-enabled cooperative NOMA strategy for users in a single BS is presented, and the outage probabilities for various user selection schemes are studied. Some prior works, such as [79] exploits the idea of cooperative NOMA to achieve performance gain. The aforementioned studies are limited to single BS scenarios, therefore, they are unable to predict how multi-tier HetNets with multi-tier interferences affect users' outage performance. There are few recent NOMA works based on large-scale HetNets. For example, in [117], the outage probability in a large-scale cognitive radio network is investigated. Similarly, in a single-tier cellular network, [118] investigates the outage and attainable rate of users. In [58], the NOMA scheme is explored for HeNet, and its coverage, ergodic rate, and energy efficiency are evaluated. [119] develops an analytical framework for a downlink NOMA systems in large-scale cellular networks and evaluates the outage performance. The works mentioned in [2]-[119] do not take into account the utilization of cooperative NOMA and SWIPT among users to enhance outage performance in a HetNet context. As a result, while employing SWIPT enabled cooperative NOMA in a HetNet, it is still unclear how to increase users' outage performance and overall system throughput which is crucial for beyond 5G sustainable systems. Furthermore, the above works are based upon the assumption of perfect CSI to be known at the BS which is not feasible in practice. The assumption of perfect CSI leads to significant system overhead and the existence of channel estimation errors and quantization errors [120]. Therefore, motivated by this practical issue this chapter also investigates the proposed system model under

an imperfect CSI scheme. The main contributions of the chapter are highlighted below:

- An analytical framework for SWIPT enabled cooperative NOMA is proposed in a multi-tier heterogeneous downlink network to improve the performance of the CEU using cooperation from the CCU. The CCUs are enabled with SWIPT to prevent their battery from draining while performing cooperation. Unlike the existing works, the CCU performs EH using the superimposed signal and the aggregate co-tier and cross-tier interference (EHSI). In the existing literature, EHSI has not been considered in the previous literature.
- Apart from EHSI, this chapter also investigates a practical case of imperfect CSI, and its impact on the system.
- Using tools from stochastic geometry, closed-form expressions for the outage probability at the CCU and the CEU with imperfect CSI are derived for the proposed EHSI at the CCU. To obtain the overall system performance, the throughput of the system is analyzed.
- Comparison of outage probability for the CCU and CEU both, with and without SWIPT, is investigated. Furthermore, the proposed system with EHSI is compared with commonly used EH models where EH is performed using only the superimposed signal (EHS), and new insights from the proposed system model are drawn. The analytical results are validated using Monte Carlo simulations.

## 2.2 System Model

The proposed system model considers a two-tier heterogeneous network comprising of an MBS tier and an FBS tier, such that the locations of MBS and FBS follow independent homogeneous PPP denoted by  $\Omega_t$  such that  $t \in \{m, f\}$  where  $m$  stands for MBS tier and  $f$  represents FBS tier, with density  $\lambda_t$ . Users are distributed uniformly with density  $\lambda_u$ . The transmit power of MBS and FBS is denoted as  $P_m$  and  $P_f$ . The coverage range of MBS tier and FBS tier are denoted as  $\mathcal{Y}_m$  and  $\mathcal{Y}_f$ , respectively. The analysis is carried out at a NOMA pair in the FBS tier wherein the

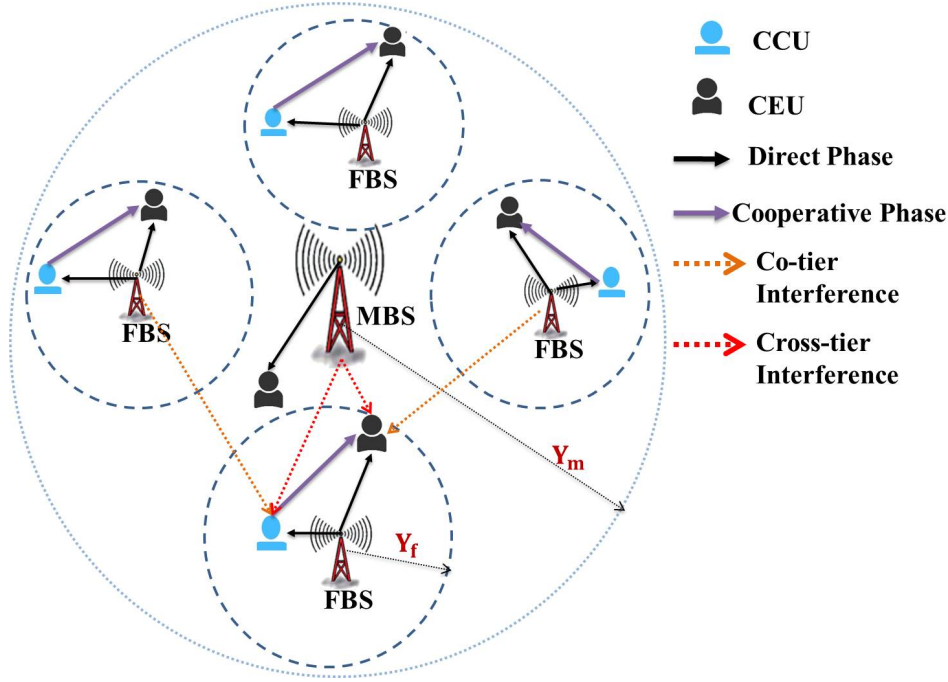


Figure 2.1: Illustration of a downlink cooperative NOMA-SWIPT system model with a tagged FBS and a NOMA user pair in a multi-tier scenario. The spatial distributions of the MBS and the FBS follow PPP assumption.

CCU and CEU are paired by the FBS based on their channel condition. The overall system transmission bandwidth is assumed to be 1 Hz [1] and the total resource time block is divided into two equal phases a direct phase and a cooperative phase each of equal duration. In the direct phase of transmission, the proposed model considers a NOMA downlink transmission in which FBS transmits the signal to both CCU and CEU. In the cooperative phase of the transmission, CCU acts as energy harvesting DF relay to forward information to CEU as shown in Fig. 2.1. The channel between the BS of  $t$  and the typical  $i^{th}$  user is denoted by  $h_i/\sqrt{1+r_i^{\alpha_t}}$ , where  $h_i \sim \mathcal{CN}(0,1)$  such that  $\mathcal{CN}(a,b)$  is the complex Gaussian distribution with mean  $a$  and variance  $b$ ,  $r_i$  is the distance of  $i^{th}$  user from the BS of  $t^{th}$  tier,  $\alpha_t$  is the path loss exponent for the  $t^{th}$  tier. Following the minimum mean square error (MMSE) estimation error [121]:

$$\hat{h}_i = h_i + e_i, \quad (2.1)$$

where  $e_i$  is the channel estimation error for  $i^{th}$  user, such that  $e_i \sim \mathcal{CN}(0, \sigma_e^2)$ ,  $\hat{h}_i$  is the estimate for  $h_i$ . Thus, the estimate  $\hat{h}_i$  follows complex Gaussian distribution with mean 0 and variance  $(1+r_{t,i}^{\alpha_t})^{-1} + \sigma_e^2$ . The quality of channel estimation is based on the value of  $\sigma_e^2$ .

### 2.2.1 SINR at CCU and CEU

Let the two users, to be served using NOMA, are selected using a random selection scheme [2]. Their estimated channel gains are ordered as  $\hat{h}_1 \leq \hat{h}_2$  and their power allocation coefficients are ordered as  $a_1 \geq a_2$ , respectively. User-2 with a better channel condition is the CCU, and user-1 with a poorer channel condition is the CEU. Therefore,  $\hat{h}_1$  is the channel power gain corresponding to the CEU and  $\hat{h}_2$  corresponds to the CCU.

#### Direct Transmission

The FBS sends the signal  $X_f = \sum_{i=1}^2 x_i \sqrt{a_i P_f}$  to users based on NOMA transmission, where  $x_i$  is the intended signal for the  $i^{th}$  user such that expectation  $\mathbb{E}[x_i^2] = 1$  and is assumed to be equal  $\forall i \in (1, 2)$ . The observation at the  $k^{th}$  typical user is given by

$$Y_k = \hat{h}_k \sqrt{(1 + r_k^\alpha)^{-1}} X_f + n_k, \quad (2.2)$$

where  $n_k$  is the additive white Gaussian noise (AWGN) at the  $k^{th}$  user. Using the NOMA principle, SIC is carried out at CCU which decodes and removes the message of CEU to detect its own message. The received SINR at CCU to detect message of CEU is expressed as

$$\gamma_{2 \rightarrow 1}^1 = \frac{\beta \rho_f a_1 |\hat{h}_2|^2 (1 + r_2^\alpha)^{-1}}{\beta \rho_f a_2 |\hat{h}_2|^2 (1 + r_2^\alpha)^{-1} + \beta \sum_t \rho_t \mathcal{I}_t + \rho_f \sigma_e^2 + 1}, \quad (2.3)$$

where  $\beta$  is the power splitting coefficient and  $\rho_t = P_t / \sigma_f^2$  is the transmit SNR at FU.  $\rho_f \mathcal{I}_f$  denotes co-tier interference from FBS tier such that  $\mathcal{I}_f = \sum_{y \in \Omega_f / \{f_o\}} |\hat{h}_y|^2$ , where  $|\hat{h}_y|^2$  denotes the estimate of channel gain from the  $y^{th}$  FBS to the typical user and  $f_o$  is the tagged FBS. Similarly  $\rho_m \mathcal{I}_m$  denotes the cross-tier interference from MBS tier such that  $\mathcal{I}_m = \sum_{y \in \Omega_m} |\hat{h}_v|^2$ , where  $|\hat{h}_v|^2$  denotes the estimate of the channel gain from  $v^{th}$  MBS to the typical user. Thus, the SINR at the CCU to detect its own message is given as

$$\gamma_2^1 = \frac{\beta \rho a_2 |\hat{h}_2|^2 (1 + r_2^\alpha)^{-1}}{\beta \sum_t \rho_t \mathcal{I}_t + \rho_f \sigma_e^2 + 1}. \quad (2.4)$$

Here, it is assumed that the CCU has rechargeable storage ability [103], and PS technique [2] is applied at CCU to perform SWIPT. The observation at CCU is divided into two parts. One part is used for information decoding and another for EH to power CCU for cooperation. The energy harvested ( $E_2$ ) at CCU from the source and the interference from MBSs and FBSs is given as

$$E_2 = \frac{T}{2}\eta(1 - \beta) \left( P_f |\hat{h}_2|^2(1 + r_2^\alpha)^{-1} + P_f \mathcal{I}_f + P_m \mathcal{I}_m \right), \quad (2.5)$$

where  $T$  is the total transmission time block, and  $\eta$  is the conversion efficiency of the energy harvester. The transmit power from CCU can be expressed as

$$\begin{aligned} P_2 &= \frac{E_2}{\frac{T}{2}} \\ &= \eta(1 - \beta) \left( P_f |\hat{h}_2|^2(1 + r_2^\alpha)^{-1} + P_f \mathcal{I}_f + P_m \mathcal{I}_m \right), \end{aligned} \quad (2.6)$$

where  $P_2$  denotes the harvested power from the energy harvester which is also the transmit power of the CCU. In this chapter, it is assumed that the energy consumed by the cell CCU for information decoding is negligible as compared to information transmission during the cooperative phase. The use of this assumption is consistent with prior works (which uses power amplifier) [103], [122], [123]. Also, the SINR at the CEU during the first phase of transmission is given by

$$\gamma_1^1 = \frac{\rho a_1 |\hat{h}_1|^2 (1 + r_1^\alpha)^{-1}}{\rho a_2 |\hat{h}_1|^2 (1 + r_1^\alpha)^{-1} + \sum_t \rho_t \mathcal{I}'_t + \rho_f \sigma_e^2 + 1}, \quad (2.7)$$

where  $\rho_f \mathcal{I}'_f$  denotes co-tier interference from FBS to the CEU and  $\rho_m \mathcal{I}'_m$  denotes the cross-tier interference from MBS tier to the CEU.

### Cooperative Transmission

In the second phase, the CCU forwards the message to the CEU. The received SINR at CEU to detect  $x_1$  forwarded from CCU user is given by

$$\gamma_1^2 = \frac{P_2 |\hat{h}_{12}|^2 (1 + r_{12}^\alpha)^{-1}}{P_f \mathcal{I}'_f + P_m \mathcal{I}'_m + P_f \sigma_e^2 + \sigma_1^2}, \quad (2.8)$$

where  $|\hat{h}_1|^2$  is the estimated channel power gain between CCU and CEU, and  $r_{12}$  denotes the distance between the CCU and CEU. The CEU combines the signal from FBS and CCU using selection combining (SC) [124], since maximal ratio combining (MRC) increases the receiver system complexity [125]. Even though only one SINR is used in SC the diversity order is same as compared to MRC which coherently combines all SINR especially when the number of links is less than five [126]. Here, SC is performed by taking the maximum of the received SINR of the direct phase (2.7) and the cooperative phase (2.8). The received SINR at the CEU is expressed as

$$\gamma_1^{sc} = \max(\gamma_1^1, \gamma_1^2). \quad (2.9)$$

## 2.3 Performance Analysis

### 2.3.1 Outage Probability at CCU

The outage probability of CCU relies on the SIC of the signal for CEU. The outage probability at the CCU can occur in two ways: first when CCU is unable to decode the message of CEU and secondly when CCU decodes the message of CEU, however is unable to decode its own message. Therefore, the outage probability at CCU is calculated as

$$P_{out}^{cc} = \mathcal{P}(\gamma_{2 \rightarrow 1}^1 < \phi_1) + \mathcal{P}(\gamma_{2 \rightarrow 1}^1 \geq \phi_1, \gamma_2^1 < \phi_2), \quad (2.10)$$

where  $\phi_1 = 2^{2R_1} - 1$  and  $\phi_2 = 2^{2R_2} - 1$ , with  $R_1$  and  $R_2$  being the target rate to detect the message of CCU and CEU.

*Proposition 1:* The outage probability of the CCU based on PPP assumptions is given as

$$P_{out}^{cc} = \frac{1}{2} \sum_{n=0}^N b_n e^{-\frac{c_n(\epsilon_1 + \rho_f \sigma_e^2)}{1 + c_n \sigma_e^2}} \mathcal{L}_{I_p}[s_p], \quad (2.11)$$

where  $\mathcal{L}_{I_p}[s_p] = \mathcal{L}_{I_f}[s_f] \mathcal{L}_{I_m}[s_m]$ ,  $s_f = \frac{\rho_f c_n \epsilon_1}{1 + c_n \sigma_e^2}$ ,  $s_m = \frac{\rho_m c_n \epsilon_1}{1 + c_n \sigma_e^2}$ ,  $\epsilon_1 = \frac{\phi_1}{\beta \rho (a_1 - \phi_1 a_2)}$ ,  $\epsilon_2 = \frac{\phi_2}{\beta \rho_f a_2}$ ,  $b_n = -\omega_N (1 + \theta_n) \sqrt{1 - \theta_n^2}$ ,  $b_0 = -\sum_{n=1}^N b_n$ ,  $\omega_N = \pi/N$ ,  $\theta_n = \cos\left(\frac{2n-1}{2N}\pi\right)$ ,  $c_n = 1 + \left(\frac{\gamma_f}{2}\theta_n + \frac{\gamma_f}{2}\right)^\alpha$ ,  $c_0 = 0$ ,  $N$  is complexity-accuracy trade-off parameter for the Gaussian-Chebyshev (G-C) quadrature. The two terms in equation (2.11), i.e.,  $\mathcal{L}_{I_f}(s)$  and  $\mathcal{L}_{I_m}(s)$  correspond to

the Laplace of co-tier and cross-tier interference from FBS and MBS tier respectively. The Laplace transform of interference by the  $t^{th}$  tier is calculated [1] as

$$\mathcal{L}_{I_t}(s) = e^{\pi\lambda_t(s^{\delta_t}\Gamma(1-\delta_t,s) - s^{\delta_t}\Gamma(1-\delta_t))}, \quad (2.12)$$

where  $\delta_t = \frac{2}{\alpha_t}$ ,  $\Gamma(a, x) = \int_x^\infty t^{a-1}e^{-t}dt$  and  $\Gamma(z) = \int_0^\infty x^{z-1}e^{-x}dx$ .

*Proof:* Let the channel gain be denoted as  $X = \hat{h}_1(1+r_1^\alpha)^{-1}$ ,  $Y = \hat{h}_2(1+r_2^\alpha)^{-1}$ , and  $Z = \hat{h}_{12}(1+r_{12}^\alpha)^{-1}$ . The cumulative distribution function (CDF) of channel gain  $Y$  can be expressed as

$$F_Y(y) = \frac{2}{\mathcal{Y}_f^2} \int_0^{\mathcal{Y}_f} \left( 1 - e^{-\frac{(1+r_2^{\alpha_f})y}{1+(1+r_2^{\alpha_f})\sigma_e^2}} \right) r_2 dr_2. \quad (2.13)$$

Applying G-C quadrature [127], CDF can be approximated as

$$F_Y(y) \approx \frac{1}{2} \sum_{n=0}^N b_n e^{-\frac{c_n}{1+c_n\sigma_e^2}y}, \quad (2.14)$$

where  $b_n = -\omega_N \alpha (1 + \theta_n) \sqrt{1 - \theta_n^2}$ ,  $b_0 = -\sum_{n=1}^N b_n$ ,  $\omega_N = \pi/N$ ,  $\theta_n = \cos\left(\frac{2n-1}{2N}\pi\right)$ ,  $c_n = 1 + \left(\frac{\mathcal{Y}_f}{2}\theta_n + \frac{\mathcal{Y}_f}{2}\right)$ ,  $c_0 = 0$ ,  $N$  is complexity-accuracy trade-off parameter for the G-C quadrature. (2.10) can be rewritten in terms of random variable  $Y$  as

$$P_{cc}^1 = \mathcal{P}(Y < \epsilon_1) + \mathcal{P}(Y \geq \epsilon_1, Y < \epsilon_2). \quad (2.15)$$

Second part of (2.15) gives outage for condition  $\epsilon_1 < \epsilon_2$ . Thus, for the case when  $\epsilon_1 \geq \epsilon_2$ , the outage probability is given by the CDF of  $Y$  with  $y = \epsilon_1(1 + \beta \sum_t \rho_t \mathcal{I}_t + \rho_f \sigma_e^2)$ , and substituting  $y$  in (2.14) to get (2.11).

### 2.3.2 Outage Probability at CEU

The outage probability at the CEU can occur in two ways, firstly when neither the CCU nor the CEU can detect the message of the CEU, and secondly when the CCU can detect the message of the CEU however overall SINR at the CEU can not support the targeted rate. Therefore, the outage probability at the CEU can be expressed as

$$P_{out}^{ce} = \underbrace{\mathcal{P}(\gamma_{2 \rightarrow 1}^1 < \phi_1, \gamma_1^1 < \phi_1)}_{\Theta_1} + \underbrace{\mathcal{P}(\gamma_{2 \rightarrow 1}^1 > \phi_1, \gamma_1^{sc} < \phi_1)}_{\Theta_2}. \quad (2.16)$$

*Proposition 2:* The outage probability at the CEU based on PPP assumption is given by

$$\begin{aligned}
 P_{out}^{ce} = & \frac{1}{4} \sum_{n=0}^N \sum_{k=0}^K b_n b_k e^{-\frac{(c_n+c_k)(\epsilon_1+\rho_f\sigma_e^2)}{(1+c_n\sigma_e^2)(1+c_k\sigma_e^2)}} \mathcal{L}_{I_p}[s_p] \mathcal{L}'_{I_p}[s_p] + \frac{1}{2} \sum_{n=0}^N b_n e^{-\frac{c_n(\epsilon_1+\rho_f\sigma_e^2)}{(1+c_n\sigma_e^2)}} \mathcal{L}_{I_p}[s_p] \times \\
 & \left( 1 - \lim_{B \rightarrow \infty} \frac{\pi^2 B}{\alpha^2 N M \mathcal{Y}_f^3} \sum_{n=1}^N (1 - \theta_n^2)^{\frac{1}{2}} \frac{e^{-K_n}}{K_n^{1+\frac{2}{\alpha}}} \left( (2 + \alpha K_n) \Gamma\left(\frac{2}{\alpha}\right) - \alpha K_n \Gamma\left(\frac{2}{\alpha}, \mathcal{Y}_f^\alpha K_n\right) \right) \times \right. \\
 & \left. \sum_{m=1}^M b_m e^{-\frac{c_m Q_1}{(1+c_m\sigma_e^2)K_n}} - \alpha \Gamma\left(\frac{2+\alpha}{\alpha}, \mathcal{Y}_f^\alpha K_n\right) \right) \mathcal{L}_{I_p} \left[ \frac{d_m Q \rho_m}{(1+d_m\sigma_e^2)K_n} \right] \quad (2.17)
 \end{aligned}$$

*Proof:* Let the first and the second term of (2.16) be denoted as  $\Theta_1$  and  $\Theta_2$ . The terms of  $\Theta_1$  are independent. Therefore,  $\Theta_1$  can be obtained as

$$\Theta_1 = \mathcal{P}(\gamma_{2 \rightarrow 1}^1 < \phi_1) \mathcal{P}(\gamma_1^1 < \phi_1), \quad (2.18)$$

$\mathcal{P}(\gamma_{2 \rightarrow 1}^1 < \phi_1)$  is given by (2.11) and the analysis for  $\mathcal{P}(\gamma_1^1 < \phi_1)$  is carried in the same manner, i.e., by assuming the channel gain  $X = \hat{h}_1(1+r_1^\alpha)^{-1}$  and following the same steps as in the Appendix A. The expression of  $\Theta_1$ , is given as

$$\Theta_1 = \frac{1}{4} \sum_{n=0}^N \sum_{k=0}^K b_n b_k e^{-\frac{(c_n+c_k)\epsilon_1}{(1+c_n\sigma_e^2)(1+c_k\sigma_e^2)}} \mathcal{L}_{I_p}[s_p] \mathcal{L}'_{I_p}[s_p] \quad (2.19)$$

where  $\mathcal{L}_I[s]$  and  $\mathcal{L}'_I[s]$  represents the Laplace transform of the interference at CEU during the direct phase transmission and cooperative phase transmission, respectively.  $\Theta_2$  can be written as

$$\Theta_2 = \underbrace{\mathcal{P}(\gamma_1^1 < \phi_1)}_{\Theta_{21}} \underbrace{\mathcal{P}(\gamma_{2 \rightarrow 1}^1 \geq \phi_1, \gamma_1^2 < \phi_1)}_{\Theta_{22}}, \quad (2.20)$$

The evaluation of  $\Theta_{21}$  is completed in (2.19). Therefore, the expression of  $\Theta_{21}$  is given as

$$\Theta_{21} = \frac{1}{2} \sum_{n=0}^N b_n e^{-\frac{c_n(\epsilon_1+\rho_f\sigma_e^2)}{(1+c_n\sigma_e^2)}} \mathcal{L}_{I_p}[s_p]. \quad (2.21)$$

Consider  $\rho_f\sigma_e^2 + \rho_f\mathcal{I}_f + \rho_m\mathcal{I}_m = \mathcal{I}$ , and  $\epsilon'_1 = \epsilon_1(\beta\mathcal{I} + 1)$ , using this  $\Theta_{22}$  can be given

from (2.20) as

$$\Theta_{22} = \mathcal{P}\left(Z < \frac{\phi_1(\mathcal{I} + 1)}{\eta(1 - \beta)(\rho y + \mathcal{I})}, Y \geq \epsilon'_1\right). \quad (2.22)$$

Consider high SNR approximation, i.e., assuming  $\rho \rightarrow \infty$ , which approximate  $\rho y + \mathcal{I} \approx \rho y$  and  $\epsilon'_1 \approx 0$ . Using these approximations  $\Theta_{22}$  can be rewritten as

$$\Theta_{22} = \int_0^{\mathcal{Y}_f} \int_0^{\mathcal{Y}_f} \underbrace{\int_0^\infty F_Z\left(\frac{\phi_1(\mathcal{I} + 1)}{\eta(1 - \beta)\rho y}\right) f_Y(y) dy}_{I_1} f_{\mathcal{Y}_f}(r_1) dr_1 f_{\mathcal{Y}_f}(r_2) dr_2. \quad (2.23)$$

Consider  $Q = \frac{\phi_1}{\eta(1 - \beta)\rho_f}$  and replacing the upper integral of  $I_1$  to be B and take the limit as  $B \rightarrow \infty$ . Applying G-C Quadrature to find the approximation of  $I_1$  as

$$I_1 \approx 1 - \lim_{B \rightarrow \infty} \frac{\pi B}{2N} \sum_{n=1}^N \frac{(1 + r_2^{\alpha_f})}{(1 + r_2^{\alpha_f} \sigma_e^2)} \left( e^{-\frac{2(1+r_{12}^{\alpha_f})Q}{(1+r_{12}^{\alpha_f} \sigma_e^2)(1+\theta_n)B}} \right) \times \\ \mathcal{L}_{I_p}[s_p] e^{-\frac{(1+r_2^{\alpha_f})(1+\theta_n)B}{2(1+r_2^{\alpha_f} \sigma_e^2)}} (1 - \theta_n^2)^{\frac{1}{2}}, \quad (2.24)$$

where  $s_p = \frac{2(1+r_{12}^{\alpha_f})Q}{(1+r_{12}^{\alpha_f} \sigma_e^2)(1+\theta_n)B}$ ,  $\theta_n = \cos\left(\frac{2n-1}{2N}\right) \pi$ . Substituting the value of  $I_1$  in (2.23), applying  $f_{\mathcal{Y}_f}(r_1) = \frac{2r_1}{\mathcal{Y}_f^2}$ ,  $f_{\mathcal{Y}_f}(r_2) = \frac{2r_2}{\mathcal{Y}_f^2}$  and approximating the distance as  $r_{12} \approx r_1$ ,  $\Theta_{22}$  is given as

$$\Theta_{22} = 1 - \lim_{B \rightarrow \infty} \frac{2\pi B}{N\mathcal{Y}_f^4} \sum_{n=1}^N (1 - \theta_n^2)^{\frac{1}{2}} \underbrace{\int_0^{\mathcal{Y}_f} \frac{(1 + r_2^\alpha)}{(1 + r_2^\alpha \sigma_e^2)} e^{-\frac{(1+r_2^\alpha)K_n}{(1+r_2^\alpha \sigma_e^2)}} r_2 dr_2}_{I_2} \times \\ \underbrace{\int_0^{\mathcal{Y}_f} \left( e^{-\frac{(1+r_1^{\alpha_f})Q}{(1+r_1^{\alpha_f} \sigma_e^2)K_n}} \right) \mathcal{L}_{I_p}[s_p] r_1 dr_1}_{I_3} \quad (2.25)$$

where  $K_n = \frac{(1+\theta_n)B}{2}$ ,  $s_m = \frac{(1+r_1^{\alpha_f})Q_1\rho_m}{(1+r_1^{\alpha_f} \sigma_e^2)K_n}$ ,  $s_f = \frac{(1+r_1^{\alpha_f})Q_1\rho_f}{(1+r_1^{\alpha_f} \sigma_e^2)K_n}$ . After solving for  $I_2$  and applying G-C quadrature to get approximation of  $I_3$ . The expression of  $\Theta_{22}$  is given

as

$$\Theta_{22} = 1 - \lim_{B \rightarrow \infty} \frac{\pi^2 B}{\alpha^2 N M \mathcal{Y}_f^3} \sum_{n=1}^N (1 - \theta_n^2)^{\frac{1}{2}} \frac{e^{-K_n}}{K_n^{1+\frac{2}{\alpha}}} \left( (2 + \alpha K_n) \Gamma\left(\frac{2}{\alpha}\right) - \alpha K_n \Gamma\left(\frac{2}{\alpha}, \mathcal{Y}_f^\alpha K_n\right) \right) \sum_{m=1}^M b_m e^{-\frac{c_m Q_1}{(1+c_m \sigma_e^2) K_n}} - \alpha \Gamma\left(\frac{2+\alpha}{\alpha}, \mathcal{Y}_f^\alpha K_n\right) \mathcal{L}_{I_p} \left[ \frac{d_m Q \rho_m}{(1+d_m \sigma_e^2) K_n} \right], \quad (2.26)$$

where  $c_m = 1 + \left( (1 + \varphi_m) \frac{\mathcal{Y}_f}{2} \right)^\alpha$ ,  $d_m = 1 + (1 + \varphi_m) \frac{\mathcal{Y}_f}{2}$ ,  $\varphi_m = \cos\left(\frac{2m-1}{2M}\pi\right)$  and  $M$  is the complex accuracy trade-off parameter. After substituting  $\Theta_{21}$  and  $\Theta_{22}$  from (2.21) and (2.26) into (2.20), respectively to get  $\Theta_2$ . Then, substituting for  $\Theta_1$  and  $\Theta_2$  in (2.16) to get closed form expression for outage probability of CEU as given in (2.17).

### 2.3.3 System Throughput

To obtain overall system performance the throughput of the system is evaluated. The system throughput, based on the outage probability of the CCU and the CEU at fixed target rates, is given as

$$T_{sys} = (1 - P_{out}^{cc}) R_1 + (1 - P_{out}^{ce}) R_2, \quad (2.27)$$

where  $P_{out}^{cc}$  and  $P_{out}^{ce}$  is obtained from (2.11) and (2.17).

### 2.3.4 Proportional Fairness Index

In NOMA, since the total transmit power is split between users with different channel gains, the users may achieve different performance such that one user have better performance than the other [128]. Therefore, user fairness becomes important consideration in NOMA. It is desired that the performance gap between the users should not increase and user fairness be maintained. The proportional fairness (PF) index is used to compare users' performances based on the outage probability. In case if the fairness is not maintained, one of the users may have higher outage probability than the other. To alleviate this unfairness, PF index for outage probability is defined [129]

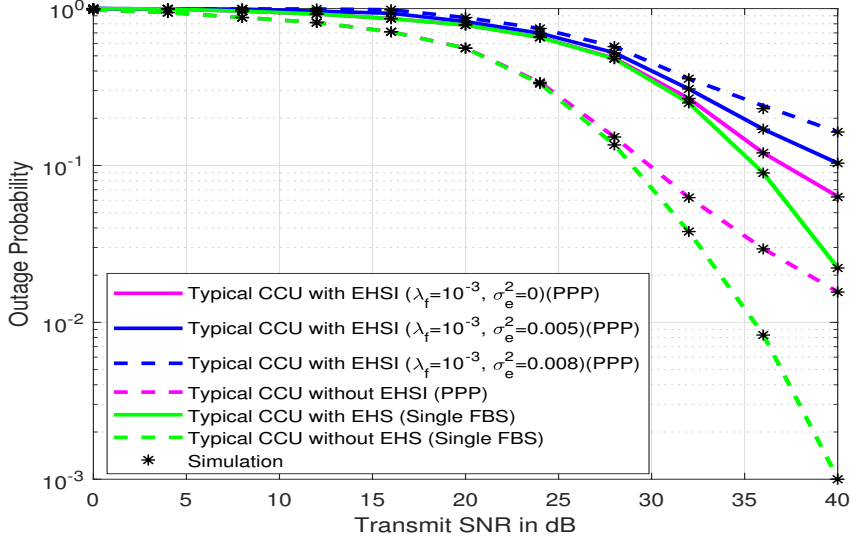


Figure 2.2: Variation of outage probability at the CCU with transmit SNR.

$$PF = \frac{P_{out}^{cc}}{P_{out}^{ce}}, \quad (2.28)$$

The expressions for  $P_{out}^{cc}$  and  $P_{out}^{ce}$  can be obtained from (10) and (13). We observe that the optimum value for PF can be considered as 1 which means that both user have exactly the same outage probability.

## 2.4 Results and Discussions

This section discusses the numerical results based on the derived expressions for the outage probability and system throughput obtained in Section IV for the proposed system model. The analytical results are validated using Monte Carlo simulation for an ensemble of  $10^5$ . Parameters for the numerical results are considered as  $\eta=0.7$ ,  $\beta=0.5$ ,  $N=10$ ,  $M=10$ ,  $B=1000$ , and the network parameters for the analytical plots and the simulation plots are given as [1]  $P_m = 40\text{W}$ ,  $P_f = 1\text{W}$ ,  $\lambda_m = 10^{-4}\text{m}^{-2}$ ,  $\lambda_f = 10^{-3}\text{m}^{-2}$ ,  $\mathcal{Y}_m = 1\text{km}$ ,  $\mathcal{Y}_f = 5\text{m}$ ,  $a_1 = 0.8$ ,  $a_2 = 0.2$ ,  $\alpha_f = 4$  and  $\alpha_m = 3$ . The channel estimation error variance  $\sigma_e^2$  is assumed to take the values 0.005 and 0.008. For comparison, to plot the rate outage probability based on perfect CSI, the channel estimation variance is considered as  $\sigma_e^2 = 0$ . For analysis, the transmit SNR at the FBS tier is varied from 0 to 40dB, while, comparisons are performed at a transmit SNR of 36dB. In this chapter, EHSI-PPP refers to the proposed

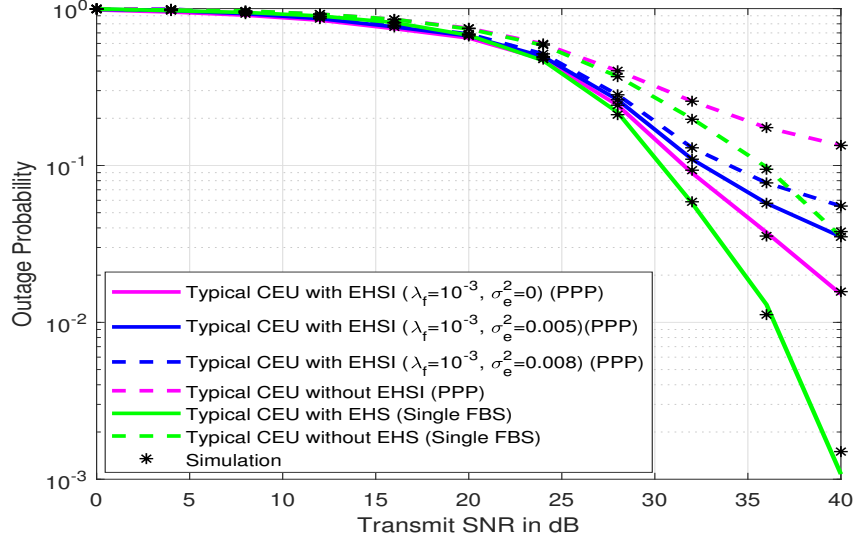


Figure 2.3: Variation of outage probability at the CEU with transmit SNR.

system model in which the CCU performs EH using the superimposed signal and the aggregate co-tier and cross-tier interference. Further, it indicates that the BSs follow PPP distribution. EHS-SBS refers to the system wherein the CCU performs EH using only the superimposed signal and the network contains a single FBS as in [2]. EHS-PPP refers to the system wherein the CCU performs EH using only the superimposed signal and the distribution of BSs follow PPP assumptions. Furthermore, the systems without EHSI-PPP, without EHS-PPP and without EHS-PPP are the cooperative NOMA systems that do not perform EH as considered in [79].

Fig. 2.2 shows the outage probability of the CCU versus transmit SNR plot. A degradation of 89.37% in the outage performance of CCU with EHS-SBS compared with the CCU without EHS-SBS is observed. The reason for the observed degradation is because the CCU with EHS-SBS dedicates only a part of the energy for information decoding and only half of its time block is used for cooperative transmission. For the same reason, the outage probability of the CCU with EHSI-PPP achieves degradation of 75.56% when compared with the outage probability of the CCU without EHSI-PPP. The CCU with EHS-SBS achieves better outage performance by 25.52% as compared to the CCU with EHSI-PPP. The reason is that the CCU with EHSI-PPP suffers from co-tier and cross-tier interference. However, no interference is experienced at the CCU with EHS-SBS since only a single BS is

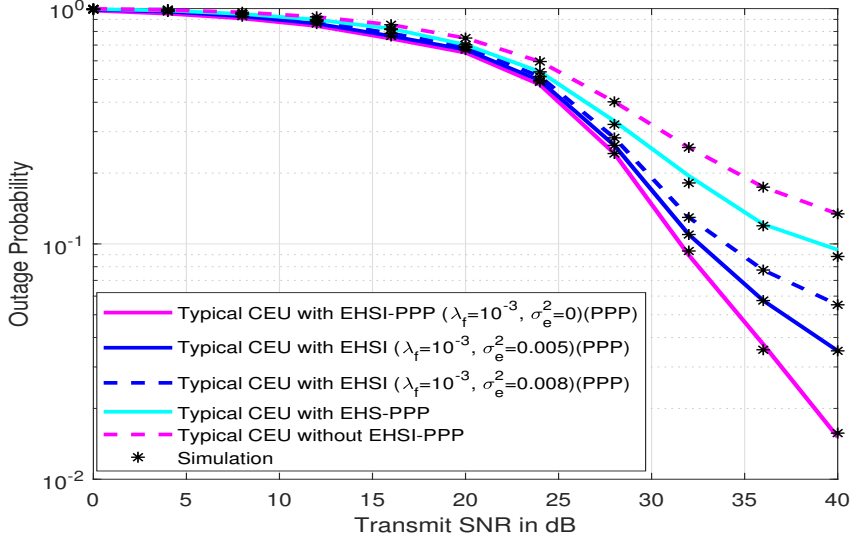


Figure 2.4: Comparison of proposed EHSI-PPP system with EHS-PPP system.

considered for the analysis.

Fig. 2.3 shows the plot for the outage probability of the CEU versus transmit SNR. It can be inferred that an improvement of 88.16% is achieved in the outage performance of CEU with EHS-SBS as compared to that achieved at the CEU without EHS-SBS. The reason being that the CEU with EHS-SBS detects its signal using SC from both phases, while, the CEU without EHS-SBS receives signal only from the direct phase. For the same reason, the outage performance of the CEU with EHSI-PPP achieves an improvement of 79.63% when compared with CEU without EHSI-PPP. The CEU with EHS-SBS achieves better outage performance by 68.45% as compared to the CEU with EHSI-PPP. It can be seen from Fig. 2.2 and Fig. 2.3 that imperfect CSI deteriorates the outage probability as compared to perfect CSI. This is because the channel estimation error acts as a source of interference, thus causing degradation in the outage probability. However, the complexity of the system can be reduced using imperfect CSI at the cost of increased outage probability. Also, a further degradation in the outage probability can be observed with the increase in error variance from 0.005 to 0.008. The error variance indicates the quality of channel estimation.

In Fig. 2.4, the outage performance of CEU with EHS-PPP shows an improvement of 31.49% as compared with the system without EHS-PPP. Also, the outage performance of the proposed CEU with EHSI-PPP shows an improvement of 79.63%

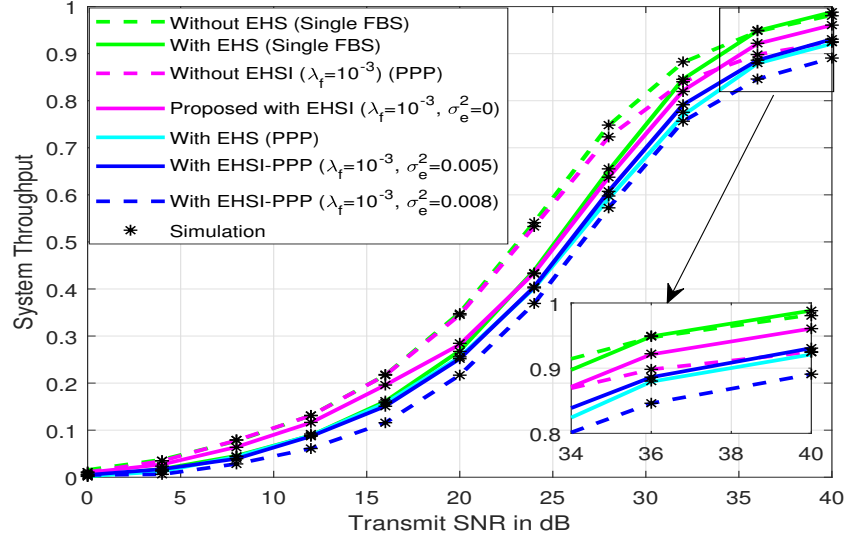


Figure 2.5: System throughput versus transmit SNR for the target rates  $R_1=0.5$  and  $R_2=0.5$

as compared with the system without EHSI-PPP. The outage performance of the CEU with the proposed EHSI-PPP achieves an improvement of 70.27% as compared to the CEU with EHS-PPP.

To obtain the overall system performance, the throughput of the system is obtained as shown in Fig. 2.5. As can be observed from Fig. 2.5 that at low values of the transmit SNR, the system without EH performs better in terms of throughput as compared to the system with EH. This is because at low transmit SNR, degradation in the outage performance of the CCU dominates the improvement in the outage performance of the CEU. Also, the amount of harvested energy is proportional to the transmit SNR. Therefore, at low values of the transmit SNR the harvested power for cooperation is also lower. At high values of transmit SNR, the outage performance of the EH-enabled system surpasses the system without EH. The throughput performance of the proposed system with EHSI-PPP enabled at the CCU achieves better performance as compared to the system with EHS-PPP.

Fig. 2.6 shows the comparison of user PF index between the systems, without EHS-SBS, without EHSI-PPP, with EHS-SBS, with EHS-PPP, and EHSI-PPP, for the same parameter values as for the outage probabilities with the target rates of  $R_1 = R_2 = 0.5$ . It can be seen from Fig. 2.6 that the proposed system with EHSI-PPP provides better user fairness than all other systems except for the system with

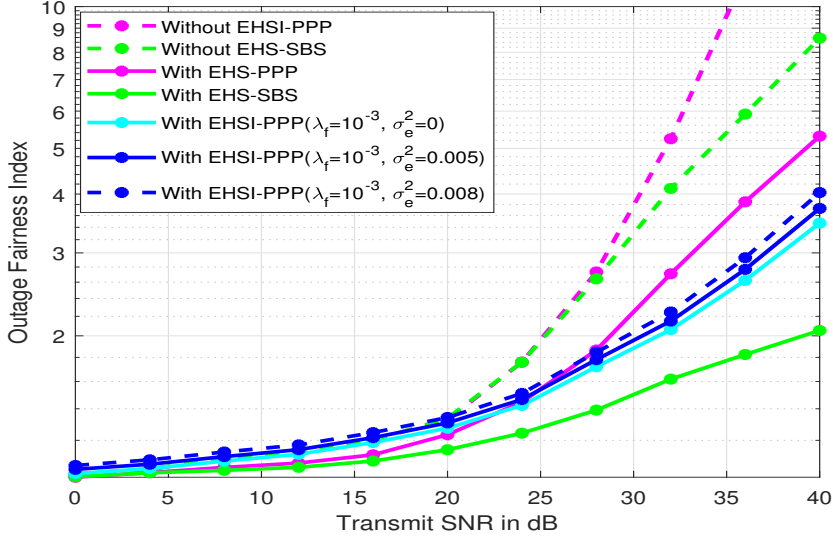


Figure 2.6: Proportional fairness (PF) index versus transmit SNR.

EHS-SBS. The CCU has outage probability closer to the CEU for the systems, with EHS-SBS, with-EHS-PPP, and EHSI-PPP. Hence the PF index is less than 2, till the transmit SNR of 28dB. The systems, without EHS-SBS and without EHSI-PPP have the most significant difference between the outage probabilities of users, this is because the outage probability at the CEU in a non-SWIPT system depends only on the transmission from one of the two phases. However, in the SWIPT enabled systems the CEU combines the SINR from both transmission phases.

## 2.5 Summary

This chapter investigates the application of SWIPT in a PPP-distributed two-tier downlink cooperative NOMA network with imperfect CSI. Closed-form expressions in terms of outage probability and system throughput have been derived at the CCU and the CEU. It is observed that the CCU with EHSI-PPP suffers degradation in outage probability. Further, the outage performance of the CEU experiences significant improvement by employing cooperation from the CCU. The throughput analysis also highlights that the performance of the proposed system with EHSI-PPP surpasses a cooperative NOMA system without EHSI-PPP at high transmit SNR. The PF index plot shows that the system with EHSI-PPP achieves a better user PF index than all other systems except for the system with EHS-SBS.

# Chapter 3

## SWIPT Enabled Heterogeneous Networks with NOMA and Carrier Sensing

In the previous chapter, PPP is commonly used to model location of MBSs and SBSs. PPP assumes that the locations of the BSs are independent and hence uncorrelated. This assumption is true for the BSs locations in random wireless networks with high BSs density and also for the networks where BSs access channel independently such as in ALOHA [83]. However, need for models with practical BSs distribution are desired. The random distribution of SBSs makes the channel access strategies troublesome [130]. Dearth of planning between the BSs' channel access leads to performance degradation [131]. The problem can be rectified by employing a suitable MAC protocol. One possible solution is to employ carrier sensing to manage interference at the SBS tier such that the SBS transmission does not use the channel that is already being accessed by other SBS. Carrier sensing prevents the transmission of SBSs using the same channel simultaneously.

Carrier sensing maintains a region around the SBS, known as exclusion region where no additional SBSs are granted transmission. The radius of the exclusion region is known as contention radius (CR) which can be thought of as a minimum distance between the two transmitting SBS. This implies correlation between the SBSs' location as encountered in scenarios with practical deployment. To model the dependence of SBSs', PPP modeling is not accurate [65], thus the repulsive point

process (RPP), for e.g., HCPP, with a hard core parameter (HCP), is used to model the formation of exclusion region around SBSs.

### 3.1 Motivation and Contribution

In NOMA, one of the most popular technique for user pairing is based on users' channel condition [132], where a user with a good channel condition is termed as CCU, and the user with a poor channel condition is called as cell edge user CEU [1]. Although, NOMA is more spectrally efficient than OMA, pairing CCU and CEU together results in degradation of performance at the CEU due to power splitting [128]. Thus, to improve performance at CEU, a cooperative NOMA scheme is proposed in [79]. The basic idea of cooperative NOMA is to make CCU act as relays to help the CEU with poor channel condition. The underlying principle of cooperative NOMA systems is that CCU performs SIC to remove the message of CEU thereby it has the information of CEU's message too. Therefore, the knowledge of CEU's message at the CCU can be exploited to improve reliability at the CEU [1]. CCU is considered as a DF relay that forwards information to CEU. However, relaying drains the CCU battery [2]. In this chapter, to maintain energy levels, CCU harvests energy from the RF signal using SWIPT. However, unlike performing EH from only the superimposed signal [2], this chapter utilizes the interference, which is lying latent in the RF environment, from the SBSs and MBSs to harvest energy at the CCU along with EH from the superimposed signal. In this chapter, the aforementioned concepts of NOMA and SWIPT are combined to attain performance enhancement at the CEU. Main contributions of the chapter are highlighted below:

- An analytical framework is proposed for a two-tier HetNet, where SBS tier is enabled with NOMA for power splitting, to improve reliability at the CEU using cooperation from the CCU. SBS tier also utilizes carrier sensing for managing the co-tier interference.
- The CCUs are enabled with SWIPT to prevent their battery from draining while performing cooperation. Unlike the existing works, the CCU performs EH using the superimposed signal and the aggregate co-tier and cross-tier interference (EHSI).

- Closed-form expressions for the outage probability at the CCU and the CEU are derived using the proposed EH at the CCU. To obtain the overall system performance, the throughput and energy efficiency of the system are analyzed.
- Comparison of outage probability plots for the CCU and CEU both with and without SWIPT is shown. Furthermore, the proposed system with EHSI is compared with the scenario when EH is performed using the superimposed signal (EHS) only, and new system insights are drawn.

## 3.2 System Model

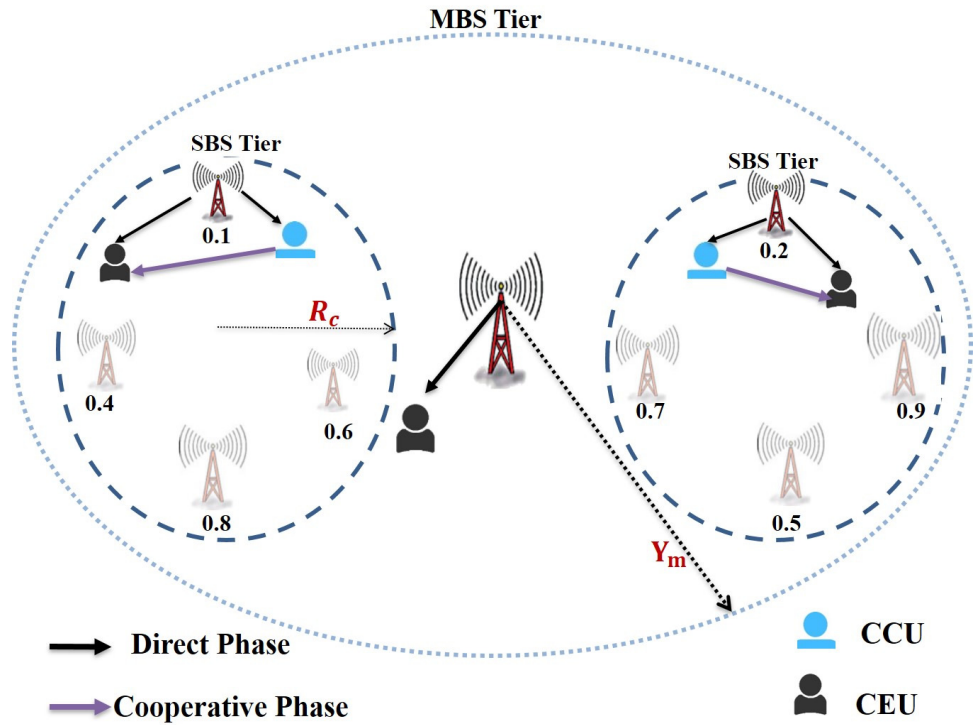


Figure 3.1: Illustration of a downlink cooperative NOMA-SWIPT system model with a tagged SBS and a NOMA user pair in a multi-tier scenario. The spatial distributions of the SBS follow marked PPP assumption.

The proposed system model considers a two-tier heterogeneous network comprising of MBS tier under-laid with SBS tier. The locations of MBS follow independent homogeneous PPP model denoted by  $\Omega_m$  with densities  $\lambda_m$ . The distribution of SBSs follow marked PPP denoted by  $\Omega_s = \{(x_i^s, p_i^s); i = 1, 2, 3, \dots\}$ , where the points  $\Omega = \{x_i^s; i = 1, 2, 3, \dots\}$  construct a PPP with density  $\lambda_s$  in  $\mathbb{R}^2$ , and the time marks  $\{p_i^s; i = 1, 2, 3, \dots\}$  are uniformly distributed in the range  $[0, 1]$ . The time marks

are independent of each other as well as independent from  $\Omega$ . The transmit power of MBS and SBS is denoted as  $P_m$  and  $P_s$ , with coverage range, denoted as  $\mathcal{Y}_m$  and  $\mathcal{Y}_s$  respectively.  $\Omega$  denotes the spatial distribution of all the potential SBSs. The analysis is carried out at a NOMA pair inside SBS tier, wherein the CCU and CEU are paired by the SBS based on their channel condition. In the direct phase of transmission, the proposed model considers a NOMA downlink transmission in which SBS transmits the signal to both CCU and CEU. In the cooperative phase of the transmission, CCU acts as energy harvesting DF relay to forward information to CEU as shown in Fig. 3.1. In the literature, the energy efficiency analysis is based on the simple linear energy harvesting model. In practical systems, there is a non-linear relationship between the received signal power and the harvested energy. Moreover, after a certain received power level, the energy harvester reaches power saturation, which limits the harvested energy [133]. Fading between the links is Rayleigh distributed, hence the power is distributed exponentially with unity variance. The bounded path-loss model assumes that the received power is proportional to  $(1 + r_k^\alpha)^{-1}$ , where  $r_k$  denotes the Euclidean distance between the SBS and the  $k^{th}$  user, and  $\alpha$  is the path-loss exponent. Therefore, the total channel power gain can be expressed as  $h_k(1 + r_k^\alpha)^{-1}$ , where  $h_k$  denotes the channel power gain between the SBS and the  $k^{th}$  user.

### 3.2.1 SINR at CCU and CEU

Let the two users, to be served using NOMA, are selected using random selection scheme [2]. Their channel gains are ordered as  $h_1 \leq h_2 \leq h_3 \dots$ , and their power allocation coefficients are ordered as  $a_1 \geq a_2 \geq a_3 \dots$ , respectively. Hence for a two user NOMA case, the User-2 with a better channel condition is termed as CCU, and the User-1 with a poorer channel condition is termed as CEU. This work assumes perfect CSI at the BS.

#### Direct Transmission

The SBS sends the signal  $X_s = \sum_{i=1}^2 x_i \sqrt{a_i P_s}$  to user pair based on NOMA transmission, where  $x_i$  is the intended signal for the  $i^{th}$  user such that  $\mathbb{E}[x_i^2] = 1$ , and is

assumed to be equal  $\forall i \in (1, 2)$ . The observation at the  $k^{th}$  typical user is given by

$$Y_k = \sqrt{h_k(1 + r_k^\alpha)^{-1}} X_f + n_k, \quad (3.1)$$

where  $n_k$  is the additive white Gaussian noise (AWGN) at the  $k^{th}$  user. Using the NOMA principle, SIC is carried out at CCU which decodes and removes the CEU's signal to detect its own signal. The received signal to interference and noise ratio (SINR) at CCU to detect message of CEU is expressed as

$$\gamma_{2 \rightarrow 1}^1 = \frac{\beta \rho_s a_1 h_2 (1 + r_2^\alpha)^{-1}}{\beta \rho_s a_2 h_2 (1 + r_2^\alpha)^{-1} + \beta \rho_s \mathcal{I}_s + \beta \rho_m \mathcal{I}_m + 1}, \quad (3.2)$$

where  $\beta$  is the power splitting coefficient and  $\rho_s = P_s / \sigma_s^2$  is the transmit SNR at the user, and  $\rho_m = P_m / \sigma_f^2$ .  $\rho_s \mathcal{I}_s$  denotes co-tier interference from SBS tier such that  $\mathcal{I}_s = \sum_{y \in \Omega_s / \{s_o\}} h_y$ , where  $h_y$  denotes the total channel gain from the  $y^{th}$  SBS to the typical user and  $s_o$  is the tagged SBS. Similarly,  $\rho_m \mathcal{I}_m$  denotes the cross-tier interference from MBS tier such that  $\mathcal{I}_m = \sum_{v \in \Omega_m} h_v$ , where  $h_v$  denotes the total channel gain from  $v^{th}$  MBS to the typical user. Thus, the SINR at the CCU to detect its own message is given as

$$\gamma_2^1 = \frac{\beta \rho_s a_2 h_2 (1 + r_2^\alpha)^{-1}}{\beta \rho_s \mathcal{I}_s + \beta \rho_m \mathcal{I}_m + 1}. \quad (3.3)$$

Here, it is assumed that the CCU have rechargeable battery [103] and, to apply SWIPT PS technique [2] is implemented at the CCU. The received signal power at CCU is divided into two parts. One part is treated for information decoding and another for EH to power the CCU for cooperation. The energy harvested ( $E_2$ ) at CCU from the source and the interference from MBSs and SBSs is given as

$$E_2 = \frac{T}{2} \eta (1 - \beta) (P_s h_2 (1 + r_2^\alpha)^{-1} + P_s \mathcal{I}_s + P_m \mathcal{I}_m), \quad (3.4)$$

where  $\eta$  is the conversion efficiency of the energy harvester. The transmit power from CCU can be expressed as

$$\begin{aligned} P_2 &= \frac{E_2}{\frac{T}{2}} \\ &= \eta(1 - \beta) (P_f |h_2|^2(1 + r_2^\alpha)^{-1} + P_f \mathcal{I}_f + P_m \mathcal{I}_m), \end{aligned} \quad (3.5)$$

where  $P_2$  denotes the harvested power from the energy harvester which is also the transmit power of the CCU. In this chapter, it is assumed that the energy consumed by the cell center user (CCU) for information decoding is negligible as compared to information transmission during the cooperative phase. The use of this assumption is consistent with prior works (which uses power amplifier) [103], [122], [123]. Also, the SINR at the CEU during the first phase of transmission is given by

$$\gamma_1^1 = \frac{\rho_s a_1 h_1 (1 + r_1^\alpha)^{-1}}{\rho_s a_2 h_1 (1 + r_1^\alpha)^{-1} + \rho_s \mathcal{I}'_s + \rho_m \mathcal{I}'_m + 1}. \quad (3.6)$$

### Cooperative Transmission

In the second phase, the CCU forwards the message to the CEU. The received SINR at CEU to detect  $x_1$  forwarded from CCU user is given by

$$\gamma_1^2 = \frac{P_2 g (1 + r_{12}^\alpha)^{-1}}{P_s \mathcal{I}'_s + P_m \mathcal{I}'_m + \sigma_1^2}, \quad (3.7)$$

where  $g(1+r_{12}^\alpha)^{-1}$  is the total channel power gain between CCU and CEU,  $r_{12}$  denotes the distance between the CCU and CEU.  $P_s \mathcal{I}'_s$  denotes co-tier interference from the SBS tier such that  $\mathcal{I}'_s = \sum_{y \in \Omega_s / \{s_o\}} h'_y$ , where  $h'_y$  denotes the total channel gain from the  $y^{th}$  SBS to the CEU and  $s_o$  is the tagged SBS. Similarly,  $\rho_m \mathcal{I}'_m$  denotes the cross-tier interference from the MBS tier such that  $\mathcal{I}'_m = \sum_{v \in \Omega_m} h'_v$ , where  $h'_v$  denotes the total channel gain from  $v^{th}$  MBS to the CEU. The CEU combines the signal from SBS and CCU using SC [124]. SC is used over MRC, since MRC increases the receiver complexity [125]. Even though only one SINR is used in SC the diversity order is same as compared to MRC which coherently combines all SINR especially when the number of links is less than five [126]. Here, SC is performed by taking the maximum of the received SINR of direct phase (3.6) and cooperative phase (3.7).

The received SINR at the CEU is expressed as

$$\gamma_1^{sc} = \max(\gamma_1^1, \gamma_1^2). \quad (3.8)$$

### 3.3 Modeling SBS Tier

In this section, the density of simultaneous transmitting SBSs is derived by applying carrier sensing. The process, which is used here for finding simultaneous transmitters is known as thinning process. The distribution of all SBSs is based on the marked PPP which acts as a parent model. However, the distributions of SBSs that are retained for transmission is based on a hard core point process (HCPP) with hard core parameter  $r_c$ , which is generated by independent thinning of this marked PPP as shown in Fig. 3.1.

To implement contention, the neighborhood set of a generic SBS,  $x_i^s$  contending for accessing the channel, are formed.  $\mathcal{N}_{x_i^s}$  denotes the neighborhood set of generic SBS,  $x_i^s$ . The concept of received signal strength is utilized to determine  $\mathcal{N}_{x_i^s}$ . Mathematically,  $\mathcal{N}_{x_i^s}$  can be written as  $N_{x_i^s} = \{(x_i^s, p_j^s) \in \Omega_s | \gamma(x_i^s, x_j^s) > \mathcal{T}_B\}_{i \neq j}$  where  $\gamma(a, b)$  is the signal-to-noise ratio (SNR) received at node a from node b. This implies that  $N_{x_i^s}$  is the group of SBSs, such that the received SNR at the generic SBS,  $x_i^s$ , from  $x_j^s$  is greater than the BS sensing threshold,  $\mathcal{T}_B$ . The SBS is selected amongst the neighborhood set on the basis of their time marks. The SBS with the lowest time mark amongst all the SBSs in the neighborhood set is retained (qualifies to transmit), as can be seen from Fig. 3.1. This process is analogous to the general carrier sensing multiple access (CSMA) protocol [67], [66]. In agreement with the above consideration, the retaining probability of an SBS is derived, wherein the CR denoted as  $r_c$ , is calculated first. The observation region denoted as  $B_{x_i^s}$ , centered at the SBS  $x_i^s$  of radius  $r_c$ , gives all the SBSs contending for the channel. The CR is considered to be sufficiently large such that the probability of an SBS in the neighborhood of SBS  $x_i^s$  located beyond  $r_c$  is negligible. Mathematically, it can be written as

$$\mathcal{P}\{\rho_s h_{(i,j)}(1 + r_j^\alpha)^{-1} > \mathcal{T}_B | r_j > r_c\} \leq \epsilon, \quad (3.9)$$

where  $\rho_f = P_s/\sigma_s^2$  denotes the transmit SNR of SBS tier,  $\sigma_s^2$  is the noise variance,  $h_{(i,j)}$  denotes the channel power gain between the SBS  $x_i^s$  and  $x_j^s$  in the disc  $B_{x_i^s}$ , and  $r_j$  is the distance of SBS  $x_j^s$  from SBS  $x_i^s$  in the disc  $B_{x_i^s}(r_c)$ . Evaluating probability at  $r_c$ , (3.9) can be rewritten as

$$\mathcal{P}\left\{h_{(i,j)} > \frac{r_c^\alpha \mathcal{T}_B}{\rho_s}\right\} \leq \epsilon, \quad (3.10)$$

Assuming  $X = h_{(i,j)}$  and  $F_X(x)$  as the complementary cumulative distribution function (CCDF) of  $X$ , (3.10) is rewritten as

$$F_X\left(\frac{r_c^\alpha \mathcal{T}_B}{\rho_s}\right) \leq \epsilon. \quad (3.11)$$

By taking inverse on both the sides of (3.11), the CR can be calculated as

$$r_c = \left(\frac{\rho_s}{\mathcal{T}_B} F_X^{-1}(\epsilon)\right)^{\frac{1}{\alpha_s}}, \quad (3.12)$$

where  $F_X^{-1}(\epsilon)$  represents the inverse of the CCDF of  $X$  evaluated at infinitesimal  $\epsilon$ . The neighborhood success probability (NSP) is described as the probability that an SBS  $x_j^f$  satisfies the carrier sensing threshold of  $\mathcal{T}_B$  around SBS  $x_i^s$  and becomes its neighbor. The SBS associated with the lowest time mark acquire the contention and is permitted to access the channel neighboring SBS in  $N_{x_i^s}^s$ . The NSP is calculated using (3.12) as

$$\mathcal{P}_s = \mathcal{P}\{\rho_s X r_j^{-\alpha_s} \geq \mathcal{T}_B | x_j^s \in B_{x_i^s}(r_c)\}. \quad (3.13)$$

On the assumption that the small scale fading is Rayleigh distributed and the large scale fading is based on bounded path loss model, thus (3.13) can be expressed as

$$\mathcal{P}_s = \int_0^1 f(r_j) \left(1 - F_X\left(\frac{r_j^\alpha \mathcal{T}_B}{\rho_s}\right)\right) dr_j + \int_1^{r_c} f(r_j) \left(1 - F_X\left(\frac{r_j^\alpha \mathcal{T}_B}{\rho_s}\right)\right) dr_j, \quad (3.14)$$

where  $f(r_j) = 2r_j/r_c^2$ . Solving (3.14), the NSP can be expressed as

$$\mathcal{P}_s = \frac{1}{r_c^2} e^{-\frac{\mathcal{T}_B}{\rho_s}} + \frac{2 \left( \frac{\mathcal{T}_B}{\rho_s} \right)^{-\frac{2}{\alpha_s}} \Gamma \left( \frac{2}{\alpha_s}, \mathcal{T}_B/\rho_s \right)}{\alpha_s r_c^2} - \frac{2 \left( \left( \mathcal{T}_B/\rho_s \right) r_c^{\alpha_s} \right)^{-\frac{2}{\alpha_s}} \Gamma \left( \frac{2}{\alpha_s}, \mathcal{T}_B/\rho_s \right)}{\alpha_s}, \quad (3.15)$$

where  $\Gamma(a, x)$  is the incomplete gamma function. From [65], the retaining probability for CSMA protocol can be written as  $\mathcal{P}_R = \frac{1-e^{-N_e P_s}}{N_e P_s}$ , where  $N_e = \pi \lambda_s r_c^2$  is the average number of SBS in the observation region  $B_{x_i^s}(r_c)$ , of radius  $r_c$ , centered at  $x_i^s$ . The intensity of active number of transmitting SBS using carrier sensing is given by  $\lambda_s^R = \lambda_s \mathcal{P}_R$ , where  $\lambda_s$  is the intensity of the PPP distributed SBS without carrier sensing. This means that the intensity of simultaneously transmitting SBS under the applied carrier sensing is reduced by  $\mathcal{P}_R$  ( $0 \leq \mathcal{P}_R \leq 1$ ). For example Fig. 10(a) in [65] shows the effect of intensity of primary PPP versus the intensity of simultaneous active transmitters. The figure shows that the RPP reduces the intensity of the primary PPP by 30%. This decreases the co-tier interference at the CCU and the CEU but also reduces the harvested power at the CCU. Due to the decrease in the intensity from (3.5) the term  $\mathcal{I}_s$  decreases which decreases the amount of harvested power at the CCU.

## 3.4 Performance Analysis

### 3.4.1 Outage probability at CCU

The outage probability of CCU relies on the efficient SIC of the signal for CEU. The outage probability at the CCU can occur in two ways: first when CCU is unable to decode the message of CEU and secondly when CCU decodes the message of CEU, however is unable to decode its own message. Therefore, the outage probability at CCU is calculated as

$$P_{out}^{cc} = \mathcal{P}(\gamma_{2 \rightarrow 1}^1 < \phi_1) + \mathcal{P}(\gamma_{2 \rightarrow 1}^1 \geq \phi_1, \gamma_2^1 < \phi_2), \quad (3.16)$$

where  $\phi_1 = 2^{2R_1} - 1$  and  $\phi_2 = 2^{2R_2} - 1$ , with  $R_1$  and  $R_2$  being the target rate to detect the message of CCU and CEU.

**Proposition 1**

The outage probability of the CCU based on PPP assumptions is given as

$$P_{out}^{cc} = \frac{1}{2} \sum_{n=0}^N b_n e^{-c_n \epsilon_1} \mathcal{L}_{I_m}[s_m] e^{\mu_s}, \quad (3.17)$$

where  $\mu_s = \mathbb{E}_{\Omega_s} \left[ -\sum_{v \in \Omega_s} \ln(1 + s_s r_v^\alpha) \right]$ ,  $s_s = \rho_s \epsilon_1 c_n$ ,  $s_m = \rho_m \epsilon_1 c_n$ ,  $\epsilon_1 = \frac{\phi_1}{\beta \rho_s (a_1 - \phi_1 a_2)}$  and  $\epsilon_2 = \frac{\phi_2}{\beta \rho_s a_2}$ ,  $b_n = -\omega_N (1 + \theta_n) \sqrt{1 - \theta_n^2}$ ,  $b_0 = -\sum_1^N b_n$ ,  $\omega_N = \pi/N$ ,  $\theta_n = \cos\left(\frac{2n-1}{2N}\pi\right)$ ,  $c_n = 1 + \left(\frac{\mathcal{Y}_s}{2}\theta_n + \frac{\mathcal{Y}_s}{2}\right)^\alpha$ ,  $c_0 = 0$ ,  $N$  is complexity-accuracy trade-off parameter for the Gaussian-Chebyshev (G-C) quadrature.  $\mathcal{L}_{I_m}(s)$  in (3.17), corresponds to the Laplace of cross-tier interference from MBS tier and  $e^{\mu_s}$  term correspond to co-tier interference from SBS tier. The Laplace transform of interference by the  $t^{th}$  tier is calculated [134] as

$$\mathcal{L}_{I_t}(s) = e^{\pi \lambda_t (s^{\delta_t} \Gamma(1 - \delta_t, s) - s^{\delta_t} \Gamma(1 - \delta_t))}, \quad (3.18)$$

where  $\delta_t = \frac{2}{\alpha_t}$ , and  $\Gamma(z)$  is the gamma function.

$$\mu_s = \frac{-\lambda_s^R}{\alpha'} r_g^{-\alpha'} (\alpha_s s F(r_g, \alpha) - \alpha' K), \quad (3.19)$$

where  $K = r_g^\alpha \ln(s_s r_g^{-\alpha} + 1)$ ,  $F(r_g, \alpha_s) = {}_2F_1\left(1, \frac{\alpha'}{\alpha_s}; 2 - \frac{1}{\alpha_s}; -s_s r_g^{-\alpha_s}\right)$  is the hypergeometric function and  $\alpha' = \alpha_s - 1$ .

*Proof:* Let the channel gain be denoted as  $X = h_1(1+r_1^\alpha)^{-1}$ ,  $Y = h_2(1+r_2^\alpha)^{-1}$ , and  $Z = h_{12}(1+r_{12}^\alpha)^{-1}$ . The probability density function (PDF) of the random variables  $X$ ,  $Y$ , and  $Z$  are expressed as  $f_X(x) = (1+r_1^\alpha)^{-1} e^{-(1+r_1^\alpha)x}$ ,  $f_Y(y) = (1+r_2^\alpha)^{-1} e^{-(1+r_2^\alpha)y}$ , and  $f_Z(z) = (1+r_{12}^\alpha)^{-1} e^{-(1+r_{12}^\alpha)z}$ . Also,  $r_1$  is the distance of CEU from SBS,  $r_2$  is the distance of the CCU from SBS and  $r_{12}$  is the distance of CEU from CCU. The cumulative distribution function (CDF) of channel gain  $Y$  can be expressed as

$$F_Y(y) = \frac{2}{\mathcal{Y}_f^2} \int_0^{\mathcal{Y}_s} \left(1 - e^{-(1+r_2^\alpha)y}\right) r_2 dr_2. \quad (3.20)$$

Applying G-C quadrature [127], CDF can be approximated as

$$F_Y(y) \approx \frac{1}{2} \sum_{n=0}^N b_n e^{-c_n y}. \quad (3.21)$$

(3.16) can be rewritten in terms of random variable  $Y$  as

$$P_{out}^{cc} = \mathcal{P}(Y < \epsilon_1) + \mathcal{P}(Y \geq \epsilon_1, Y < \epsilon_2). \quad (3.22)$$

Second part of (3.22) gives outage for condition  $\epsilon_1 < \epsilon_2$ . Thus, for the case when  $\epsilon_1 \geq \epsilon_2$ , the outage probability is given by the CDF of  $Y$  with  $y = \epsilon_1(1 + \beta\rho_s\mathcal{I}_s + \beta\rho_m\mathcal{I}_m)$ , and substituting  $y$  in (3.21) to get

$$\begin{aligned} P_{out}^{cc} &= \frac{1}{2} \sum_{n=0}^N b_n e^{-c_n \epsilon_1} \mathbb{E}[s_m I_m] \mathbb{E}[s_s I_s] \\ &= \frac{1}{2} \sum_{n=0}^N b_n e^{-c_n \epsilon_1} \mathcal{L}_{I_m}[s_m] \mathcal{F}_I, \end{aligned} \quad (3.23)$$

where  $\mathbb{E}[s_m I_m] = \mathcal{L}_{I_m}[s_m]$  and  $\mathbb{E}[s_s I_s] = \mathcal{F}_I$ . Now, we evaluate the co-tier interference at the typical user from SBS tier applying similar steps as in [135].

$$\begin{aligned} \mathcal{F}_I &= \mathbb{E}[s_s I_s] \\ &\stackrel{(a)}{=} \mathbb{E}_{\mathcal{I}_s} \left[ e^{-s_s \sum_{\nu \in \Omega_f^R} h_\nu r_\nu^{-\alpha_s}} \right] \\ &= \mathbb{E}_{\Omega_s^R} \left[ \prod_{\nu \in \Omega_s^R} \mathbb{E} \left[ e^{-s_s \sum_{\nu \in \Omega_s^R} h_\nu r_\nu^{-\alpha_s}} \right] \right] \\ &= \mathbb{E}_{\Omega_s^R} \left[ e^{-\sum_{\Omega_s^R} \ln \left( 1 + s_s r_\nu^{-\alpha_s} \right)} \right] \\ &\geq e^{\mathbb{E}_{\Omega_s^R} \left[ -\sum_{\Omega_s^R} \ln \left( 1 + s_s r_\nu^{-\alpha_s} \right) \right]} \end{aligned} \quad (3.24)$$

where (a) comes after the consideration of a guard zone around receiving nodes  $r_g > 1$ , therefore, the bounded path loss model is scaled down to  $r_\nu^{-\alpha_s}$  for the evaluation of interference, where  $r_\nu$  is the distance between the typical FU to the  $\nu^{th}$  SBS and (3.24) comes from Jensen's inequality. Let  $\mu_s = \mathbb{E}_{\Omega_s^R} \left[ -\sum_{\Omega_s^R} \ln \left( 1 + s_m^s r_\nu^{-\alpha_s} \right) \right]$ . Using Campbell's theorem [37], we can rewrite  $\mu_s$  as

$$\begin{aligned} \mu_s &= \mathbb{E}_{\Omega_s^R} \left[ -\sum_{\Omega_s^R} \ln \left( 1 + s_s r_\nu^{-\alpha_s} \right) \right] \\ &= \int_{r_g}^{\infty} -\lambda_s^R \ln \left( 1 + s_s r_\nu^{-\alpha_s} \right) dr_\nu \\ &= \frac{-\lambda_s^R}{\alpha'} r_g^{-\alpha'} \left( \alpha_s F(r_g, \alpha) - \alpha' r_g^{\alpha_s} \ln \left( 1 + s_s r_\nu^{-\alpha_s} \right) \right) \end{aligned} \quad (3.25)$$

From (3.25) and (3.24),  $\mathcal{F}_I = e^{\mu_s}$ . Substituting  $\mathcal{F}_I$  in (3.23) to get (3.17).

Proposition 1 derives the outage probability at the CCU when the CCU harvests energy from the superimposed signal transmitted by the SBS using NOMA principle and the aggregate co-tier and cross tier interference. The outage probability at the CCU in (3.17) depends upon, the power splitting ratio  $\beta$ , the co-tier interference from the SBS tier, and the cross tier interference from the MBS tier. The outage probability decreases as  $\beta$  varies from 0 to 1. We observe this by considering two extreme cases of  $\beta = 0$  and  $\beta = 1$ .  $\beta = 0$  means that the total received power at the CCU is used for EH and no power left for information decoding which results in outage at the CCU, where as  $\beta = 1$  signifies that the total power at the CCU is used for information decoding and no power is left for EH which improves outage and hence decreases the outage probability. Co-tier interference at the CCU decreases on increasing the intensity of the SBS  $\lambda_s$  which also reduces the outage probability at the CCU. This is due to removal of dominant interferers under the applied carrier sensing. On the contrary cross-tier interference at the CCU depends upon the intensity of the MBS  $\lambda_m$  and increases with increase in  $\lambda_m$ . The outage probability at the CCU also increases with increase in  $\lambda_m$ .

### 3.4.2 Outage Probability at CEU

The outage probability at the CEU can occur in two ways, firstly when neither the CCU nor the CEU can detect message of the CEU, and secondly when the CCU can detect message of the CEU but the CEU is unable to decode its message by using SC scheme. Therefore, the outage probability at the CEU can be expressed as

$$P_{out}^{ce} = \underbrace{\mathcal{P}(\gamma_{2 \rightarrow 1}^1 < \phi_1, \gamma_1^1 < \phi_1)}_{\Theta_1} + \underbrace{\mathcal{P}(\gamma_{2 \rightarrow 1}^1 > \phi_1, \gamma_1^{sc} < \phi_1)}_{\Theta_2}. \quad (3.26)$$

*Proposition 2:* The outage probability at the CEU, based on RPP assumption

of the SBS tier and PPP assumption of MBS tier, is expressed in (3.27).

$$\begin{aligned}
 P_{out}^{ce} &= \frac{1}{4} \sum_{n=0}^N \sum_{k=0}^K b_n b_k e^{-(c_n+c_k)\epsilon_1} \mathcal{L}_{I_m}[s_m I_m] \mathcal{L}'_{I_m}[s_m I_m] e^{\mu_s} e^{\mu'_s} + \frac{1}{2} \sum_{n=0}^N b_n e^{-c_n \epsilon_1} \times \\
 &\mathcal{L}_{I_m}[s_m] e^{\mu_s} \left( 1 - \lim_{B \rightarrow \infty} \frac{\pi^2 B}{\alpha^2 N M \mathcal{Y}_s^3} \sum_{n=1}^N (1 - \theta_n^2)^{\frac{1}{2}} \frac{e^{-K_n}}{K_n^{1+\frac{2}{\alpha}}} \left( (2 + \alpha K_n) \Gamma\left(\frac{2}{\alpha}\right) \right. \right. \\
 &\left. \left. - \alpha K_n \Gamma\left(\frac{2}{\alpha}, \mathcal{Y}_s^\alpha K_n\right) \sum_{m=1}^M b_m e^{-\frac{c_m^\alpha Q_1}{K_n}} - \alpha \Gamma\left(\frac{2+\alpha}{\alpha}, \mathcal{Y}_f^\alpha K_n\right) \right) \mathcal{L}_{I_m}\left[\frac{d_m Q \rho_m}{K_n}\right] \times \right. \\
 &\left. e^{-\frac{\lambda_s^R}{\alpha'} r_g^{-\alpha} \left( \alpha \left( \frac{d_m Q \rho_f}{K_n} \right) F(r_g, \alpha) - \alpha' r_g^\alpha \ln \left( 1 + \left( \frac{d_m Q \rho_f}{K_n} \right) r_g^{-\alpha} \right) \right)} \right) \quad (3.27)
 \end{aligned}$$

*Proof:* Let the first and the second term of (3.26) be denoted as  $\Theta_1$  and  $\Theta_2$ . The terms of  $\Theta_1$  are independent. Therefore,  $\Theta_1$  can be obtained as

$$\Theta_1 = \mathcal{P}(\gamma_{2 \rightarrow 1}^1 < \phi_1) \mathcal{P}(\gamma_1^1 < \phi_1), \quad (3.28)$$

$\mathcal{P}(\gamma_{2 \rightarrow 1}^1 < \phi_1)$  is given by (3.17) and the analysis for  $\mathcal{P}(\gamma_1^1 < \phi_1)$  is carried in the same manner, i.e., by assuming the channel gain  $X = h_1(1 + r_1^\alpha)^{-1}$  and following the same steps as in the Appendix A. The expression of  $\Theta_1$ , is given as

$$\Theta_1 = \frac{1}{4} \sum_{n=0}^N \sum_{k=0}^K b_n b_k e^{-(c_n+c_k)\epsilon_1} \mathcal{L}_{I_m}[s_m] \mathcal{L}'_{I_m}[s_m] e^{\mu_s} e^{\mu'_s}, \quad (3.29)$$

where  $\mathcal{L}_{I_m}[s_m]$  and  $\mathcal{L}'_{I_m}[s_m]$  represents the Laplace transform of the interference from MBS tier at CCU and CEU, respectively during the direct phase transmission.  $e^{\mu_s}$  and  $e^{\mu'_s}$  represents the interference from SBS tier at CCU and CEU, respectively during the direct phase transmission.  $\Theta_2$  can be written as

$$\Theta_2 = \underbrace{\mathcal{P}(\gamma_1^1 < \phi_1)}_{\Theta_{21}} \underbrace{\mathcal{P}(\gamma_{2 \rightarrow 1}^1 \geq \phi_1, \gamma_1^2 < \phi_1)}_{\Theta_{22}}, \quad (3.30)$$

The expression for  $\Theta_{21}$  is given in (3.29). Therefore, the expression of  $\Theta_{21}$  is given as

$$\Theta_{21} = \frac{1}{2} \sum_{n=0}^N b_n e^{-c_n \epsilon_1} \mathcal{L}'_{I_m}[s_m] e^{\mu'_s}. \quad (3.31)$$

Considering  $\rho_s \mathcal{I}_s + \rho_m \mathcal{I}_m = \mathcal{I}$ , and  $\epsilon'_1 = \epsilon_1(\beta \mathcal{I} + 1)$ ,  $\Theta_{22}$  can be written from (3.30) as

$$\Theta_{22} = \mathcal{P}\left(Z < \frac{\phi_1(\mathcal{I} + 1)}{\eta(1 - \beta)(\rho y + \mathcal{I})}, Y \geq \epsilon'_1\right). \quad (3.32)$$

Considering high SNR approximation, i.e., assuming  $\rho \rightarrow \infty$ , gives  $\rho y + \mathcal{I} \approx \rho y$  and  $\epsilon'_1 \approx 0$ . Using these approximations  $\Theta_{22}$  can be rewritten as

$$\Theta_{22} = \int_0^{\mathcal{Y}_s} \int_0^{\mathcal{Y}_s} \underbrace{\int_0^\infty F_Z\left(\frac{\phi_1(\mathcal{I} + 1)}{\eta(1 - \beta)\rho y}\right) f_Y(y) dy}_{I_1} \times f_{\mathcal{Y}_s}(r_1) dr_1 f_{\mathcal{Y}_s}(r_2) dr_2. \quad (3.33)$$

Considering  $Q = \frac{\phi_1}{\eta(1 - \beta)\rho}$ , replacing the upper integral of  $I_1$  to be  $B$ , taking the limit as  $B \rightarrow \infty$ , and applying G-C Quadrature,  $I_1$  can be approximated as,

$$I_1 \approx 1 - \lim_{B \rightarrow \infty} \frac{\pi B}{2N} \sum_{n=1}^N (1 + r_2^\alpha) \left( e^{-\frac{2(1+r_2^\alpha)Q}{(1+\theta_n)B}} \right) \mathcal{L}_{I_m}[s_m] \times e^{\mu s} e^{-\frac{(1+r_2^\alpha)(1+\theta_n)B}{2}} (1 - \theta_n^2)^{\frac{1}{2}}, \quad (3.34)$$

where  $s = \frac{2(1+r_{12})Q}{(1+\theta_n)B}$ ,  $\theta_n = \cos\left(\frac{2n-1}{2N}\right)\pi$ . Substituting the value of  $I_1$  in (3.33), applying  $f_{\mathcal{Y}_s}(r_1) = \frac{2r_1}{\mathcal{Y}_s^2}$ ,  $f_{\mathcal{Y}_s}(r_2) = \frac{2r_2}{\mathcal{Y}_s^2}$  and approximating the distance as  $r_{12} \approx r_1$ ,  $\Theta_{22}$  is given as

$$\Theta_{22} = 1 - \lim_{B \rightarrow \infty} \frac{2\pi B}{N\mathcal{Y}_s^4} \sum_{n=1}^N (1 - \theta_n^2)^{\frac{1}{2}} \underbrace{\int_0^{\mathcal{Y}_s} (1 + r_2^\alpha) e^{-(1+r_2^\alpha)K_n} r_2 dr_2}_{I_2} \times \underbrace{\int_0^{\mathcal{Y}_s} \left( e^{-\frac{(1+r_1^\alpha)Q}{K_n}} \right) \mathcal{L}_{I_m}[s_m] e^{\mu} r_1 dr_1}_{I_3}, \quad (3.35)$$

where  $K_n = \frac{(1+\theta_n)B}{2}$ ,  $s_m = \frac{(1+r_1)Q_1\rho_m}{K_n}$ ,  $s_s = \frac{(1+r_1)Q_1\rho_s}{K_n}$ . After solving for  $I_2$  and applying G-C quadrature to get approximation of  $I_3$ , the expression of  $\Theta_{22}$  is given

as

$$\begin{aligned}
 \Theta_{22} = & 1 - \lim_{B \rightarrow \infty} \frac{\pi^2 B}{\alpha^2 N M \mathcal{Y}_s^3} \sum_{n=1}^N (1 - \theta_n^2)^{\frac{1}{2}} \frac{e^{-K_n}}{K_n^{1+\frac{2}{\alpha}}} \times \\
 & \left( (2 + \alpha K_n) \Gamma\left(\frac{2}{\alpha}\right) - \alpha K_n \Gamma\left(\frac{2}{\alpha}, \mathcal{Y}_s^\alpha K_n\right) \sum_{m=1}^M b_m e^{-\frac{c_m^\alpha Q_1}{K_n}} \right. \\
 & \left. - \alpha \Gamma\left(\frac{2 + \alpha}{\alpha}, \mathcal{Y}_f^\alpha K_n\right) \right) \mathcal{L}_{I_m} \left[ \frac{d_m Q \rho_m}{K_n} \right] \times \\
 & e^{-\frac{\lambda_s^R}{\alpha^2} r_g^{-\alpha} \left( \alpha \left( \frac{d_m Q \rho_s}{K_n} \right)^{F(r_g, \alpha)} - \alpha' r_g^\alpha \ln \left( 1 + \left( \frac{d_m Q \rho_f}{K_n} \right) r_g^{-\alpha} \right) \right)}, \tag{3.36}
 \end{aligned}$$

where  $c_m = 1 + \left( (1 + \varphi_m) \frac{\mathcal{Y}_f}{2} \right)^\alpha$ ,  $d_m = 1 + (1 + \varphi_m) \frac{\mathcal{Y}_s}{2}$ ,  $\varphi_m = \cos\left(\frac{2m-1}{2M}\pi\right)$  and  $M$  is the complexity accuracy trade-off parameter. On substituting  $\Theta_{21}$  and  $\Theta_{22}$  from (3.31) and (3.36) into (3.30), respectively, to get the expression for  $\Theta_2$ . Afterwards, substituting for  $\Theta_1$  and  $\Theta_2$  in (3.26) to get closed form expression for outage probability of CEU as given in (3.27).

Proposition 2 derives the outage probability at the CEU. The CEU receives signal from SBS in direct transmission phase where it detects its signal considering the CCU signal as interference. The CEU also receives signal from the CCU where the CCU uses harvested energy to forward information to the CEU in the cooperative phase transmission. The outage probability at the CEU in (3.27) depends upon the power splitting ratio  $\beta$  and increases when the  $\beta$  is close to 0 or 1, this is because at  $\beta = 0$  the CCU does not decode the incoming signal and at  $\beta = 1$  the CCU does not perform EH, both the cases impact the cooperative transmission phase and increases the outage probability at the CEU.

### 3.4.3 System Throughput

In the previous subsection, the outage probabilities have been evaluated individually at the CCU and at the CEU, however to evaluate the overall system performance the delay-sensitive system throughput is calculated in this subsection. In delay sensitive mode [103], the SBS transmits information at a fixed rate and the system throughput is determined from the outage probability at the CCU and the outage probability at the CEU. The system throughput, based on the outage probability

at the CCU and the CEU at fixed target rates, is given as

$$T_{sys} = (1 - P_{out}^{ce}) R_1 + (1 - P_{out}^{cc}) R_2, \quad (3.37)$$

where  $P_{out}^{cc}$  and  $P_{out}^{ce}$  is obtained from (3.17) and (3.27).

### 3.4.4 System Energy Efficiency

Hereby, we compare the energy efficiency of the proposed EHSI-RPP with EHSI-PPP and EHS-SBS. Fundamentally, the energy efficiency for the system can be defined as the total amount of data delivered to the total amount of consumed energy. The total amount of data delivered can be quantified by system throughput defined in (3.37). While the total energy consumed in the system is the energy consumed by SBS. Consequently, the expression of energy efficiency, for a delay-limited system, can be given as

$$\begin{aligned} \eta_{sys} &= \frac{T_{sys}}{P_s} \\ &= \frac{(1 - P_{out}^{ce}) R_1 + (1 - P_{out}^{cc}) R_2}{P_s}. \end{aligned} \quad (3.38)$$

## 3.5 Results and Discussions

This section discusses the numerical results based on the derived expressions for the outage probability and system throughput obtained in Section IV for the proposed system model. The analytical results are validated using Monte Carlo simulation for an ensemble of  $10^5$ . Network parameters for the analytical plots and the simulation plots are given as [1]  $\eta=0.7$ ,  $\beta=0.5$ ,  $N=10$ ,  $M=10$ ,  $B=1000$ ,  $P_m = 40\text{W}$ ,  $P_s = 1\text{W}$ ,  $\lambda_m = 10^{-4}\text{m}^{-2}$ ,  $\lambda_s = 10^{-3}\text{m}^{-2}$ ,  $\mathcal{Y}_m = 500\text{m}$ ,  $\mathcal{Y}_s = 5\text{m}$ ,  $a_1 = 0.8$ , and  $a_2 = 0.2$ . For analysis, the transmit SNR of the SBS tier is varied from 0 to 40dB, while, comparisons are performed at a transmit SNR of 36dB.

In this chapter, EHSI-RPP refers to the proposed system in which the CCU performs EH using the superimposed signal and the aggregate cross-tier and co-tier interference. Further, it indicates that the SBSs are equipped with carrier sensing hence their locations follow RPP distribution. EHSI-PPP refers to the system in

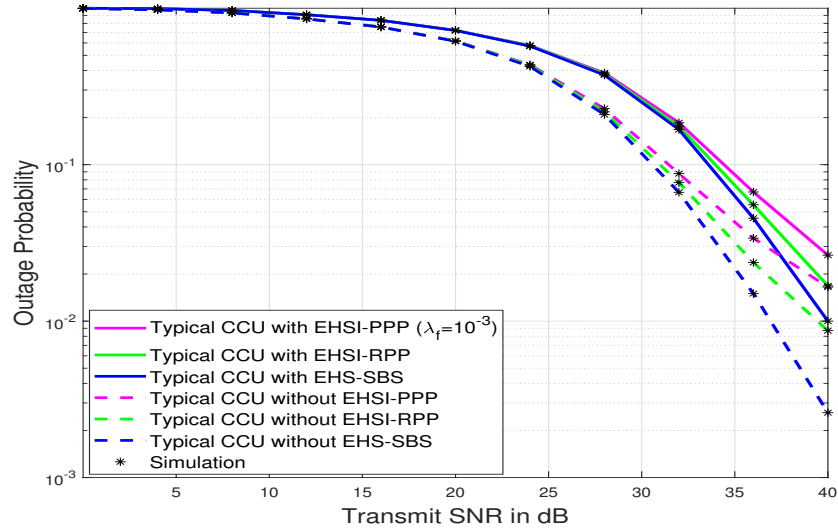


Figure 3.2: Variation of outage probability at the CCU with transmit SNR.

which the CCU performs EH using the superimposed signal, and the aggregate cross-tier and co-tier interference. Further, it indicates that the BSs follow PPP distribution. EHS-SBS refers to the system wherein the CCU performs EH using only the superimposed signal and the network contains a single SBS. EHS-PPP refers to the system wherein the CCU performs EH using only the superimposed signal and the distribution of the BSs follow PPP assumption.

Fig. 3.2 shows outage probability of the CCU versus transmit SNR plot. The degradation of 62.38% in the outage performance is shown by the proposed system with EHSI-RPP as compared to the system without EHSI-RPP. The reason is that the proposed EHSI-RPP uses only a fraction of power for information decoding in the direct phase transmission however, the system without EHSI-RPP dedicates all the power for decoding. For the same reason, the outage probability of the CCU with EHSI-PPP and EHS-SBS achieve degradation of 48.30% and 68.94% when compared with the outage probability of the CCU without EHSI-PPP and EHS-SBS, respectively. The proposed CCU with EHSI-RPP performs better as compared to EHSI-PPP by 12.58%. This is due to the application of proposed carrier sensing in the SBS tier which removes the simultaneously transmitting SBSs among its neighborhood set thereby reducing the co-tier interference. However, the CCU with EHSI-PPP suffers from randomized co-tier and cross-tier interference which degrades its performance. The CCU with EHS-SBS achieves better outage

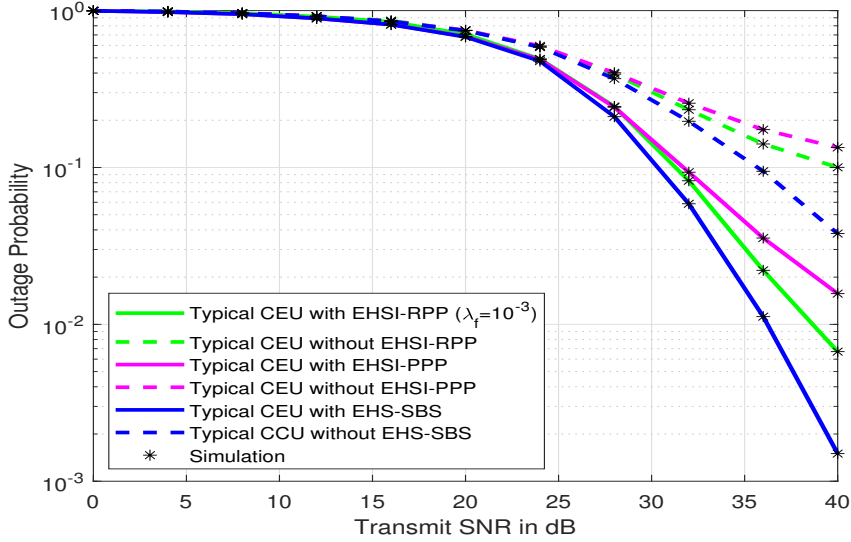


Figure 3.3: Variation of outage probability at the CEU with transmit SNR.

performance by 22.68% and 32.50% as compared to the CCU with EHSI-RPP and EHSI-PPP, respectively. The reason is that the CCU with EHSI-RPP and EHSI-PPP suffers from co-tier and cross-tier interference. However, no interference is experienced at the CCU with EHS-SBS since only a single BS is considered for the analysis.

Fig. 3.3 shows the plot for outage probability of the CEU versus transmit SNR. It can be inferred from Fig. 3.3 that an improvement of 59.26%, 79.12% and 50.82% is achieved in the outage performance of CEU with EHSI-RPP, EHSI-PPP and EHS-SBS, respectively as compared to that achieved at the CEU without EHSI-RPP, EHSI-PPP and EHS-SBS, respectively. The reason being that the CEU enabled with EH detects its signal using SC from both phases, while, the CEU without EH receives signal only from the direct phase. The proposed CEU with EHSI-RPP achieves better outage performance by 39.43% as compared to the CEU with EHSI-PPP. The reason is that the system with EHSI-PPP suffers from larger co-tier interference as compared to the system with EHSI-RPP, because of the applied carrier sensing in EHSI-RPP. Though, the performance at CEU with EHSI-PPP is enhanced by harvesting energy from the co-tier and cross-tier interference however the same interference also degrades its performance. The outage performance of the CEU with EHS-SBS achieves better performance by 48.36% and 72.35% as compared to the proposed system with EHSI-RPP and the system with EHSI-PPP, respec-

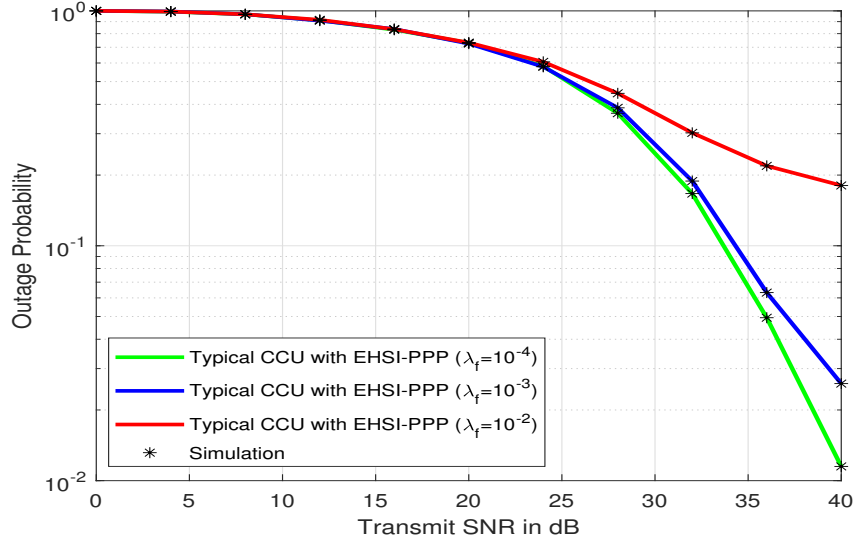


Figure 3.4: Variation of outage probability at the CCU with transmit SNR for different values of  $\lambda_s$

tively. This is because the system with EHS-SBS depicts an ideal situation with no co-tier and cross-tier interference, therefore achieves better outage performance.

Fig. 3.4 shows the plot for outage probability of the proposed CCU with EHSI-RPP versus transmit SNR for different values of SBS intensity  $\lambda_s$ . As the intensity of the SBS increases, the outage probability at the proposed CCU with EHSI-RPP increases. The reason is that the intensity of simultaneously transmitting SBS using carrier sensing ( $\lambda_s^R$ ) increases with increasing the intensity of the SBS ( $\lambda_s$ ) which in turn increases the co-tier interference at the CCU. However, this has a constructive effect on the amount of energy harvested at the CCU. The harvested energy  $E_2$  at the CCU increases with the increase in the co-tier interference. The increased harvested energy at the CCU boosts the cooperative phase transmission as evident from Fig. 3.5. Fig. 3.5 shows the plot for outage probability of the proposed CEU with EHSI-RPP versus transmit SNR for different values of SBS intensity  $\lambda_s$ . The proposed CEU with EHSI-RPP shows near similar performances for different values of SBS intensity. This is due to the fact that the degradation in the outage probability with the increased intensity is compensated by the boost in the cooperative phase transmission due to increased harvested energy at the CCU.

For detailed comparative study, Fig. 3.6 presents comparison between the outage probability of CEU with, the proposed EHSI-RPP, EHS-RPP, EHSI-PPP and EHS-

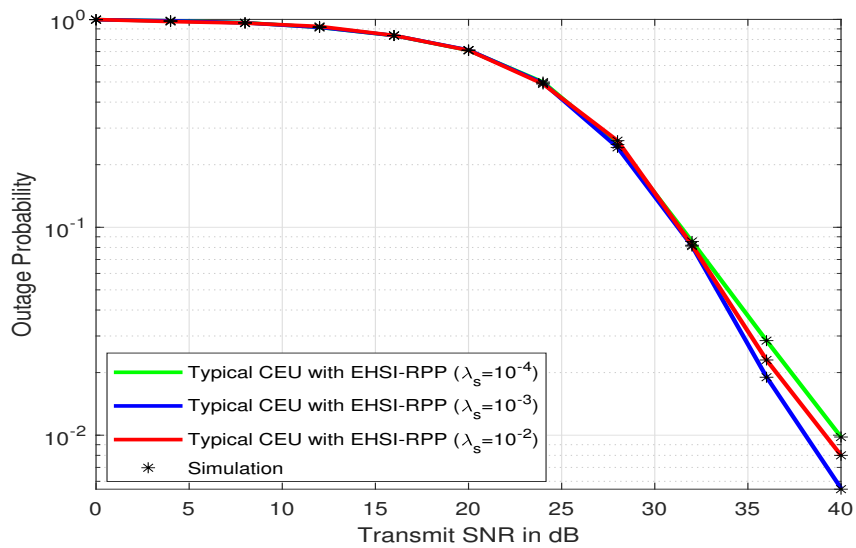


Figure 3.5: Variation of outage probability at the CEU with transmit SNR for different values of  $\lambda_s$

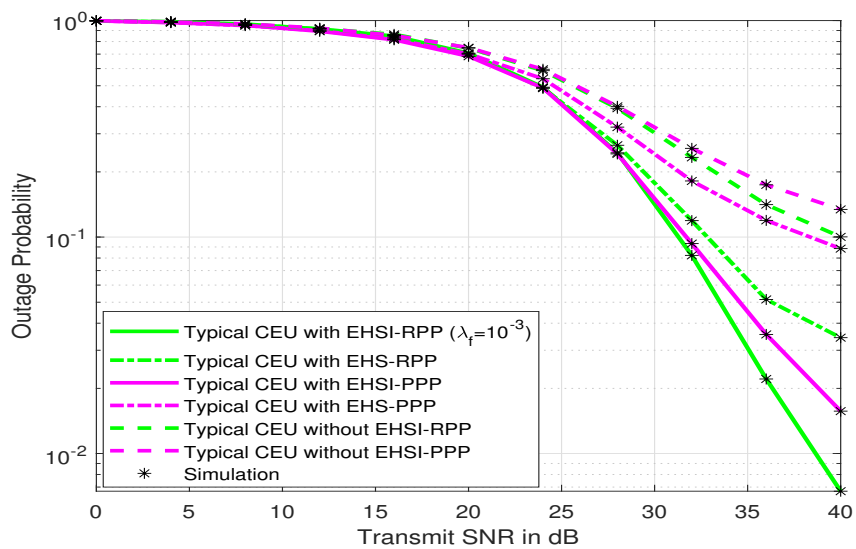


Figure 3.6: Comparison of proposed EHSI-RPP system with EHSI-PPP system.

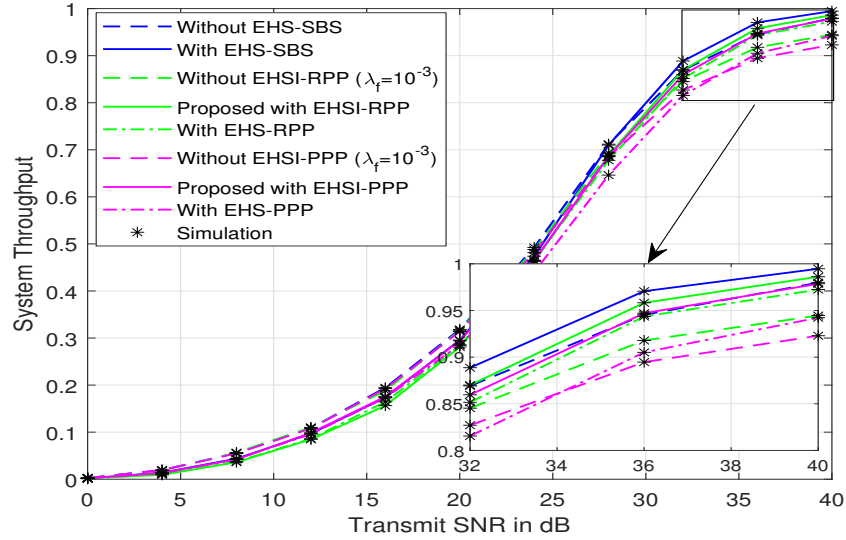


Figure 3.7: System throughput versus transmit SNR for the target rates  $R_1=0.5$  and  $R_2=0.5$

PPP. Primarily, the study tries to distinguish the system in which the CCU is harvesting only from the superimposed signal to that from the system in which the CCU is harvesting from superimposed signal as well as aggregate interference from co-tier and cross-tier. In Fig. 3.6, the outage performance of CEU with the proposed EHS-RPP shows an improvement of 31.49% as compared with the system with EHS-PPP. This is because both the systems' CCU harvests energy only from superimposed signal and hence the cooperative signal in both the systems have nearly same power however, the aggregate interference at the CEU with EHS-PPP is greater than the aggregate interference at the CEU with EHS-RPP which degrades its performance. The proposed CEU with EHSI-RPP performs better than the CEU with EHS-RPP, similarly the CEU with EHSI-PPP achieves improvement than the CEU with EHS-PPP. Because in both cases, i.e., the CEU with EHSI-RPP and the CEU with EHSI-PPP, the CCU harvest energy together from aggregate interference and superimposed signal. However, in the case of the CEU with EHS-RPP and the CEU with EHS-PPP, the CCU harvests energy only from superimposed signal.

To obtain the overall system performance, the throughput of the system is obtained as shown in Fig. 3.7. As can be observed from Fig. 3.7 that at low values of the transmit SNR, the system without EHSI-RPP, the system without EHSI-PPP, the system without EHS-SBS performs better in terms of throughput as compared

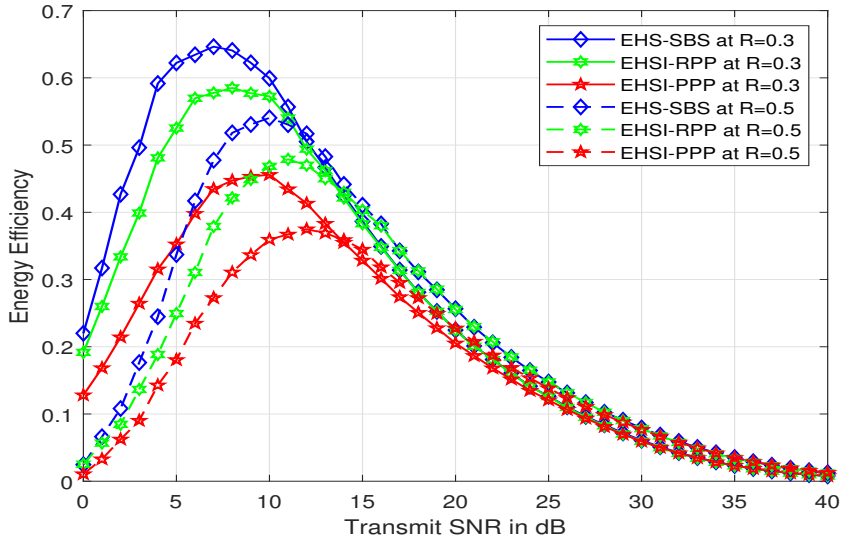


Figure 3.8: System Energy Efficiency versus transmit SNR

to the system with EHSI-RPP, the system with EHSI-PPP, the system with EHS-SBS, respectively. This is because at low transmit SNR, degradation in the outage performance of the CCU dominates the improvement in the outage performance of the CEU when using EH. Also, the amount of harvested energy is proportional to the transmit SNR. Therefore, at low values of the transmit SNR, the harvested power for cooperation is also lower. At high values of transmit SNR, the outage performance of the EH enabled system surpasses the system without EH. This is because at high transmit SNR, the improvement in the outage performance of the CEU dominates the degradation in the outage performance of the CCU. Also, the amount of harvested power for cooperation is considerable at high SNR. The system throughput performance of the proposed system with EHSI-RPP enabled at the CCU achieves better performance as compared to the system with EHSI-PPP. This is because the outage performance at the proposed, CCU with EHSI-RPP and the CEU with EHSI-RPP, performs better than the CCU with EHSI-PPP and the CEU with EHSI-PPP, respectively.

Fig. 3.8 plots the energy efficiency of the proposed EHSI-RPP system versus transmit SNR for different values of target rates  $R = R_1 = R_2$ . Plot also compares the energy efficiency of the proposed EHSI-RPP system with EHS-SBS system and EHSI-RPP system. From Fig. 3.8, it can be observed that the EHS-SBS system achieves higher energy efficiency as compared to the proposed EHSI-RPP system and

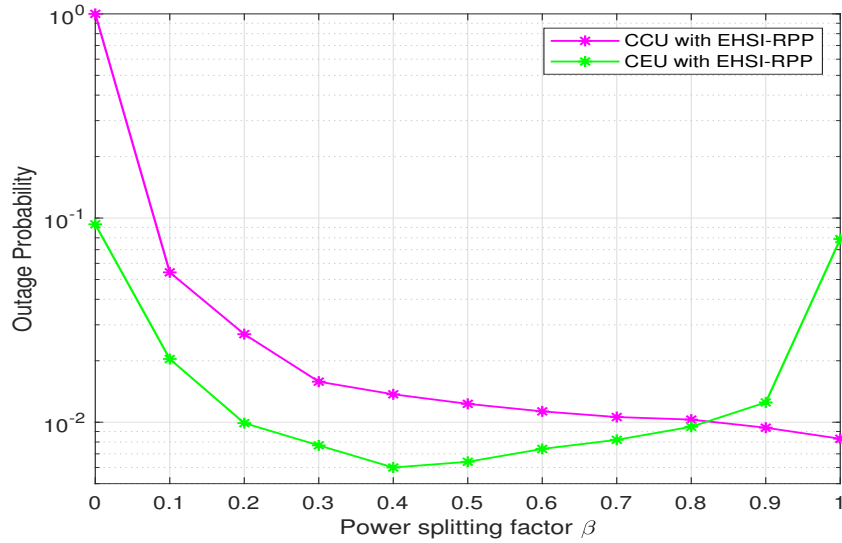


Figure 3.9: Outage Probability versus PS factor  $\beta$  at transmit SNR of 36dB.

EHSI-PPP system, for both target rates  $R = 0.3$  and  $R = 0.5$ . The energy efficiency of the proposed EHSI-RPP system is higher than the EHSI-PPP system. This is because the proposed EHSI-RPP system achieves better throughput performance as compared to EHSI-PPP system. From the plot, one can also observe that the systems exhibits maximum energy efficiency at a certain SNR value for a given target rate and if the target rate changes to a different value, the SNR value for which system attains maximum energy efficiency also changes. One can also note that energy efficiency of the considered system is decreases with SNR. This is because, for higher values of transmit SNR, the consumed power is higher than the achieved system throughput.

The optimal value of  $\beta$  is defined as the value, which results in the lowest outage probability at the CCU and the CEU. Because of the complicated analytical expressions of the outage probability at the CCU and the CEU, it is intractable to evaluate the closed-form expressions for the optimal value of  $\beta$ . Therefore, to obtain the optimal value of power splitting ratio  $\beta$  Fig. 3.9 plots the outage probabilities at the CCU and the CEU versus the power splitting ratio  $\beta$  at the transmit SNR of 36dB.  $\beta$  is the power splitting coefficient for SWIPT at the CCU, such that  $\beta$  times the received power at the CCU is used for information decoding during the direct phase transmission and the rest i.e.,  $1 - \beta$  times received power at the CCU is used for EH. It is observed from Fig. 3.9 that as  $\beta$  increases from  $\beta = 0$  to  $\beta = 1$  the

outage probability at the CCU decreases.  $\beta = 0$  means that the total received power at the CCU is used for EH. Therefore, no power is left for information decoding that results in an outage at the CCU.  $\beta = 1$  signifies that the total power at the CCU is used for information decoding that results in the decrease in the outage probability. It is also observed from Fig. 3.9 that as  $\beta$  increases from  $\beta = 0$  to  $\beta = 1$  the outage probability at the CEU first decreases until reaches a minimum value at  $\beta = 0.4$  and then again starts increasing. The outage probability of the CEU remains below  $10^{-2}$  for the  $\beta$  values between 0.4 to 0.6. For the CEU  $\beta = 0.4$  achieves the best outage performance and, for the CCU  $\beta = 1$  achieves the best outage performance. For the proposed scheme we selected  $\beta = 0.5$  from the intuitive perspective as the received power at the CCU be divided equally for information decoding and EH, and  $\beta = 0.5$  also ensures the outage probability to be less than  $10^{-2}$  for the CEU.

## 3.6 Summary

This work explores the application of SWIPT in a CNOMA enabled two-tier heterogeneous network. The locations of the MBSs are based on PPP assumption. The SBS tier supports NOMA and the location of SBS are modelled using RPP due to the applied carrier sensing for interference management. Closed-form expressions of outage probability and system throughput are obtained at the CCU and the CEU. It is inferred that the CCU with EHSI-RPP shows improvement in outage probability in comparison with the CCU with EHSI-PPP, however, suffers degradation in outage probability in comparison with the CCU with EHS-SBS. Also, CCU achieves flexibility in terms of energy consumption due to EH. Furthermore, the outage performance of the CEU experiences significant improvement by employing cooperation from the CCU. The throughput analysis highlights that the proposed system with EHSI-RPP surpasses a cooperative NOMA system with EHSI-PPP at high transmit SNR. The energy efficiency analysis also depicts that the energy efficiency of the proposed EHSI-RPP is higher as compared to EHSI-PPP. The optimal value of PS coefficient is also obtained for the proposed system model as  $\beta = 0.5$ . However, the previous chapters are based upon the PS protocol for energy harvesting models in HetNets. In the PS protocol the receiver has separate circuits for EH and ID to

process the received signal simultaneously. The PS ratio determines the portion of the received signal allocated for EH and ID, respectively. In the next chapter, we choose the TS relaying protocol in the considered model as it has been shown to require less complicated circuitry than the PS protocol.



# Chapter 4

## Time Switching based Energy Harvesting Enabled Cooperative NOMA HetNets

The existing literature on the performance in EH enabled NOMA in two-tier Het-Net, considering the two-tier interference is limited. The NOMA-enabled system is investigated in [76], by evaluating the ergodic rate and outage rate, the results indicate that the NOMA reaches a higher sum rate. Work in [2] investigates the utilization of EH to NOMA networks wherein the users are randomly located. Some previous works, such as [79] and [136], have also used cooperative NOMA to improve performance. In [137], a novel implementation of EH in a cooperative NOMA network with PS relaying protocol is proposed, and the data rate maximization problem of the NOMA users is formulated for the case of multiple-input single-output. In [138], a PS relaying protocol for a DF relay is investigated, and outage probability and throughput expressions in closed form are evaluated in a delay-limited transmission mode. In [139], a novel PS relaying protocol for an EH cooperative NOMA system is proposed, and the outage probability at NOMA users is investigated, and analytical expression is also obtained. The system throughput is also evaluated for a delay-limited transmission mode. [86] analyzes the utilization of EH in cooperative NOMA, where analytical closed-form outage expressions are evaluated for the weak and strong users. [140] derives the analytical secrecy outage probability in a cooperative NOMA cellular network for distinct energy harvesting relay selection schemes.

---

These aforementioned studies are based upon a single tier scenario with a single BS and thus they are not able to estimate how the outage performance of users are affected by multi-tier HetNets with multi-tier interference. The works [141] and [142] are based upon the PS protocol wherein the received signal is split into two parts: one for EH and the other for ID. The receiver has separate circuits to process these two signals simultaneously and the PS ratio determines the portion of the received signal allocated for EH and ID, respectively. Furthermore, the studies in [86, 137–140] are based upon PS relaying protocol. In this work, we choose the TS relaying protocol in the considered model as it has been shown to require less complicated circuitry than the PS protocol [143]. There have been few works that are related to large-scale networks. For instance, in [80], outage probability is analyzed in a dense cognitive network. In the large-scale systems, [118] and [144] investigate the outage and energy efficiency of users, respectively. In [58], the system enabled with NOMA is implemented in a HetNet, and the performance of the coverage and ergodic rate are examined. The work in [112] focuses on resource allocation in energy cooperation enabled two-tier HetNets with NOMA, high-power MBS is underlaid with a group of pico BSs, and renewable energy can be shared between BSs. In [145], NOMA is introduced in the SBS tier to enhance the spectrum efficiency. However, in [145], SBS additionally harvests energy from the RF signal to supplement the energy consumed in transmission phase. Furthermore [145] have not considered the distributions of the MBS and SBS into account. [146] proposes the fair energy-efficient resource allocation for the downlink of a power domain NOMA-based HetNet system by considering energy harvesting. [146] formulates various fairness methods for the optimization problems based on which the trade-off between energy efficiency, fairness, and system sum rate is investigated. [147] studies the problem of joint subcarrier allocation, beamforming design, decoding order for the user, and energy beam for EH users in a NOMA-assisted SWIPT while considering a non-linear energy harvesting model. However, [147] does not consider the distribution of MBS, and the interference from the MBSs. As observed, the application of cooperative NOMA and the application of EH between the users to influence the performances in a HetNet scenario are not addressed in these previous works. As a result, it is currently unknown how to improve user outage performance and system throughput

when using EH-enabled cooperative NOMA in a multi-tier HetNet. Furthermore, few studies have examined user fairness in HetNets involving cooperative NOMA and EH. Technical contributions of the work are summarized as follows:

- A time switching-based EH-enabled cooperative NOMA communication scheme has been considered in a two-tier HetNet, constituting MBS-tier and SBS-tier. The locations of MBS and SBS are based upon the independent PPP assumption. An analytical framework is developed at a typical SBS tier. The strong user (SU), powered with EH prevents their battery from draining while acting as a DF relay to transmit the message to WU.
- Unlike existing works in [2], where EH is performed by only utilizing the transmitted NOMA signal, in this work, the SU of the considered system model carries out EH utilizing the transmitted signal and additionally the aggregate two-tier interference (EH-ATI).
- Closed-form expressions characterizing outage probability have been obtained. The throughput is evaluated to analyze the overall system performance.
- The outage probability at SU and WU of the proposed system is studied with the existing systems [2], where EH is achieved by only utilizing the superimposed signal (EH-SS). Furthermore, the outage probabilities are also analyzed with the existing systems [1], [148], [149], that do not employ EH at the cooperative node.
- Finally, a proportional fairness index is defined utilizing the outage probability, demonstrating that the suggested system with EH-ATI delivers greater user fairness than the system with EH-SS and the system without EH.

## 4.1 System and Channel Model

A wireless network comprising of SBS tier and MBS tier is considered as shown in Fig. 4.1. Without the loss of generality the location of SBS and MBS follows independent PPP distribution,  $\Omega_t$  with density  $\lambda_t$  for the  $t^{th}$  tier, such that  $t \in \{m, s\}$ , where  $m$  stands for MBS-tier and  $s$  stands for SBS-tier, respectively. The PPP

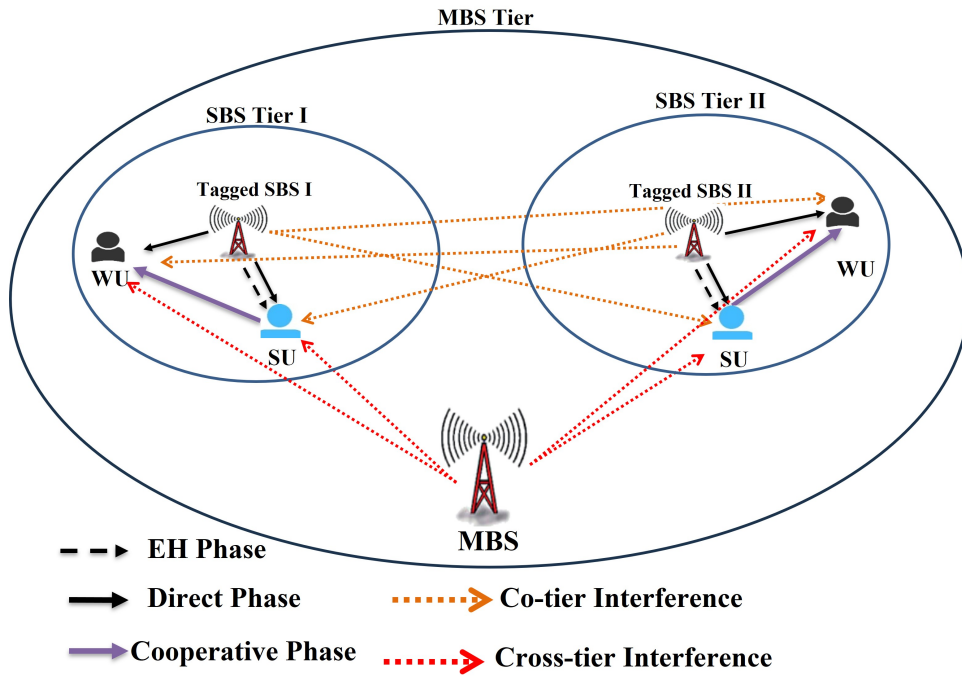


Figure 4.1: A downlink EH enabled cooperative NOMA system model in a two-tier situation with a tagged SBS broadcasting to NOMA user pair. The MBS and SBS spatial distributions are consistent with the PPP assumption.

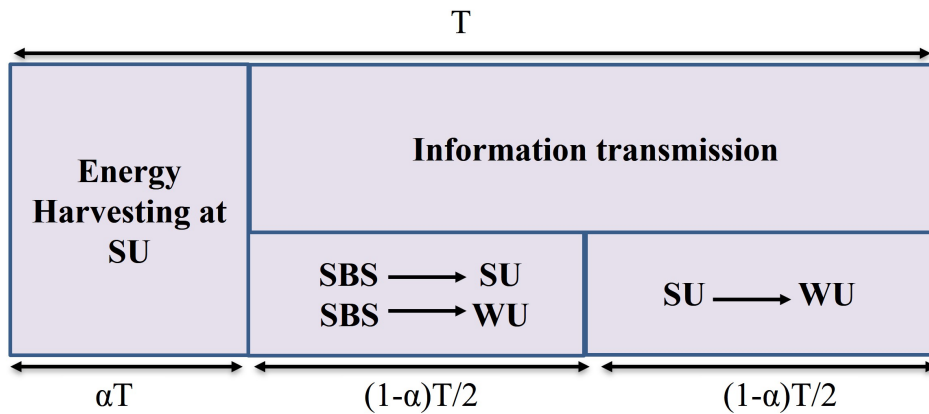


Figure 4.2: Total transmission time block  $T$

model is used to distribute the nodes since it provides a mathematically tractable and spatially realistic model for wireless networks, which can be used for system design and performance evaluation [1, 149].  $\mathcal{P}_m$  and  $\mathcal{P}_s$  indicate the power transmitted by the MBS and the SBS, respectively. The coverage area of MBS-tier and SBS-tier is designated as  $\mathcal{Y}_m$  and  $\mathcal{Y}_s$ , respectively. The main focus of analysis is at SBS-tier enabled with NOMA as shown in Fig. 4.1. The use of NOMA in SBS ensures that users with different channel conditions can be served using the same spectrum [132, 150]. In the SBS-tier, distribution of users follows independent PPP [80],  $\Omega_u$  with density  $\lambda_u$  such that  $\lambda_u \gg \lambda_s$ . The SBS selects NOMA pair based on random selection scheme [2]. Random selection schemes can be beneficial in specific scenarios where associating BS with users which would provide the best performance for the user device may be difficult. For example, in a dense urban environment with large number of users in proximity, a random selection scheme may be more effective than manually determining which user received the strongest signal. The channel gains between the links are considered to be Rayleigh distributed and accordingly the channel power gains are exponentially distributed with unit variance. A bounded path loss model is taken into account for the large-scale path-loss model. Hence, the total channel gain is given as  $\frac{h_t}{(1+r_t^{\nu_t})}$ , where  $\nu_t$  denotes the path loss exponent for the  $t^{th}$  tier, such that  $t \in \{m, s\}$ ,  $h_k$  and  $r_k$ , are the channel power gain and separation between the  $k^{th}$  NOMA user and the tagged SBS, respectively. Fig. 4.2 describes the total transmission time block  $T$ , which is divided into the EH phase, and the information transmission (IT) phase [151]. In the EH phase, the SU performs EH from the transmitted NOMA signal and additionally the aggregate two-tier interference (EH-ATI) for  $\alpha T$  of the time block, where  $\alpha$  is the fractional time block, such that  $0 \leq \alpha \leq 1$ . The IT phase is further divided into two parts Phase-1 and Phase-2 each of  $(1 - \alpha)T/2$  of the time block. In Phase-1, the SBS transmits information to the two NOMA users (the SU and the WU). In Phase-2, the SU performs cooperative transmission to the WU. It is important to acknowledge that [141] and [142] divide the signal transmission into two distinct phases: the direct transmission phase and the cooperative transmission phase, with both phases of equal duration. During the direct transmission phase, the research works consider a NOMA downlink transmission, where the SBS transmits the signal

to both the CCU and the CEU. The signal received at CCU is split into two parts using the PS coefficient  $\beta$ .  $\beta$  times the received signal is utilized for EH, while  $1 - \beta$  times the received signal is used for ID. In the cooperative phase of the transmission, CCU functions as an energy harvesting DF relay to relay information to CEU. Such architecture allows for simultaneous EH and ID, however it requires more complex hardware implementation.

#### 4.1.1 SINR at SU and WU

SBS selects two users, based on random selection scheme [2], for the NOMA transmission. Let us assume  $\frac{h_1}{(1+r_1^{\nu_s})} \leq \frac{h_2}{(1+r_2^{\nu_s})}$  to be ordered channel gains. Hence their ordering of power allocation coefficients are given as  $a_1 \geq a_2$ , such that  $a_1 + a_2 = 1$ . Therefore, WU is the user-1 having a lower channel gain as compared to user-2 which is the SU, where, the channel corresponding to the WU and the SU are  $h_1$  and  $h_2$ , respectively.  $r_1$  corresponds to the distance between the SBS and WU whereas  $r_2$  corresponds to the distance between the SBS and SU. The SBS is considered to have knowledge of CSI.

#### Phase-1 Transmission

The SBS transmitted message is given as  $X_s = \sum_{i=1}^2 x_i \sqrt{a_i \mathcal{P}_s}$  utilizing PD-NOMA, where the signal meant for the  $i^{th}$  user is denoted by  $x_i$ . The transmitted power in the message  $x_i$  is assumed to be unity i.e.  $\mathbb{E}[x_i^2]=1$  and is equal  $\forall i \in (1, 2)$ . The received message at the typical  $k^{th}$  user is expressed as

$$Y_k = \sqrt{h_k(1 + r_k^{\nu_s})^{-1}} X_s + n_k, \quad (4.1)$$

where  $n_k \sim \mathcal{N}(0, \sigma_k^2)$  is the noise at the  $k^{th}$  user. Utilizing NOMA principle, SU does SIC to decodes its message by eliminating the WU's message. The SINR received at the SU for detecting the WU messages is described as

$$\gamma_{2 \rightarrow 1}^1 = \frac{\rho a_1 h_2 (1 + r_2^{\nu_s})^{-1}}{\rho a_2 h_2 (1 + r_2^{\nu_s})^{-1} + \rho_s I_s + \rho_m I_m + 1}, \quad (4.2)$$

where  $\rho = \rho_s = \mathcal{P}_s/\sigma_2^2$  is the transmit signal to noise ratio (SNR) at SU, and  $\rho_m = \mathcal{P}_m/\sigma_2^2$ .  $I_s = \sum_{y \in \Omega_s/\{s_o\}} h_y$  is the total SBS-tier interference at the SU, where  $h_y$  is the channel gain between the the SU and  $y^{th}$  SBS, and  $s_o$  represent the assigned SBS. Likewise  $I_m = \sum_{y \in \rho_m} h_v$  is the total MBS-tier interference at the SU, such that  $h_v$  represent the channel gain between the typical SU and the  $v^{th}$  MBS. Hence, the SU's SINR for detecting its message is described as

$$\gamma_2^1 = \frac{\rho a_2 h_2 (1 + r_2^\nu)^{-1}}{\rho_s I_s + \rho_m I_m + 1}. \quad (4.3)$$

Here, it is presumed that the SU have energy storage ability [2] and TS protocol [103] is incorporated at SU to perform EH. In EH phase, the SU harvests energy for cooperative transmission in Phase-2. The energy harvested ( $\mathcal{E}_2$ ) at SU from the transmitted NOMA signal and additionally the aggregate two-tier interference, i.e., interference from MBS-tier and SBS-tier is given as

$$\mathcal{E}_2 = \alpha T \zeta (\mathcal{P}_s h_2 (1 + r_2^\nu)^{-1} + \mathcal{P}_s I_s + \mathcal{P}_m I_m), \quad (4.4)$$

where  $\zeta$  represents the energy conversion efficiency of the harvester. Let  $\mathcal{P}_2$  represents the transmit power from SU, to be used in Phase-2 transmission, is given by

$$\begin{aligned} \mathcal{P}_2 &= \frac{\mathcal{E}_2}{\frac{(1-\alpha)T}{2}} \\ &= \frac{2\alpha}{1-\alpha} \zeta (\mathcal{P}_s h_2 (1 + r_2^\nu)^{-1} + \mathcal{P}_s I_s + \mathcal{P}_m I_m). \end{aligned} \quad (4.5)$$

It is assumed that the strong user will always be able to execute the cooperative transmission after harvesting energy in the direct phase. It must be noted that the user grouping process used in the work may not consider the battery life of the users, it is possible to develop more sophisticated algorithms that take into account energy harvesting and other constraints of the users which can be a future extension of the proposed scheme. The SINR received at the typical WU is given by

$$\gamma_1^1 = \frac{\mathcal{P}_s a_1 h_1 (1 + r_1^{\nu_s})^{-1}}{\mathcal{P}_s a_2 h_1 (1 + r_1^{\nu_s})^{-1} + \mathcal{P}_s I'_s + \mathcal{P}_m I'_m + \sigma_1^2}, \quad (4.6)$$

where  $I'_s = \sum_{y \in \Omega_s / \{s_o\}} h_y$  is the total SBS-tier interference at the WU, where  $h_w$  is the channel gain between the WU and  $w^{th}$  SBS, and  $s_o$  represent the assigned SBS. Likewise  $I'_m = \sum_{y \in \rho_m} h_u$  is the total MBS-tier interference at the WU, such that  $h_u$  represent the channel gain between the typical WU and the  $u^{th}$  MBS.

### Phase-2 Transmission

In this phase, the message is forwarded to the WU by the SU. The SINR to decode  $x_1$  at WU is given by

$$\gamma_1^2 = \frac{\mathcal{P}_2 h_{12} (1 + r_{12}^{\nu_s})^{-1}}{\mathcal{P}_s I'_s + \mathcal{P}_m I'_m + \sigma_1^2}, \quad (4.7)$$

where  $h_{12} (1 + r_{12}^{\nu_s})^{-1}$  is the total channel gain for the link  $SU \rightarrow WU$ ,  $r_{12}$  denotes the distance between the SU and WU. The WU utilizes SC [124] technique to choose the highest signal from SBS and SU. This is achieved by considering the maximal received SINR from (4.6) and (4.7), the received SINR at the WU is given by

$$\gamma_1^{sc} = \max(\gamma_1^1, \gamma_1^2). \quad (4.8)$$

## 4.2 Performance Analysis

### 4.2.1 Outage probability at SU

The outage probability at SU depends upon the successful SIC of WU's message. The SU goes into outage when SU is not able to detect the message of WU, and when SU detects the message of WU however is unable to detect its own message. Therefore, outage probability expression at the WU is described as

$$P_{out}^{su} = \mathcal{P}(\gamma_{2 \rightarrow 1}^1 < \phi_1) + \mathcal{P}(\gamma_{2 \rightarrow 1}^1 \geq \phi_1, \gamma_2^1 < \phi_2), \quad (4.9)$$

where  $\phi_1 = 2^{\frac{2R_1}{1-\alpha}} - 1$  and  $\phi_2 = 2^{\frac{2R_2}{1-\alpha}} - 1$ , with  $R_1$  and  $R_2$  represents the targeted rate to successfully decode the messages of SU and WU.

*Proposition 1:* Depending on the PPP model, the outage probability at the SU

is defined as

$$P_{out}^{su} = \frac{1}{2} \sum_{l=0}^L b_l e^{-c_l \epsilon_1} \mathcal{L}_{I_s}[s_l \rho_s] \mathcal{L}_{I_m}[s_l \rho_m], \quad (4.10)$$

where  $s_l = \epsilon_1 c_l$ ,  $\epsilon_1 = \frac{\phi_1}{\rho(a_1 - \phi_1 a_2)}$ ,  $b_l = -\omega_L (1 + \psi_l) \sqrt{1 - \psi_l^2}$ ,  $b_0 = -\sum_{l=1}^L b_l$ ,  $c_l = 1 + \left(\frac{\gamma_s}{2} \psi_l + \frac{\gamma_s}{2}\right)^{\nu_s}$ ,  $\psi_l = \cos\left(\frac{2l-1}{2L}\pi\right)$ ,  $\omega_L = \pi/L$ ,  $c_0 = 0$ ,  $L$  is a parameter to provide complexity-accuracy trade-off for the Gaussian-Chebyshev (G-C) quadrature. The Laplace transform (LT) of the  $t^{th}$  tier is described [134] as

$$\mathcal{L}_{I_t}(s) = e^{\pi \lambda_t (s^{\delta_t} \Gamma(1 - \delta_t, s) - s^{\delta_t} \Gamma(1 - \delta_t))}, \quad (4.11)$$

where  $\delta_t = \frac{2}{\nu_t}$ ,  $\Gamma(a, x)$  is the lower incomplete gamma function, and  $\Gamma(z)$  is the gamma function.

*Proof:* Look at Appendix A.

## 4.2.2 Outage probability at WU

The WU goes into outage when both the SU and the WU are not able to decode the signal of the WU, and when the SU decodes signal of the WU however the WU is not able to attain the targeted rate in Phase-2. Thus, the outage probability expression at the WU is described as

$$P_{out}^{wu} = \underbrace{\mathcal{P}(\gamma_{2 \rightarrow 1}^1 < \phi_1, \gamma_1^1 < \phi_1)}_{\Theta_1} + \underbrace{\mathcal{P}(\gamma_{2 \rightarrow 1}^1 > \phi_1, \gamma_1^{sc} < \phi_1)}_{\Theta_2}. \quad (4.12)$$

*Proposition 2:* Depending on the PPP model, the outage probability at the WU is defined in (4.13).

*Proof:* Look at Appendix B.

## 4.2.3 System Throughput

The system's throughput is calculated to determine overall system performance. It is evaluated utilizing the outage probability at the SU and at the WU at constant

$$\begin{aligned}
 P_{out}^{wu} &= \frac{1}{4} \sum_{l=0}^L \sum_{n=0}^N b_l b_n e^{-(c_l+c_n)\epsilon_1} \mathcal{L}_{I_s}[s_l \rho_s] \mathcal{L}_{I_m}[s_l \rho_m] \mathcal{L}'_{I'_s}[s_n \rho_s] \mathcal{L}'_{I'_m}[s_n \rho_m] + \\
 &\frac{1}{2} \sum_{n=0}^N b_n e^{-c_n \epsilon_1} \mathcal{L}'_{I'_s}[s_n \rho_s] \mathcal{L}'_{I'_m}[s_n \rho_m] \left( 1 - \lim_{\mathcal{B} \rightarrow \infty} \frac{\pi^2 \mathcal{B}}{\nu_s^2 K M \mathcal{Y}_s^3} \sum_{k=1}^K \sum_{m=1}^M (1 - \psi_k^2)^{\frac{1}{2}} \right. \\
 &\left. \left( (2 + \nu_s Q_k) \Gamma\left(\frac{2}{\nu_s}\right) - \nu_s Q_k \Gamma\left(\frac{2}{\nu_s}, \mathcal{Y}_s^{\nu_s} Q_k\right) - \nu_s \Gamma\left(\frac{2 + \nu_s}{\nu_s}, \mathcal{Y}_s^{\nu_s} Q_k\right) \right) \times \right. \\
 &\left. \frac{b_m e^{-\frac{c_m Q}{Q_k}} e^{-Q_k}}{Q_k^{1+\frac{2}{\nu_s}}} \mathcal{L}'_{I'_s}\left[\frac{c_m Q \rho_s}{Q_k}\right] \mathcal{L}'_{I'_m}\left[\frac{c_m Q \rho_m}{Q_k}\right] \right). \tag{4.13}
 \end{aligned}$$


---

targeted rates, and is expressed as

$$T_{sys} = \frac{(1 - \alpha)R_1}{2}(1 - P_{out}^{wu}) + \frac{(1 - \alpha)R_2}{2}(1 - P_{out}^{su}), \tag{4.14}$$

where  $P_{out}^{su}$  and  $P_{out}^{wu}$  are given in (4.10) and (4.13).

#### 4.2.4 System Energy Efficiency

The energy efficiency, represented as  $\zeta_{sys}$ , of the proposed EH-ATI system is studied together with EH-SS system and without EH system. Basically,  $\zeta_{sys}$  is described as the ratio of successful data delivered and the total energy consumed by the system. The successful data delivered is measured by the system throughput performance obtained from (4.14). The total amount of energy used by the system as a whole is the amount used by SBS. The expression of  $\zeta_{sys}$  can therefore be given as

$$\begin{aligned}
 \zeta_{sys} &= \frac{T_{sys}}{1/2(1 + \alpha)\mathcal{P}_s} \\
 &= \frac{(1 - \alpha)(1 - P_{out}^{wu})R_1 + (1 - \alpha)(1 - P_{out}^{su})R_2}{(1 + \alpha)\mathcal{P}_s}. \tag{4.15}
 \end{aligned}$$

#### 4.2.5 PF Index

The total transmitted power is divided among the users in NOMA, hence one user may attain better performance than the other [19]. As a result, user fairness has become a key factor in NOMA for ensuring minimal performance disparities among users. The PF index is used to measure the difference in users' performances [152]

Table 4.1: Parameters used for obtaining the mathematical and simulation results [1], [2].

Parameters	Symbols	Value
Transmitting power from MBS, SBS	$P_m, P_s$	40W, 1W
Density	$\lambda_m, \lambda_s$	$10^{-4}\text{m}^{-2}$ , $10^{-3}\text{m}^{-2}$
Coverage radius	$\mathcal{Y}_m, \mathcal{Y}_s$	1Km, 5m
Path loss exponent	$\nu_m, \nu_s$	3, 4
Targeted rates	$R_1, R_2$	0.5bps, 0.5bps
Power allocation coefficients	$a_1, a_2$	0.8, 0.2
Energy conversion efficiency	$\zeta$	0.7
G-C quadrature complexity accuracy trade-off parameter	$K, M, L, N$	10, 10, 10, 10

and is formulated as

$$PF = \frac{P_{out}^{su}}{P_{out}^{wu}}, \quad (4.16)$$

where  $P_{out}^{su}$  and  $P_{out}^{wu}$  are from (4.10) and (4.13). The best possible value for PF is 1 indicating that users have achieved similar performances. Although, this may not be accomplished when the users have distinct quality of service (QoS) demands. If the PF index has value 2, this means that the performance of SU is two times greater than the WU. In this work, NOMA users are chosen based upon their channel conditions.

### 4.3 Results and Discussions

The mathematical results depend on the acquired results from Section 4.2 are explained in this section. The results of the analysis are validated for an ensemble of  $10^5$  using a Monte Carlo simulation. The considered parameters for obtaining the mathematical and simulation results are given in Table 4.1. For analytical ob-

Table 4.2: Outage probability comparison between the proposed system with the existing solutions at the transmit SNR of 36dB

Outage probability Comparison	SU with EH-ATI (proposed system)	WU with EH-ATI(proposed system)
Without EH [1], [148], [149]	62.38% degradation	88.46% improvement
With EH-SS [2]	remains same	81.66% improvement

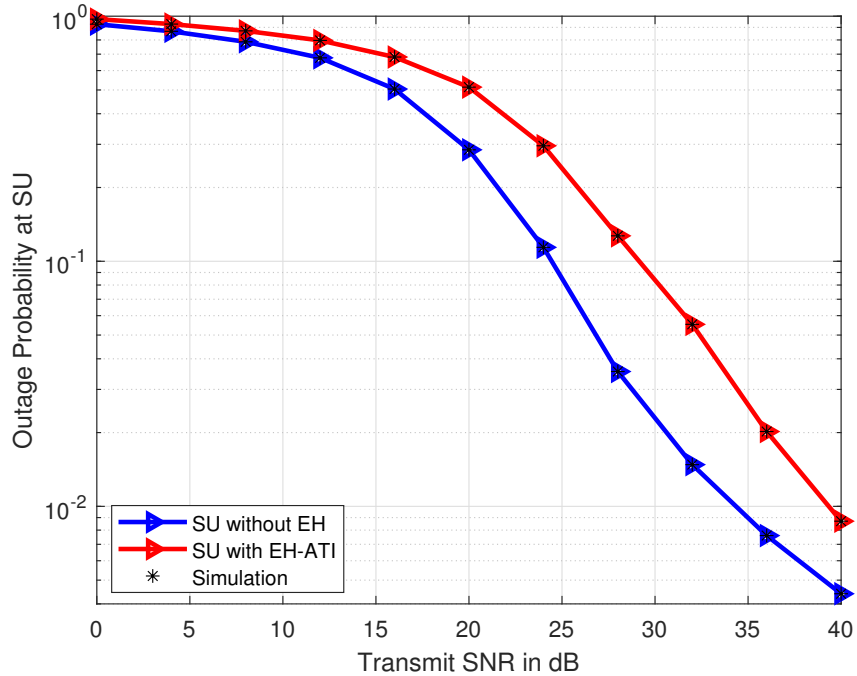


Figure 4.3: Outage probability at SU versus transmit SNR

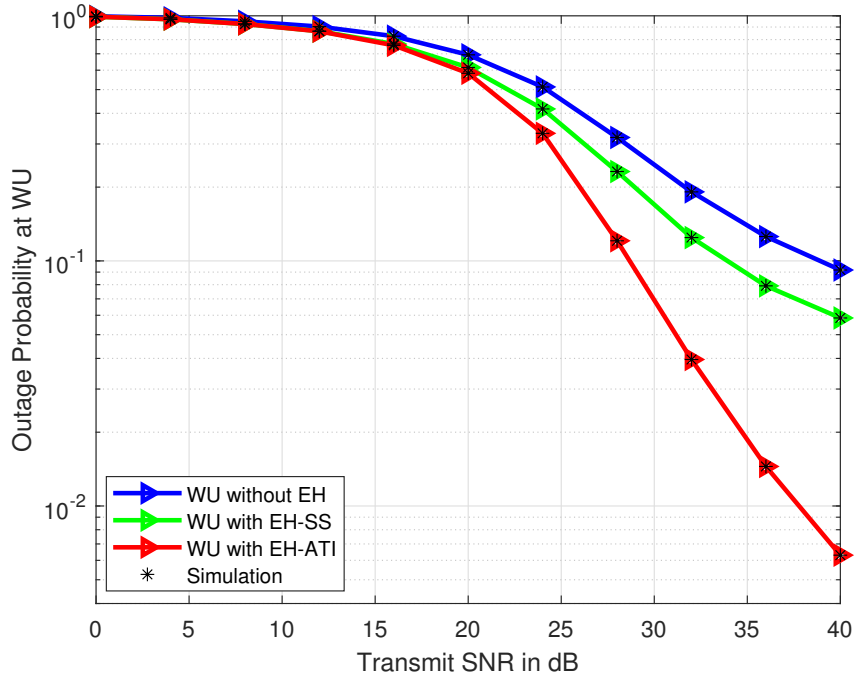


Figure 4.4: Outage probability at WU versus transmit SNR

servation, the SBS transmit SNR varies between 0 and 40 dB, while comparative results are drawn at a transmit SNR of 36 dB. In this chapter, EH-ATI refers to the proposed TS based EH enabled HetNet system wherein the SU performs EH using the transmitted NOMA signal and the aggregate two-tier interference. The EH-SS system is the same system as the proposed EH-ATI system, except in the EH-SS system, the SU performs EH by only utilizing the superimposed signal as in [2]. Furthermore, the system without EH is the two-tier NOMA system that does not perform EH as in [1], [148], [149]. The existing systems taken for comparison are assumed under the environment of two-tier HetNet.

Fig. 4.3 exhibits the outage probability of SU versus transmit SNR plot. A decline of 62.38% in the performance of SU with EH-ATI compared to the outage probability at the SU without EH is shown in Table 4.2. The reason is that the SU with EH-ATI decodes information only for  $(1 - \alpha)T/2$  of its time block, wherein the SU without EH uses its entire time block for decoding information. It is evident from Table 4.2 that the outage probability at the SU for the considered system model and the system with EH-SS are the same. The reason for this is that both the systems dedicate  $\alpha T$  for harvesting energy, and the effect of EH, whether from the transmitted signal or from both the transmitted NOMA signal and the aggregate

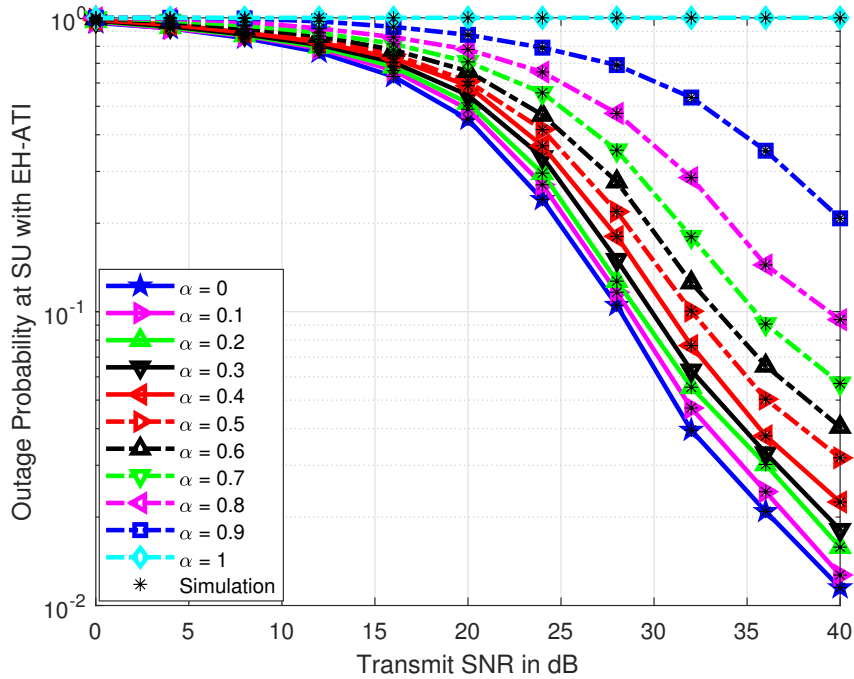


Figure 4.5: Outage probability at SU versus transmit SNR for different values of TS factor  $\alpha$

two-tier interference, has no effect on the outage probability at the SU.

Fig. 4.4 exhibits the outage probability of WU with respect to SNR. It is concluded from Table 4.2 that an enhancement of 88.46% is attained in the performance of WU with EH-ATI compared to the WU without EH. The reason is that the WU with EH-ATI obtains its signal utilizing SC from both phases, while the WU without EH obtains its signal only from Phase-1. Table 4.2 also compares the outage probabilities of the considered WU with EH-ATI and the WU with EH-SS. The difference between EH-ATI and EH-SS is that EH-SS harvests energy from the transmitted NOMA signal, whereas EH-ATI harvests energy from the aggregate two-tier in addition to the NOMA signal. Therefore, the performance of WU with the considered EH-ATI attains an enhancement of 81.66% times at 36dB compared to the WU with EH-SS. This means that the SU with EH-ATI has more energy for cooperation in comparison to the SU with EH-SS.

Fig. 4.5 and Fig. 4.6 show the outage probabilities of the SU and the WU, respectively, for different values of TS factor  $\alpha$ . It is concluded from Fig. 4.5 that the SU attains the best performance at lower values of  $\alpha$ , since the SU with EH-ATI decodes information only for  $(1 - \alpha)T/2$  of its time block. Hence for  $\alpha = 0$  the SU

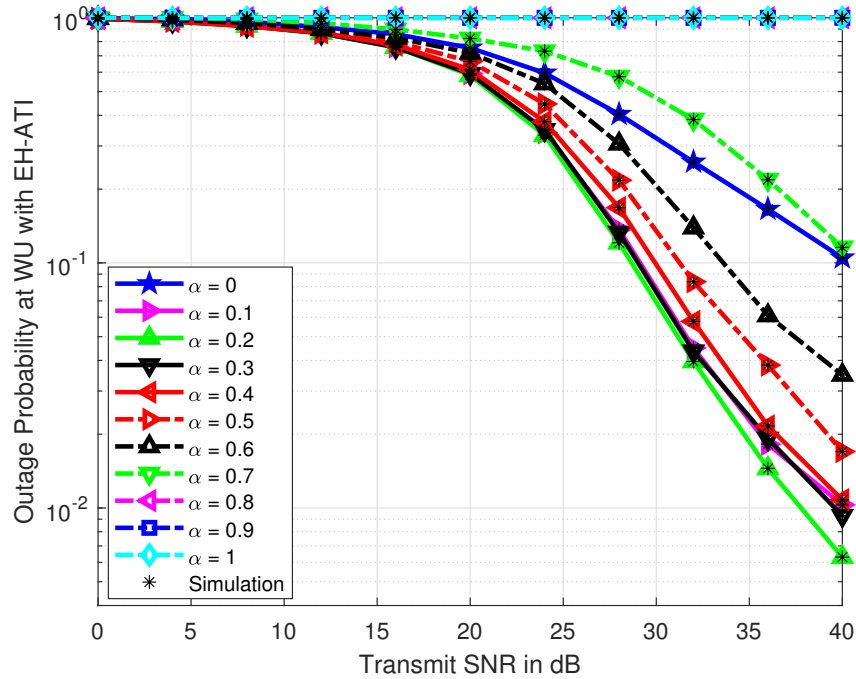


Figure 4.6: Outage probability at WU versus transmit SNR for different values of TS factor  $\alpha$

achieves the best outage performance. However, from Fig. 4.6, it is observed that WU achieves the best outage performance at  $\alpha = 0.2$ . The reason is that the SU harvests energy for  $\alpha T$  of its time block, which aids in the cooperative transmission (Phase-2 transmission) and the WU combines SINR from both phases utilizing SC thereby improving the outage performance. Hence  $\alpha = 0.2$  is used for obtaining the outage probability plots shown in Fig. 4.3 and Fig. 4.4. Furthermore, increasing the value of  $\alpha$  reduces the decoding time  $((1 - \alpha)T/2)$  for both the SU and the WU. Hence, increasing  $\alpha$  results in poor outage performance for both the WU and the SU.

The throughput of the system is calculated to obtain overall performance as demonstrated in Fig. 4.7. It is realized from Fig. 4.7 that the performance of the considered system with EH-ATI attains improvement compared to the system with EH-SS. In addition, the system with no EH is better than the system with EH at low transmit SNRs since at low transmit SNRs, the reduction in the performance of the SU prevails over the increase in the performance of the WU. Since the amount of energy harvested depends on the transmit SNR and at low SNR, the power harvested for cooperative communication is insignificant. At high SNR, the performance of

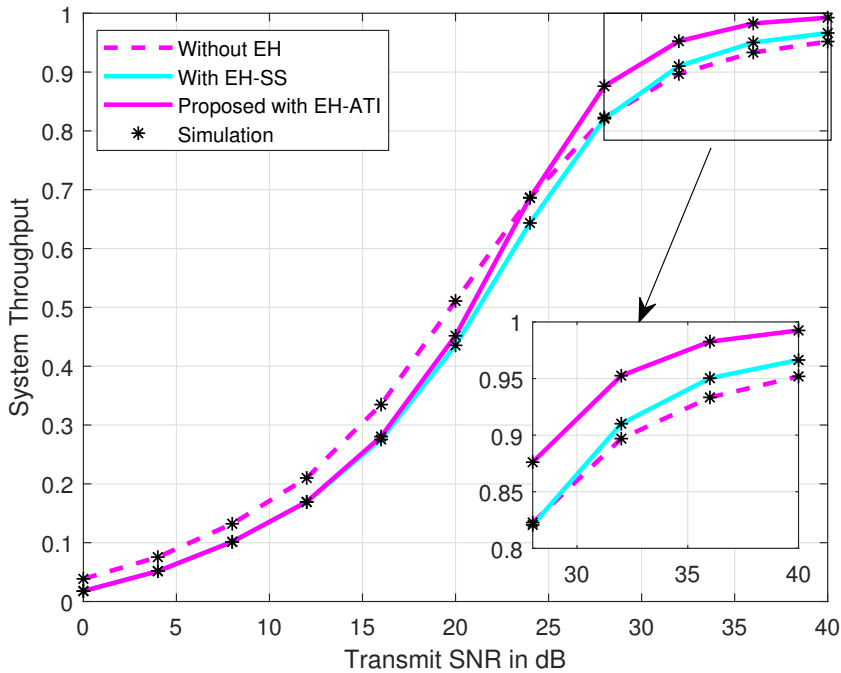


Figure 4.7: System throughput versus transmit SNR for the target rates  $R_1 = 0.5$  and  $R_2 = 0.5$

the EH-enabled system surpasses that of the system without EH. The reason is that the energy harvested is significant at high transmit SNR.

Fig. 4.8 exhibits the energy efficiency of the considered EH-ATI system with respect to transmitting SNR for distinct values of target rates  $R = R_1 = R_2$ . The considered EH-ATI system is also compared to the EH-SS system in terms of energy efficiency. From Fig. 4.8, it can be noticed that the energy efficiency of the considered EH-ATI system is higher than the EH-SS system. The reason is that the considered EH-ATI system achieves better outage performance than the EH-SS system. The plot also illustrates that for a given target rate and at a specific SNR value, the system achieves maximum energy efficiency. The SNR value at which the system achieves maximum energy efficiency varies with the target rate. It is also important to mention that as SNR increases, the energy efficiency of the system under consideration reduces. The reason is that, at high transmit SNR, the energy utilized by the system is greater than the attained system throughput.

The user PF index is compared between the systems, without EH, with EH-SS and with EH-ATI and is shown in Fig. 4.9. It can be noticed from Fig. 4.9 that the considered system with EH-ATI represents user fairness better than any

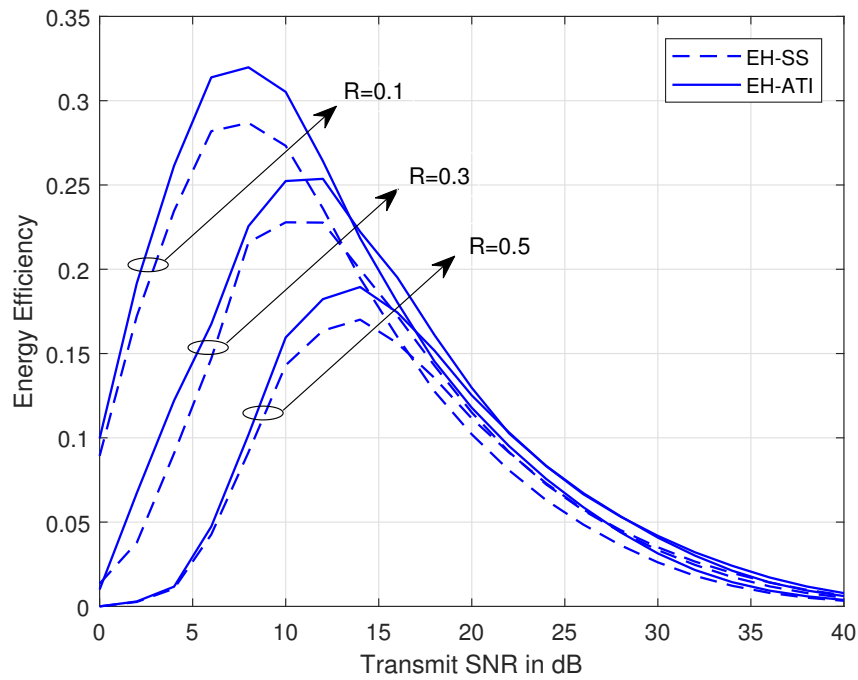


Figure 4.8: Energy efficiency versus transmit SNR

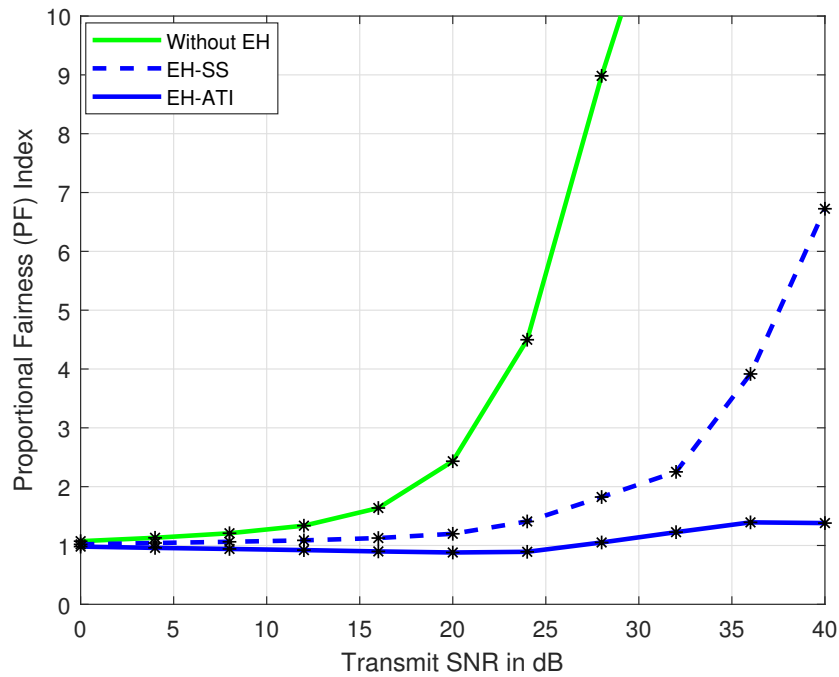


Figure 4.9: PF index versus transmit SNR

other systems. The SU has outage probability closer to the WU for the systems, with EH-SS and with EH-ATI. Also, with the increase of transmit SNR, the PF index increases. The systems, without EH, has the greatest impact on the outage probability of users. The reason is that the outage probability at the WU in the system depends only on the transmission from the direct phase. The WU in EH systems, on the other hand, considers the SINR from both phases.

## 4.4 Summary

In this chapter, the utilization of TS-based EH in a cooperative NOMA two-tier HetNet is investigated, where the distributions of the BSs are depended upon PPP assumptions. At the SU and the WU, expressions of outage probability and system throughput have been evaluated. It has been shown that the SU with EH-ATI suffers degradation in outage probability. However, SU attains flexibility with regards to energy consumption. Moreover, the outage performance of the WU undergoes notable enhancement by utilizing cooperation from SU. Throughput analysis shows that at high transmit SNR the considered system with EH-ATI achieves better performance than the system with EH-SS and the system without EH. Energy efficiency analysis also illustrates superiority of the proposed system with EH-ATI over the system with EH-SS. Finally, the considered system with EH-ATI provides better user fairness as compared to the system with EH-SS and the system without EH.

The previous chapters consider the simple linear energy harvester model where the output power is linearly proportional to the input power. However, as most rectennas include non-linear components (e.g., diodes and capacitors), the input/output relationship is non-linear, hence it is necessary to perform analysis with nonlinear harvester models. In the next chapter, a non-linear energy harvesting model is employed in the proposed models.

## Chapter 5

# SWIPT and NOMA Enabled Heterogeneous Networks with Non-linear Energy Harvesting

In the literature, there have been some recent related works for instance, in [153, 154], where outage probability is analyzed in a cooperative NOMA network however, results are calculated for single-tier scenarios considering a single BS. In the large-scale systems, [144] investigate users' outage probability and energy efficiency, respectively. In [58], the system enabled with NOMA is implemented in a HetNet, and the coverage, and ergodic rate are examined. However, the application of cooperative NOMA and the application of SWIPT between the users to influence the performances in a HetNet scenario, are not addressed in these previous works. Furthermore, the works in [153], [141] and [142] have looked into outage performance in HetNets involving cooperative NOMA utilizing SWIPT however, a linear EH model is considered.

To the best of authors knowledge, no previous research investigates the outage probability of NOMA users for a SWIPT-enabled cooperative NOMA using non-linear energy harvesting in HetNets. This is the first work to derive the outage probability expressions of NOMA users with the SU enabled with SWIPT involving non-linear EH. The proposed non-linear EH model accurately depicts the practical restrictions of the energy harvesting system, for example, the saturation effect, i.e., the maximum power at which output power does not change and brings out novel

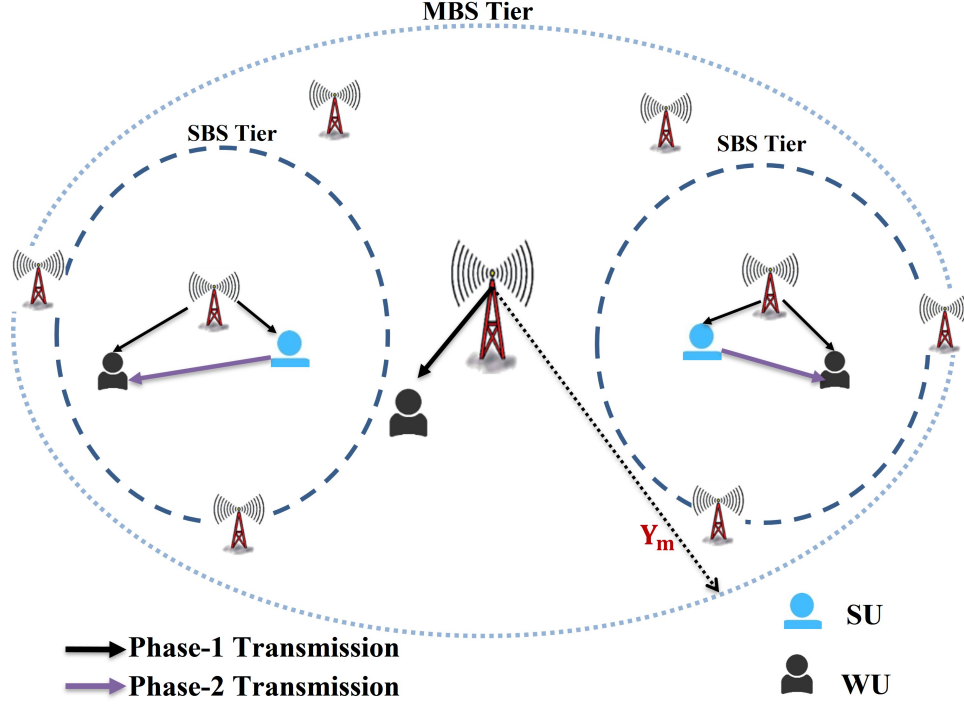


Figure 5.1: Illustration of a downlink NOMA assisted HetNet scenario.

insights into an EH-enabled NOMA-based HetNets. The major contributions of the letter are:

- A NOMA-based HetNet is investigated utilizing SWIPT at the SU considering a practical case of non-linear EH. SU performs cooperative transmission in order to achieve performance improvement at the WU.
- Closed-form expressions for the outage probability at both the NOMA users are evaluated. The system throughput is also analyzed to obtain the overall system performance. The results demonstrate that the considered scheme substantially improves the performance of the WU.
- The analytical results are confirmed through simulations. The proposed system is compared with the benchmark linear EH system [141, 142], the system without EH involving NOMA [155], and the system without EH involving OMA [156, 157].

## 5.1 System and Channel Model

A HetNet comprising of SBS tier and MBS tier is considered with locations of SBS and MBS following independent PPP distribution  $\Omega_t$ , with density  $\lambda_t$  for the  $t^{th}$  tier, such that  $t \in \{m, s\}$ , where  $m$  and  $s$  indicate the MBS-tier and the SBS-tier, respectively as illustrated in Fig. 5.1. The power transmitted by MBS and SBS is indicated as  $\mathcal{P}_m$  and  $\mathcal{P}_s$ , respectively. The coverage radius of the MBS tier and SBS tier is designated as  $\mathcal{Y}_m$  and  $\mathcal{Y}_s$ , respectively, with the focus on the SBS tier with NOMA users. The distribution of users follows independent PPP,  $\Omega_u$  with density  $\lambda_u$ , in the SBS-tier. The SBS selects the NOMA pair based on the random selection scheme [2]. The channel gains between the links are considered to be Rayleigh distributed, and accordingly, the channel gains are exponentially distributed with unit variance. A bounded path loss model for modeling large scale path-loss is considered. Hence, the total channel gain is given as  $\frac{h_t}{(1+r_t^\nu)}$ , where  $\nu$  denotes the path loss exponent,  $h_t$  and  $r_t$ , are the channel power gain and separation between the NOMA user and the tagged SBS, respectively. The total transmission time block,  $T$ , is split into two phases; the EH phase, and the information transmission (IT) phase. In the EH phase, the SU performs EH for  $\alpha T$  of the time block, where  $\alpha$  is the fractional time block wherein the SU harvests energy from the transmitted NOMA signal and the aggregate interference from both the tiers, such that  $0 \leq \alpha \leq 1$ . The IT phase is further divided into Phase-1 and Phase-2, each of  $(1-\alpha)T/2$  of the time block. In the Phase-1, the SBS transmits information to both the NOMA users (the SU and the WU). In the Phase-2, the SU performs cooperative transmission to the WU.

### Phase-1 Transmission

The SBS transmitted message is given as  $X_s = \sum_{k=1}^2 x_k \sqrt{a_k \mathcal{P}_s}$ , where, the signal of the  $k^{th}$  user is denoted by  $x_k$ . The transmitted power in the message  $x_k$  is assumed to be unity i.e.  $\mathbb{E}[x_k^2]=1$  and is equal  $\forall k \in (1, 2)$ , where the operator  $\mathbb{E}[\cdot]$  represents the statistical expectation operator. The received message at the typical  $k^{th}$  user is expressed as

$$Y_k = \sqrt{h_k(1+r_k^\nu)^{-1}} X_s + n_k, \quad (5.1)$$

where  $\frac{h_k}{1+r_k^\nu}$  is the total channel gain between the BS and the  $k^{\text{th}}$  user for  $k \in \{1, 2\}$ . It is assumed that  $\frac{h_1}{1+r_1^\nu} \leq \frac{h_2}{1+r_2^\nu}$  therefore, User 1 is WU, and User 2 is SU.  $n_k \sim \mathcal{N}(0, \sigma_k^2)$  is the noise at the  $k^{\text{th}}$  user. Utilizing the NOMA principle, SU performs SIC to decode its signal by eliminating the WU's signal. The SINR received at the SU for detecting the WU signal is described as

$$\gamma_{2 \rightarrow 1}^1 = \frac{\rho_s a_1 h_2 (1 + r_2^\nu)^{-1}}{\rho_s a_2 h_2 (1 + r_2^\nu)^{-1} + \rho_s I_s + \rho_m I_m + 1}, \quad (5.2)$$

where  $\rho_s = \mathcal{P}_s / \sigma_2^2$  is the transmit signal-to-noise ratio (SNR) at SU, and  $\rho_m = \mathcal{P}_m / \sigma_2^2$ .  $I_s = \sum_{y \in \Omega_s / \{s_o\}} h_y$  is the total SBS-tier interference at the SU, where  $h_y$  is the total channel gain between the SU and the  $y^{\text{th}}$  SBS, and  $s_o$  represents the assigned SBS. Likewise,  $I_m = \sum_{u \in \Omega_m} h_u$  is the total MBS-tier interference at the SU, such that  $h_u$  represent the total channel gain between the typical SU and the  $u^{\text{th}}$  MBS. The SU's SINR for detecting its signal is described as

$$\gamma_2^1 = \frac{\rho_s a_2 h_2 (1 + r_2^\nu)^{-1}}{\rho_s I_s + \rho_m I_m + 1}. \quad (5.3)$$

It is presumed that the SU have energy storage ability [2] and TS protocol [103] is incorporated at SU to perform EH. In the EH phase, the SU harvests energy for cooperative transmission in Phase-2. The energy harvested ( $\mathcal{E}_2$ ) at SU from the transmitted signal is given as

$$\mathcal{E}_2 = \alpha T \left( \frac{a \mathcal{P}_s h_2 (1 + r_2^\nu)^{-1} + b}{\mathcal{P}_s h_2 (1 + r_2^\nu)^{-1} + c} - \frac{b}{c} \right), \quad (5.4)$$

where  $a$ ,  $b$ , and  $c$  are values obtained from the rectifier circuit by curve fitting [158]. Note that the energy harvested based on the linear EH model is also considered, represented by  $\mathcal{E}_2 = \alpha T \zeta (\mathcal{P}_s h_2 (1 + r_2^\nu)^{-1})$ , where  $\zeta$  is the linear energy harvester's conversion efficiency. It is helpful to utilize the linear EH model as a performance standard. Let  $\mathcal{P}_2$  represent the transmit power from SU, to be used in Phase-2 transmission, which is given by

$$\mathcal{P}_2 = \frac{2\alpha}{1 - \alpha} \left( \frac{a \mathcal{P}_s h_2 (1 + r_2^\nu)^{-1} + b}{\mathcal{P}_s h_2 (1 + r_2^\nu)^{-1} + c} - \frac{b}{c} \right). \quad (5.5)$$

The SINR received at the typical WU in Phase-1 transmission is given by

$$\gamma_1^1 = \frac{\mathcal{P}_s a_1 h_1 (1 + r_1^\nu)^{-1}}{\mathcal{P}_s a_2 h_1 (1 + r_1^\nu)^{-1} + \mathcal{P}_s I'_s + \mathcal{P}_m I'_m + \sigma_1^2}. \quad (5.6)$$

### Phase-2 Transmission

In this phase, the message is forwarded to the WU by the SU. The SINR to decode  $x_1$  at WU is given by

$$\gamma_1^2 = \frac{\mathcal{P}_2 h_{12} (1 + r_{12}^\nu)^{-1}}{\mathcal{P}_s I'_s + \mathcal{P}_m I'_m + \sigma_1^2}, \quad (5.7)$$

where  $h_{12} (1 + r_{12}^\nu)^{-1}$  is the total channel power gain for the link  $SU \rightarrow WU$ ,  $r_{12}$  denotes the distance between the SU and WU. The WU utilizes the SC [124] technique to choose the highest SINR from SBS and SU. This is achieved by considering the maximal received SINR from (5.6) and (5.7), the received SNR at the WU is given by

$$\gamma_1^{sc} = \max(\gamma_1^1, \gamma_1^2). \quad (5.8)$$

## 5.2 Performance Analysis

### 5.2.1 Outage Probability at SU

The outage probability at the SU depends upon the successful SIC of WU's signal. The SU goes into outage when SU cannot detect the signal of WU, and also when SU detect the signal of WU but cannot detect its own signal. Therefore, outage probability expression at the WU is described as

$$P_{out}^{su} = \mathcal{P}(\gamma_{2 \rightarrow 1}^1 < \phi_1) + \mathcal{P}(\gamma_{2 \rightarrow 1}^1 \geq \phi_1, \gamma_2^1 < \phi_2), \quad (5.9)$$

where  $\phi_1 = 2^{\frac{2R_1}{1-\alpha}} - 1$  and  $\phi_2 = 2^{\frac{2R_2}{1-\alpha}} - 1$ , with  $R_1$  and  $R_2$  represents the targeted rate to decode the messages of SU and WU successfully.

**Proposition 1**

Depending on the PPP model, the outage probability at the SU is defined as

$$P_{out}^{su} = \frac{1}{2} \sum_{l=0}^L b_l e^{-c_l \epsilon_1} \mathcal{L}_{I_p}[s_p], \quad (5.10)$$

where  $\mathcal{L}_{I_p}[s_p] = \mathcal{L}_{I_s}[s_s] \mathcal{L}_{I_m}[s_m]$ ,  $s_s = \rho_s \epsilon_1 c_l$  and  $s_m = \rho_m \epsilon_1 c_l$ ,  $\epsilon_1 = \frac{\phi_1}{\rho_s(a_1 - \phi_1 a_2)}$  and  $\epsilon_2 = \frac{\phi_2}{\rho_s a_2}$ ,  $b_l = -\omega_L(1 + \psi_l) \sqrt{1 - \psi_l^2}$ ,  $b_0 = -\sum_1^L b_l$ ,  $\omega_L = \pi/L$ ,  $\psi_l = \cos\left(\frac{2n-1}{2L}\pi\right)$ ,  $c_l = 1 + \left(\frac{\mathcal{Y}_s}{2}\psi_l + \frac{\mathcal{Y}_s}{2}\right)^\nu$ ,  $c_0 = 0$ ,  $L$  is a parameter to provide complexity-accuracy trade-off for the Gaussian-Chebyshev (G-C) quadrature. The Laplace transform (LT) of the  $t^{th}$  tier such that  $t \in \{m, s\}$ , is described [134] as

$$\mathcal{L}_{I_t}(s) = e^{\pi \lambda_t (s^{\delta_t} \Gamma(1 - \delta_t, s) - s^{\delta_t} \Gamma(1 - \delta_t))}, \quad (5.11)$$

where  $\delta_t = \frac{2}{\nu_t}$ ,  $\Gamma(a, x)$  is lower incomplete gamma function and  $\Gamma(z)$  is the gamma function. For the SBS tier, the path-loss exponent  $\nu$  is used instead of  $\nu_s$  throughout.

**Proof**

Let us represent the total channel power gain with random variables  $X$ ,  $Y$  and  $Z$ . Such that,  $h_1(1+r_1^\nu)^{-1} = X$ ,  $h_2(1+r_2^\nu)^{-1} = Y$ , and  $h_{12}(1+r_{12}^\nu)^{-1} = Z$ . The probability density function (PDF) of  $X$ ,  $Y$ , and  $Z$  are given by expressions  $f_X(x) = (1+r_1^\nu)e^{-(1+r_1^\nu)x}$ ,  $f_Y(y) = (1+r_2^\nu)e^{-(1+r_2^\nu)y}$ , and  $f_Z(z) = (1+r_{12}^\nu)e^{-(1+r_{12}^\nu)z}$ , where,  $r_1$ ,  $r_2$  and  $r_{12}$  denote the distances from SBS to WU, from SBS to SU, and from WU to SU, respectively. The cumulative distribution function (CDF) of random variable  $Y$  is described as

$$\mathcal{F}_Y(y) = \frac{2}{\mathcal{Y}_s^2} \int_0^{\mathcal{Y}_s} \left(1 - e^{-(1+r_2^\nu)y}\right) r_2 dr_2. \quad (5.12)$$

Approximating CDF by utilizing G-C quadrature [127], as

$$\mathcal{F}_Y(y) \approx \frac{1}{2} \sum_{l=0}^L b_l e^{-c_l y}. \quad (5.13)$$

$$\begin{aligned}
P_{out}^{wu} &= \frac{1}{4} \sum_{l=0}^L \sum_{k=0}^K b_l b_k e^{-(c_l+c_k)\epsilon_1} \mathcal{L}_{I_p}[s_p] \mathcal{L}'_{I_p}[s_p] + \frac{1}{2} \sum_{l=0}^L b_l e^{-c_l \epsilon_1} \mathcal{L}_{I_p}[s_p] \times \\
&\left( 1 - \lim_{B \rightarrow \infty} \frac{\pi^2 B}{NM \mathcal{Y}_s^3} \sum_{n=1}^N \sum_{m=1}^M b_m (1 - \theta_n^2)^{\frac{1}{2}} \frac{e^{-\chi_n} e^{-c_m Q_1 K_n}}{\nu^2 \chi_n^{1+\frac{2}{\nu}}} \left( (2 + \nu \chi_n) \Gamma\left(\frac{2}{\nu}\right) - \nu \times \right. \right. \\
&\left. \left. \chi_n \Gamma\left(\frac{2}{\nu}, \mathcal{Y}_s^\nu \chi_n\right) - \nu \Gamma\left(\frac{2+\nu}{\nu}, \mathcal{Y}_s^\nu \chi_n\right) \right) \mathcal{L}_{I_s}[C_{nm} \rho_s] \mathcal{L}_{I_m}[C_{nm} \rho_m] \right) \quad (5.16)
\end{aligned}$$


---

(5.9) is rearranged in the form containing  $Y$  as

$$P_{out}^{su} = \mathcal{P}(Y < \epsilon_1) + \mathcal{P}(Y \geq \epsilon_1, Y < \epsilon_2), \quad (5.14)$$

where  $\mathcal{P}(Y \geq \epsilon_1, Y < \epsilon_2)$  of (5.14) gives outage for  $\epsilon_1 < \epsilon_2$ . Thus, for the case when  $\epsilon_1 \geq \epsilon_2$ , the  $P_{out}^{su}$  is specified by CDF of  $Y$  with  $y = \epsilon_1(1 + \rho_s I_s + \rho_m I_m)$ , and substituting  $y$  in (5.13) to obtain (5.10).

## 5.2.2 Outage Probability at WU

The WU goes into outage when both the SU and the WU are not able to decode the signal of the WU, and also when the SU decodes the signal of the WU however, the WU is not able to attain the targeted rate in Phase-2. Thus, outage probability expression at the WU is described as

$$P_{out}^{wu} = \underbrace{\mathcal{P}(\gamma_{2 \rightarrow 1}^1 < \phi_1, \gamma_1^1 < \phi_1)}_{\Theta_1} + \underbrace{\mathcal{P}(\gamma_{2 \rightarrow 1}^1 > \phi_1, \gamma_1^{sc} < \phi_1)}_{\Theta_2}. \quad (5.15)$$

### Proposition 2

The outage probability at the WU is given in (5.16).

### Proof

From equation (5.15),  $\Theta_1 = \mathcal{P}(\gamma_{2 \rightarrow 1}^1 < \phi_1, \gamma_1^1 < \phi_1)$  and  $\Theta_2 = \mathcal{P}(\gamma_{2 \rightarrow 1}^1 > \phi_1, \gamma_1^{sc} < \phi_1)$ . The conditions in  $\Theta_1$  are independent. Therefore,  $\Theta_1$  can be obtained as

$$\Theta_1 = \mathcal{P}(\gamma_{2 \rightarrow 1}^1 < \phi_1) \mathcal{P}(\gamma_1^1 < \phi_1), \quad (5.17)$$

$\mathcal{P}(\gamma_{2 \rightarrow 1}^1 < \phi_1)$  is already derived and simultaneously  $\mathcal{P}(\gamma_1^1 < \phi_1)$  is derived, i.e., by considering the random variable  $X = h_1(1 + r_1')^{-1}$ . The analytical expression of  $\Theta_1$ , is given as

$$\Theta_1 = \frac{1}{4} \sum_{l=0}^L \sum_{k=0}^K b_l b_k e^{-(c_l + c_k)\epsilon_1} \mathcal{L}_{I_p}[s_p] \mathcal{L}'_{I_p}[s_p], \quad (5.18)$$

where  $\mathcal{L}_{I_p}[s_p]$  and  $\mathcal{L}'_{I_p}[s_p]$  represent the LT of the interference at SU and the WU, during the Phase-1 transmission, respectively.  $\Theta_2$  is given as

$$\Theta_2 = \underbrace{\mathcal{P}(\gamma_1^1 < \phi_1)}_{\Theta_{21}} \underbrace{\mathcal{P}(\gamma_{2 \rightarrow 1}^1 \geq \phi_1, \gamma_1^2 < \phi_1)}_{\Theta_{22}}. \quad (5.19)$$

The evaluation of  $\Theta_{21}$  is completed in (5.18). Therefore, the expression of  $\Theta_{21}$  is given as

$$\Theta_{21} = \frac{1}{2} \sum_{l=0}^L b_l e^{-c_l \epsilon_1} \mathcal{L}_{I_p}[s_p]. \quad (5.20)$$

Consider  $\rho_s \mathcal{I}_s + \rho_m \mathcal{I}_m = \mathcal{I}$ ,  $\rho_s \mathcal{I}'_s + \rho_m \mathcal{I}'_m = \mathcal{I}'$ ,  $\epsilon_1 = \frac{\phi_1}{\rho_s(a_1 - \phi_1 a_2)}$  and  $\epsilon'_1 = \epsilon_1(\mathcal{I} + 1)$  so  $Y \geq \epsilon'_1$  using this  $\Theta_{22}$  can be given from (5.19) as

$$\begin{aligned} \Theta_{22} &= \mathcal{P}\left(Z < \frac{c(1-\alpha)\phi_1(P_s Y + c)(\mathcal{I}' + 1)}{2\alpha(ac-b)\rho_s Y}, Y \geq \epsilon'_1\right) \\ &= \int_0^{\mathcal{Y}_s} \int_0^{\mathcal{Y}_s} \underbrace{\int_{\epsilon'_1}^{\infty} F_Z\left(\frac{c(1-\alpha)\phi_1(P_s y + c)(\mathcal{I}' + 1)}{2\alpha(ac-b)\rho_s y}\right)}_{\mathcal{I}_1} \times \\ &\quad f_Y(y) dy f_{\mathcal{Y}_s}(r_1) dr_1 f_{\mathcal{Y}_s}(r_2) dr_2. \end{aligned} \quad (5.21)$$

The above expression becomes intractable due to limits of  $\mathcal{I}_1$ . Hence to solve the expression, high SNR approximation [142] is considered, i.e.  $\rho_s \rightarrow \infty$  implies  $\epsilon' \approx 0$ . let us take  $Q_1 = \frac{c(1-\alpha)\phi_1}{2\alpha(ac-b)\rho_s}$  and applying G-C Quadrature to  $\mathcal{I}_1$  after changing the upper limit of integration of  $\mathcal{I}_1$  to be  $\mathcal{B}$  and taking the limit as  $\mathcal{B} \rightarrow \infty$ ,  $\mathcal{I}_1$  in (5.21)

is approximated as

$$\begin{aligned} \mathcal{I}_1 &\approx 1 - \lim_{B \rightarrow \infty} \frac{\pi B}{2N} \sum_{n=1}^N (1 - \theta_n^2)^{\frac{1}{2}} (1 + r_2^\nu) \left( e^{(1+r_2^\nu)Q_1 K_n} \right) \times \\ &\mathbb{E}_{I'_m} \left[ e^{-s_m \mathcal{I}'_m} \right] \mathbb{E}_{I'_s} \left[ e^{-s_s \mathcal{I}'_s} \right] e^{-\frac{(1+r_2^\nu)(1+\theta_n)B}{2}}, \end{aligned} \quad (5.22)$$

where  $K_n = (P_s + \frac{2c}{(\theta_n+1)B})$ ,  $s = (1+r_2^\nu)Q_1 K_n$ ,  $s_m = \rho_m s$ ,  $s_s = \rho_s s$ ,  $\theta_n = \cos\left(\frac{2n-1}{2N}\pi\right)$ . Taking  $\mathcal{I}_1$  from (5.22) and substituting in (5.21). Applying  $f_{\mathcal{Y}_s}(r_1) = \frac{2r_1}{\mathcal{Y}_s^2}$ ,  $f_{\mathcal{Y}_s}(r_2) = \frac{2r_2}{\mathcal{Y}_s^2}$  and approximating the distance as  $r_{12} \approx r_1$ ,  $\Theta_{22}$  is given as

$$\begin{aligned} \Theta_{22} &= 1 - \lim_{B \rightarrow \infty} \frac{2\pi B}{N\mathcal{Y}_s^4} \sum_{n=1}^N \underbrace{\int_0^{\mathcal{Y}_s} (1 + r_2^\nu) e^{-\frac{(1+r_2^\nu)(1+\theta_n)B}{2}} r_2 dr_2}_{\mathcal{I}_2} \times \\ &\underbrace{(1 - \theta_n^2)^{\frac{1}{2}} \int_0^{\mathcal{Y}_s} (e^{-(1+r_1^\nu)Q_1 K_n}) \mathbb{E}_{I'} \left[ e^{-s\mathcal{I}'} \right] r_1 dr_1}_{\mathcal{I}_3}. \end{aligned} \quad (5.23)$$

Approximating  $\mathcal{I}_3$  by utilizing G-C quadrature and solving for  $\mathcal{I}_2$ , to get the expression of  $\Theta_{22}$  as

$$\begin{aligned} \Theta_{22} &= 1 - \lim_{B \rightarrow \infty} \frac{\pi^2 B}{NM\mathcal{Y}_s^3} \sum_{n=1}^N \sum_{m=1}^M b_m (1 - \theta_n^2)^{\frac{1}{2}} \times \\ &\frac{e^{-\chi_n} e^{-c_m Q_1 K_n}}{\nu^2 \chi_n^{1+\frac{2}{\nu}}} \left( (2 + \nu \chi_n) \Gamma\left(\frac{2}{\nu}\right) - \nu \chi_n \Gamma\left(\frac{2}{\nu}, \mathcal{Y}_s^\nu \chi_n\right) - \right. \\ &\left. \nu \Gamma\left(\frac{2 + \nu}{\nu}, \mathcal{Y}_s^\nu \chi_n\right) \right) \mathcal{L}_{I_s} [C_{nm} \rho_s] \mathcal{L}_{I_m} [C_{nm} \rho_m], \end{aligned} \quad (5.24)$$

where  $\chi_n = \frac{(1+\theta_n)B}{2}$ ,  $b_m = (1 + \varphi_m)(1 - \varphi_m^2)^{\frac{1}{2}}$ ,  $c_m = 1 + ((1 + \varphi_m)\frac{\mathcal{Y}_s}{2})^\nu$ ,  $\varphi_m = \cos\left(\frac{2m-1}{2M}\pi\right)$ , and  $C_{nm} = Q_1 c_m K_n$ . Substituting  $\Theta_{21}$  and  $\Theta_{22}$  from (5.20) and (5.24) into (5.19), respectively to obtain  $\Theta_2$ . Then, substituting for  $\Theta_1$  and  $\Theta_2$  in (5.15) to get a close form expression of outage probability at WU.

### 5.2.3 System Throughput

Utilizing the outage probability at the SU and at the WU, the throughput of the system is evaluated to determine the overall system performance [2], and is expressed

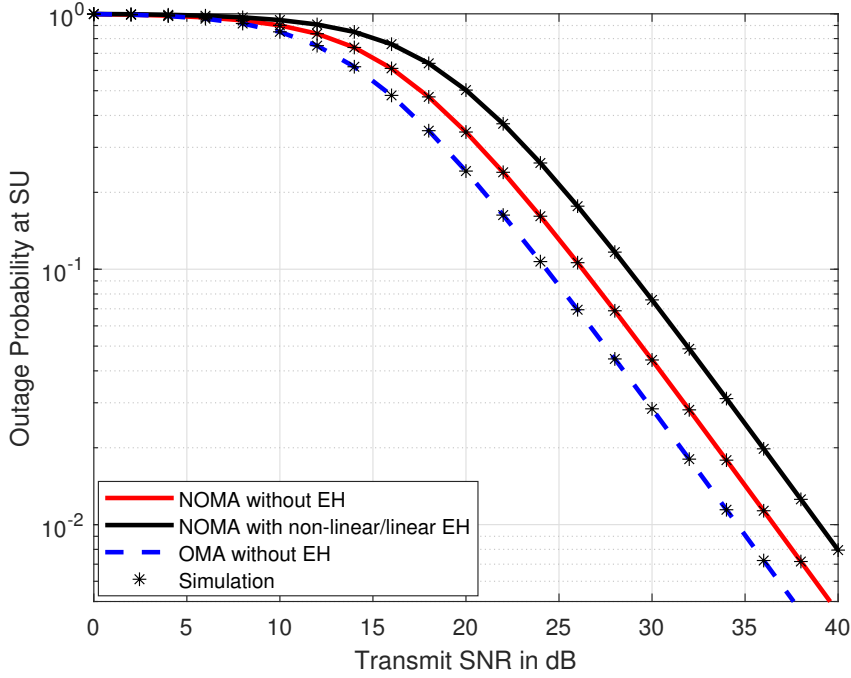


Figure 5.2: Variation of outage probability at the SU with transmit SNR.

as

$$T_{sys} = \frac{(1 - \alpha)}{2} ((1 - P_{out}^{wu})R_1 + (1 - P_{out}^{su})R_2). \quad (5.25)$$

### 5.3 Results and Discussions

The mathematical results derived in Section 5.2 are explained in this section. The results of the analysis are validated for an ensemble of  $10^5$  using Monte Carlo simulations. The considered parameters for obtaining the mathematical and simulation results are given as [1]  $L=10$ ,  $N=10$ ,  $K=10$ ,  $M=10$ ,  $\mathcal{B}=1000$ ,  $\mathcal{P}_m = 40\text{W}$ ,  $\mathcal{P}_s = 1\text{W}$ ,  $\lambda_m = 10^{-4}\text{m}^{-2}$ ,  $\lambda_s = 10^{-3}\text{m}^{-2}$ ,  $\mathcal{Y}_m = 1\text{km}$ ,  $\mathcal{Y}_s = 10\text{m}$ ,  $\nu = 4$ ,  $\nu_m = 3$ ,  $a_1 = 0.8$ , and  $a_2 = 0.2$ . The normalization constants for the non-linear EH model are set at  $a = 2.463$ ,  $b = 1.635$ , and  $c = 0.826$  [158]. The fractional time block  $\alpha$  is chosen as 0.3 [159]. For comparison, NOMA and OMA schemes are considered, such that both schemes are not employing cooperative transmission. NOMA scheme uses a single time slot to serve the two users, whereas OMA uses two different time slots to serve two users. The system with benchmark NOMA scheme [153, 155] is denoted

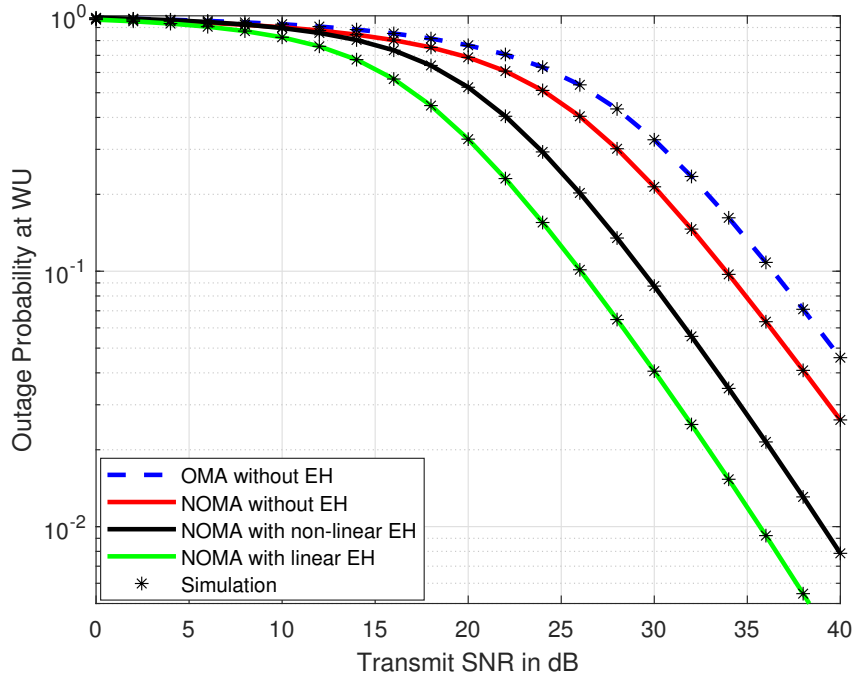


Figure 5.3: Variation of outage probability at the WU with transmit SNR.

as NOMA without EH, whereas the benchmark system with OMA [156, 157], is denoted as OMA without EH. Furthermore, the proposed scheme, denoted as NOMA with non-linear EH, is also compared with linear EH scheme [141, 142] under the same setting as the proposed scheme denoted as NOMA with linear EH.

Fig. 5.2 exhibits the outage probability of SU versus the transmit SNR plot. At the transmit SNR of 30dB, a degradation of 62% in the outage probability performance of NOMA with non-linear/linear EH, as compared to OMA without EH case, is observed. Furthermore, degradation of 42% in the performance of NOMA with non-linear/linear EH is observed in comparison to the outage probability at the SU without EH. This is observed since the SU in NOMA with non-linear/linear EH decodes information only for  $(1 - \alpha)T/2$  of its time block. However, the SU in NOMA without EH and SU in OMA without EH dedicate the entire time block and  $T/2$  of the time block for information decoding, respectively. The outage probability at the SU for the NOMA with a non-linear EH model and with linear EH are the same. This is because both systems dedicate  $\alpha T$  for harvesting energy.

Fig. 5.3 exhibits the outage probability of WU with respect to the SNR. At the transmit SNR of 30dB, it can be inferred that an enhancement of 59% and 73% is observed in the performance of NOMA with non-linear EH in comparison to the

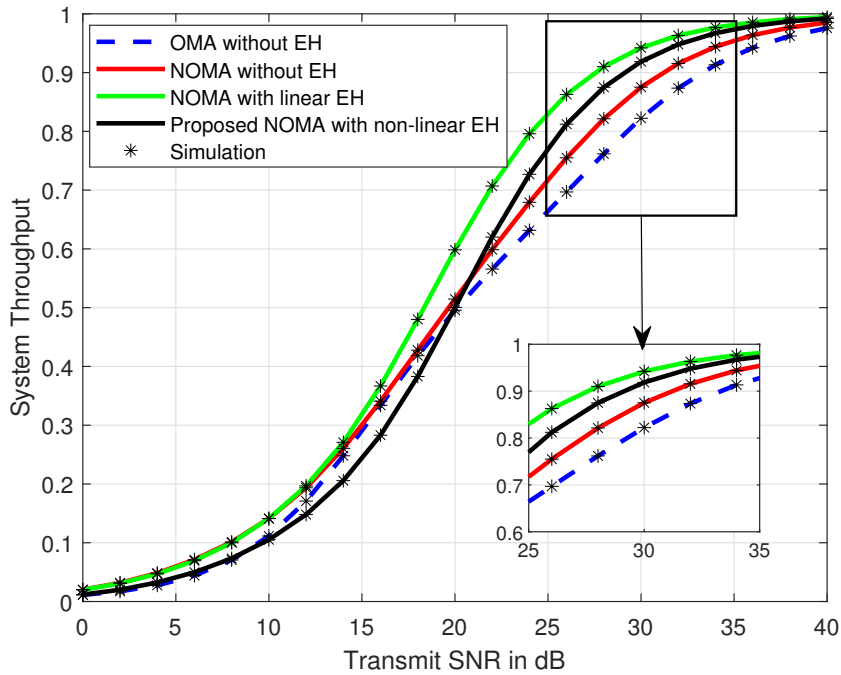


Figure 5.4: System throughput versus transmit SNR for the target rates  $R_1=0.5$  and  $R_2=0.5$ .

WU in NOMA without EH and OMA without EH, respectively. This is because the WU in NOMA with non-linear EH derives its signal through SC, while, the WU in NOMA without EH and WU in OMA without EH only obtains its signal from Phase-1. Fig. 5.3 also shows a difference between the outage probability of the considered NOMA with non-linear EH and the NOMA with linear EH, since for non-linear EH models, the performance saturates for higher transmit SNRs.

The throughput of the system is calculated to obtain overall performance as demonstrated in Fig. 5.4. It is realized from Fig. 5.4 that the performance of the system with NOMA but without EH attains better performance in comparison to the system with NOMA and non-linear EH at low transmit SNR. This is because at low transmit SNR, degradation in the performance of the SU is higher as compared to increase in the performance of the WU. Since, the amount of energy harvested depends on the transmit SNR and at low SNR, the power harvested for cooperative communication is not significant. At high SNR, the performance of the EH-enabled system surpasses that of the system without EH, Since the energy harvested is significant at high transmit SNR.

## 5.4 Summary

This work investigates the utilization of a non-linear EH model in a cooperative NOMA two-tier HetNet. At the SU and the WU, outage probability and system throughput expressions have been evaluated. It has been shown that the SU with non-linear EH suffers degradation in outage probability. However, SU attains flexibility with regard to energy consumption. Moreover, the outage performance of the WU undergoes notable enhancement by utilizing cooperation from SU. Throughput analysis shows that at high transmit SNR, the system with a non-linear EH model achieves better performance than the system without EH. Furthermore, the linear EH model fails to represent the saturation region of practical EH circuits. To overcome this limitation, a non-linear EH model is used to provide useful insights for the design and realization of HetNets. In the previous chapters SWIPT is used to power the energy constrained device however, due to a big gap between the active sensitivity of the energy harvester and that of the decoder, the SWIPT-based systems are only appropriate for short distance communication. To overcome this limitation, PB is used to supply power for wireless devices. PBs are low-cost stations for recharging wireless IoT devices as they do not require any computational capabilities and backhaul links. Therefore, they can be deployed in large numbers at locations with connections to the electrical grid. Hence, in the next chapter a practical PB-assisted downlink NOMA system model is analyzed.



# Chapter 6

## Power Beacons Assisted NOMA Based Wireless Powered Communication Networks

The number of IoT devices are increasing and evolving rapidly, which inevitably results in the ubiquitous deployment of low-powered devices and a large amounts of data flow [160]. The application of appropriate multiple access schemes is a well-known and effective method for supporting a large number of devices and data flow. Next generation multiple access (NGMA) [161] schemes are being considered in the 6G wireless systems to overcome these challenges since they combine existing schemes and incorporate novel concepts like NOMA. In comparison to the traditional multiple access schemes, NOMA is a crucial enabling technology for achieving improved performance by encouraging spectrum sharing among wireless devices with different QoS requirements [153]. Power domain NOMA connects a massive number of devices by utilizing the same time/frequency resources, thereby improving capacity and throughput performance as compared to the conventional OMA.

The growing demands for widespread connectivity for IoT devices can be met with the help of networks combined with NOMA, which can also improve spectral and energy efficiency [141]. However, the need for sufficient and constant power supplies (batteries) is one of the most prevalent challenges when deploying IoT devices in a practical context. For 6G network, Ericsson proposed their concept of zero-energy devices [162], with a battery life of up to 10 years. Additionally,

charging or replacing the batteries of these devices on a regular basis limits their usability. To overcome this issue, wireless power transfer (WPT) is proving to be a potential method for extending the lifespan of power-constrained equipment [153]. In a WPCN, PBs are set up to wirelessly provide RF power to wireless devices, and sensors [163]. PBs are low-cost stations for recharging wireless IoT devices as they do not require any computational capabilities and backhaul links [164]. Therefore, they can be deployed in large numbers at locations with connections to the electrical grid, making them suitable for mounting on the BS in the WPCN. PB-assisted EH provides a consistent and readily controllable amount of energy as compared to the BS while operating at different frequencies [165]. The WPCN assisted with NOMA and PB can be applied to various IoT applications, such as smart buildings, smart bridges, smart homes, smart healthcare, and smart agriculture. For example, in a smart agriculture scenario, when the relay communicates simultaneously with a smartphone and transmits a low data rate control signal to a device, when device is a water sprinkler, humidity sensor, pesticide sprayer, and others.

## 6.1 Communication scenarios and contribution

Many recent works highlight the advantage of NOMA combined with PB-assisted EH to improve spectral efficiency and energy efficiency. For example, in [163], and [166], the power beacon-aided wireless NOMA network has been investigated in which all the transmitting nodes use EH from a PB. However, the existing works assume a linear EH model which is far from the practical scenario. Multi-user relaying with NOMA and EH is studied in [165], and [167] with a practical non-linear EH model however, the locations of BS and relays are assumed to be fixed. [157] investigated the performance of a PB-assisted WPCN, where multiple relays are distributed to communicate with a common information receiver. However, the work in [157] did not consider NOMA. Furthermore, the distribution of BS and the use of stochastic geometry for analysis is also not considered in the present literature.

In the 6G wireless networks, the envisioned IoT devices often have low power consumption and compact sizes, which commensurate with their lower computational performances. As a result, energy harvesting devices used in IoT applications are compact sensors having a smaller hardware footprint with simple and cheap

circuitry, thus, in these situations, non linearity in EH must be taken into account, since it may be quite challenging to practically deploy different energy harvesters in order to reduce nonlinear effects. The necessity of non-linear model for IoT devices has inspired this chapter to analyze the performance of IoT devices in such networks, which to the best of authors' knowledge, has not been fully addressed in the existing works. In particular, the significant contributions are summarized as follows:

- Motivated by the advantages of PB for powering WPCN and the NOMA protocols to support massive number of IoT devices with heterogeneous QoS requirements, this chapter proposes a WPCN system that employs PB at the BS to power the battery-less IoT devices in assisting the communication.
- The model introduces an intermediate node (IN), acting as a relay to assist the BS in communicating with a blocked user (BU). IN harvests energy from the PB to power the relay transmission. Unlike the existing works, this chapter uses a non-linear EH model at IN. Furthermore, the BS and INs are distributed using the PPP. PPP provides a mathematically tractable and spatially realistic model for system design.
- IN uses the licensed band in underlay mode to forward its signal to a delay-tolerant (DT) IoT device by simultaneously superimposing the signal of the BU received from the BS using the NOMA protocol. Using IN as a relay in underlay mode encourages spectrum sharing among wireless devices with different QoS requirements and provides connectivity to the blocked users.
- The approximate closed-form expression of outage probability is evaluated at the users. Furthermore, the performance of the proposed system is analyzed in terms of outage probability, system throughput, and EE. Additionally, considering the same communication scenario, a comparison between the proposed system and the system employing OMA [124, 156, 157], is made.

## 6.2 System Model

Considering WPCN wherein the locations of the BS follow independent PPP distribution,  $\Omega_b$  with density  $\lambda_b$ , a more practical system model is proposed. The IN

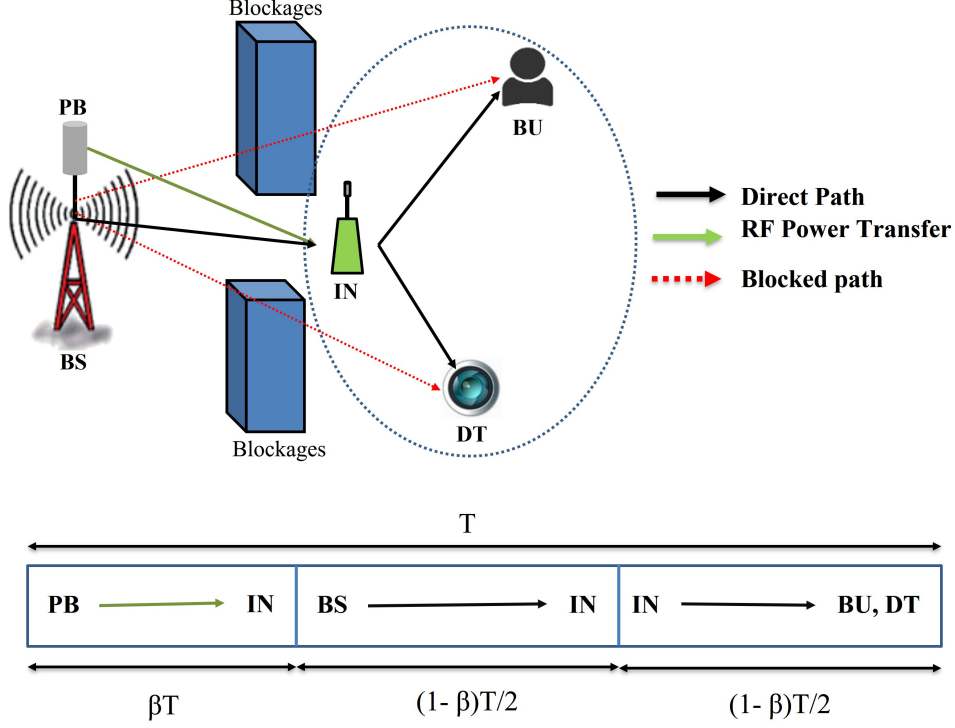


Figure 6.1: Illustration of a downlink PB assisted WPCN scenario and total transmission time block with time splitting protocol.

is distributed as an independent and stationary point process  $\Omega_u$  with density  $\lambda_i$ . BS selects IN based on a random selection scheme such that  $\lambda_i \gg \lambda_b$ . The random selection scheme is more beneficial in terms of complexity than other selection schemes as there is a dense distribution of INs [2]. The power transmitted by BS is indicated as  $\mathcal{P}_b$ . The coverage area of BS is designated as  $\mathcal{Y}_b$ . A PB is configured on the BS to broadcast RF energy to power the IN. A downlink NOMA-based IoT communication scenario [167] is considered wherein the BS communicates with the BU with the assistance of IN. In order to achieve higher SE and EE, the IN broadcasts superimposed NOMA signals for the BU and the DT. It is assumed that there is no direct link between the BS and the BU as well as the DT. The channel between the links are considered to be quasi-static Rayleigh distributed denoted by  $h_i$ , where  $i \in \{bs, ib, id\}$  for  $BS \rightarrow IN$ ,  $IN \rightarrow BU$  and  $IN \rightarrow DT$  link, respectively. Accordingly, the channel gains are exponentially distributed with unit variance. This work considers the large-scale path loss as  $\frac{1}{\sqrt{1+r_i^\nu}}$ , where  $\nu$  denotes the path loss exponent.  $r_i$  is the separation between the links, where  $i \in \{bs, ib, id\}$  for  $BS \rightarrow IN$ ,  $IN \rightarrow BU$  and  $IN \rightarrow DT$  link, respectively. Therefore the total

channel gain between the links is represented as  $\frac{|h_i|^2}{1+r_i^\nu}$ . The DT and the BU are located at a fixed distance from IN. The time splitting protocol is considered, which involves the information transmission phase and the EH phase. In the EH phase, the PB supply energy to the IN for  $\beta T$  duration, where  $\beta$  ( $0 \leq \beta \leq 1$ ), and  $T$  are the time splitting factor and the total coherence time block, respectively. The information transmission phase is divided into two phases Phase-1 and Phase-2. In Phase-1 transmission, half of the remaining duration i.e.,  $(1-\beta)T/2$ , is allocated for the BS to transmit the superimposed NOMA signal to IN. In Phase-2 transmission, the remaining duration,  $(1-\beta)T/2$ , is allocated to the IN, which uses energy that has been harvested as its power source for relaying operations.

### 6.2.1 Energy Harvesting Phase

In the EH phase, the received signal at the IN is given by

$$Y_{bs} = \sqrt{P_b} \frac{h_{bs}}{\sqrt{1+r_{bs}^\nu}} x_e + n_s, \quad (6.1)$$

where  $h_{bs}$  is the channel coefficient of the BS to IN link, and  $r_{bs}$  is the separation between the BS and IN. The  $x_e$  is the energy signal corresponding to IN and  $n_s$  is the additive white Gaussian noise (AWGN) at IN with mean zero and variance  $\sigma^2$ . The energy harvested at the IN is given by

$$E_s = \beta T \left( \frac{aP_b|h_{bs}|^2(1+r_{bs}^\nu)^{-1} + b}{P_b|h_{bs}|^2(1+r_{bs}^\nu)^{-1} + c} - \frac{b}{c} \right), \quad (6.2)$$

where  $a$ ,  $b$ , and  $c$  are values obtained from the rectification circuit by curve fitting [158]. Note that the energy that has been harvested according to the linear EH model is also considered, which is represented by  $\mathcal{E}_2 = \beta T \zeta P_b |h_{bs}|^2 (1+r_{bs}^\nu)^{-1}$ , where  $\zeta$  is the linear energy harvester's conversion efficiency. It is helpful to utilize the linear EH model as a performance standard. Let  $P_s$  represent the transmit power from IN, to be used in Phase-2 transmission,

$$\begin{aligned} P_s &= \frac{2\beta}{1-\beta} \left( \frac{aP_b|h_{bs}|^2(1+r_{bs}^\nu)^{-1} + b}{P_b|h_{bs}|^2(1+r_{bs}^\nu)^{-1} + c} - \frac{b}{c} \right) \\ &= \frac{C_1 P_b |h_{bs}|^2 (1+r_{bs}^\nu)^{-1}}{P_b |h_{bs}|^2 (1+r_{bs}^\nu)^{-1} + c}, \end{aligned} \quad (6.3)$$

where  $C_1 = \frac{2\beta(ac-b)}{c(1-\beta)}$ .

## 6.2.2 Information Transmission Phase

### Phase-1 Transmission

The BS first broadcasts signal of BU to the IN. Then, the signal received at the IN is given as

$$y_s = \sqrt{P_b} \frac{\hat{h}_{bs}}{\sqrt{1+r_{bs}^\nu}} x_b + \sqrt{P_b I_b} + \hat{n}_s, \quad (6.4)$$

where  $\hat{h}_{bs}$  is the channel coefficient of the BS to IN link in Phase-1 transmission.  $x_b$  is the signal of the BU.  $I_b = \sum_{y \in \Omega_b / \{b_o\}} |h_y|^2 (1+r_y^\nu)^{-1}$  is the total interference at the IN from neighboring BS, where  $h_y$  and  $r_y$  are the channel gain and the separation between the IN and the  $y^{\text{th}}$  BS, respectively.  $b_o$  denotes the assigned BS.  $\hat{n}_s$  is the AWGN with mean zero and variance  $\sigma^2$ , at the receiver of IN in the Phase-1 transmission. The SINR at the IN for decoding the signal  $x_b$  of BU can be written as

$$\gamma_{IN} = \frac{P_b |\hat{h}_{bs}|^2 (1+r_{bs}^\nu)^{-1}}{P_b I_b + \sigma^2}, \quad (6.5)$$

It is assumed that all the BSs transmit their signal only in Phase-1 transmission. Therefore, the interference term does not appear in the SINR expressions of the Phase-2 transmission.

### Phase-2 Transmission

After detecting the received signals of BU, the IN superimposed signals  $x_b$  of BU with  $x_d$  of DT by implementing NOMA such that the superimposed coded signal is given by  $x = \sqrt{\alpha P_s} x_b + \sqrt{(1-\alpha) P_s} x_d$ , where  $\mathbb{E}[x_b^2] = \mathbb{E}[x_d^2] = 1$ ,  $\alpha$  and  $(1-\alpha)$  are the power allocation coefficients for BU and DT, respectively. The signal transmitted from the IN that is received at the BU and the DT can be represented as

$$y_{BU} = \frac{h_{ib}}{\sqrt{1+r_{ib}^\nu}} \left( \sqrt{\alpha P_s} x_b + \sqrt{(1-\alpha) P_s} x_d \right) + n_w, \quad (6.6)$$

and

$$y_{DT} = \frac{h_{id}}{\sqrt{1+r_{id}^\nu}} \left( \sqrt{\alpha P_s} x_b + \sqrt{(1-\alpha) P_s} x_d \right) + n_s, \quad (6.7)$$

where  $n_w$  and  $n_s$  are the AWGN at the receiver of BU and DT, respectively both having zero mean and variance of  $\sigma^2$ . The SIC ordering is based on the QoS requirement of the BU and the DT [168]. Since the QoS requirement of the BU is considered to be higher than that of DT, it performs SIC. The BU first uses SIC to decode  $x_d$  and subtracts it from the received signal to decode its own message,  $x_b$ . For decoding  $x_d$  and  $x_b$  at the BU, the SINRs are written as

$$\gamma_{BU}^{x_d} = \frac{(1 - \alpha)P_s|h_{ib}|^2(1 + r_{ib}^\nu)^{-1}}{\alpha P_s|h_{ib}|^2(1 + r_{ib}^\nu)^{-1} + \sigma^2}, \quad (6.8)$$

and

$$\gamma_{BU}^{x_b} = \frac{\alpha P_s|h_{ib}|^2(1 + r_{ib}^\nu)^{-1}}{\sigma^2}. \quad (6.9)$$

Additionally, DT decodes its own message  $x_d$  while considering the message of BU as interference. The SINR at DT is expressed as

$$\gamma_{DT} = \frac{(1 - \alpha)P_s|h_{id}|^2(1 + r_{id}^\nu)^{-1}}{\alpha P_s|h_{id}|^2(1 + r_{id}^\nu)^{-1} + \sigma^2}. \quad (6.10)$$

## 6.3 Performance Analysis

### 6.3.1 Outage Performance

The definition of outage event is when a receiver's instantaneous SINR falls below a predetermined threshold [169].

#### Outage Performance at DT

The DT outage probability is defined as the event when the DT cannot successfully detect the message  $x_d$  or when the BU cannot detect  $x_d$  via SIC. The outage probability at DT is written as

$$P_{out}^{DT} = \Pr(\min(\gamma_{DT}, \gamma_{BU}^{x_d}) \leq \hat{\gamma}_{DT}), \quad (6.11)$$

where  $\hat{\gamma}_{DT} = 2^{2R_{DT}/(1-\beta)} - 1$  represents the target SINR threshold for successfully detecting  $x_d$ , and  $R_{DT}$  is the target data rate of the DT. From (6.11) the outage

probability of the DT can be expressed as

$$\begin{aligned} P_{out}^{DT} &= 1 - \Pr(\gamma_{DT} > \hat{\gamma}_{DT}, \gamma_{BU}^{x_d} > \hat{\gamma}_{DT}) \\ &= 1 - \Pr\left(Y > \frac{Q(P_b X + c)}{X}, Z > \frac{Q(P_b X + c)}{X}\right), \end{aligned} \quad (6.12)$$

where  $X = |h_{bs}|^2(1 + r_{bs}^\nu)^{-1}$ ,  $Y = |h_{id}|^2(1 + r_{id}^\nu)^{-1}$ , and  $Z = |h_{ib}|^2(1 + r_{ib}^\nu)^{-1}$ ,  $Q = \hat{\gamma}_{DT}/\rho_b C_1((1 - \alpha) - \alpha \hat{\gamma}_{DT})$ .  $\rho_b = P_b/\sigma^2$  is the transmit signal-to-noise ratio (SNR) at IN. The PDF and CDF of RVs is given by  $f_W(w) = (1 + r^\nu)e^{-w(1+r^\nu)}$  and  $F_W(w) = 1 - e^{-w(1+r^\nu)}$  such that  $W \in \{X, Y, Z\}$  and  $r \in \{r_{bs}, r_{id}, r_{ib}\}$ , respectively. On substituting the values in (6.12) to get the outage probability expression as

$$\begin{aligned} P_{out}^{DT} &\stackrel{(a)}{=} 1 - \int_0^{\mathcal{Y}_s} \int_0^\infty e^{-Q(1+r_{id}^\nu)P_b} e^{-\frac{cQ(1+r_{id}^\nu)}{x}} \times \\ &e^{-Q(1+r_{ib}^\nu)P_b} e^{-\frac{cQ(1+r_{ib}^\nu)}{x}} (1 + r^\nu) e^{-x(1+r^\nu)} \frac{2r}{\mathcal{Y}_s^2} dx dr \\ &\stackrel{(b)}{=} 1 - \frac{\pi C_2}{2N} \sum_{n=1}^N (\theta_n + 1) \sqrt{4C_3(1 - \theta_n^2)c_n} K_1\left(\sqrt{4C_3c_n}\right), \end{aligned} \quad (6.13)$$

where  $C_2 = e^{-Q(1+r_{id}^\nu)P_b} e^{-Q(1+r_{ib}^\nu)P_b}$ ,  $C_3 = cQ(2 + r_{id}^\nu + r_{ib}^\nu)$ ,  $\theta_n = \cos\left(\frac{2i-1}{2n}\pi\right)$ ,  $c_n = 1 + \left(\frac{(\theta_n+1)\mathcal{Y}_s}{2}\right)^\nu$ . (a) is obtained after taking the expectation over the coverage area  $\pi\mathcal{Y}_s^2$  of BS by substituting  $r_{bs}=r$ . (b) is obtained by using [170, eq. (3.324.1)] and applying GC quadrature to obtain the final closed-form expression.

### Outage Performance at BU

Outage probability at BU is defined as the events when the message  $x_b$  is not correctly decoded by IN or when the BU is unable to successfully detect its own message  $x_b$ .

$$P_{out}^{BU} = \Pr(\min(\gamma_{IN}, \gamma_{BU}^{x_b}) \leq \hat{\gamma}_{BU}), \quad (6.14)$$

where  $\hat{\gamma}_{BU} = 2^{2R_{BU}/(1-\beta)} - 1$  represents the SINR threshold for successfully detecting  $x_b$ , and  $R_{BU}$  is BU's desired data rate. The probability that at least one of  $\gamma_{IN}$  and  $\gamma_{BU}^{x_b}$  is smaller than  $\hat{\gamma}_{BU}$  is equivalent to one minus the probability that both  $\gamma_{IN}$  and  $\gamma_{BU}^{x_b}$  are greater than  $\hat{\gamma}_{BU}$ . Hence (6.14) can be rewritten as

$$P_{out}^{BU} = 1 - \Pr(\gamma_{IN} > \hat{\gamma}_{BU}, \gamma_{BU}^{x_b} > \hat{\gamma}_{BU}). \quad (6.15)$$

From (6.4) and (6.9), substituting the SINR expression in (6.15). Also substituting the total channel gains in terms of RVs  $X$ ,  $Y$  and  $Z$  in (6.15) and after some mathematical simplifications, the outage probability expression can be written as

$$\begin{aligned} &= 1 - \Pr\left(X > \frac{\hat{\gamma}_{BU}(\rho_b I_b + 1)}{\rho_b}, Z > \frac{\hat{\gamma}_{BU}(P_b X + c)}{\alpha C_1 \rho_b X}\right) \\ &\stackrel{(a)}{=} 1 - \int_0^{\mathcal{Y}_s} \int_0^\infty e^{-\frac{\hat{\gamma}_{BU}(\rho_b I_b + 1)}{\rho_b}(1+r^\nu)} e^{-\frac{\hat{\gamma}_{BU}(P_b x + c)}{\alpha C_1 \rho_b x}(1+r_{ib}^\nu)} \\ &\quad \times (1+r^\nu) e^{-x(1+r^\nu)} \frac{2r}{\mathcal{Y}_s^2} dx dr \\ &\stackrel{(b)}{=} 1 - \frac{\pi e^{-C_4 P_b}}{2N} \sum_{n=1}^N (\phi_n + 1) \sqrt{4cd_n C_4 (1 - \phi_n^2)} e^{-\frac{\hat{\gamma}_{BU} d_n}{\rho_b}} \times \\ &\quad K_1\left(\sqrt{4cd_n C_4}\right) \mathcal{L}_{I_b}(s_n), \end{aligned} \quad (6.16)$$

where  $C_4 = \frac{\hat{\gamma}_{BU}(1+r_{ib}^\nu)}{\alpha C_1 \rho_b}$ ,  $\phi_n = \cos\left(\frac{2i-1}{2n}\pi\right)$ ,  $d_n = 1 + \left(\frac{(\phi_n+1)\mathcal{Y}_s}{2}\right)^\nu$ ,  $s_n = \hat{\gamma}_{BU} c_n$ . (a) is obtained after taking the expectation over the coverage area  $\pi\mathcal{Y}_s^2$  of BS by substituting  $r_{bs}=r$ . (b) is obtained by using [170, eq. (3.324.1)], and applying GC quadrature in to get the final closed-form expression.  $\mathcal{L}_{I_b}(s_n)$  denotes the Laplace transform (LT) of the interference coming from PPP distributed BSs and is described [171] as

$$\mathcal{L}_{I_t}(s) = e^{\pi\lambda_t(s^{\delta_t}\Gamma(1-\delta_t, s) - s^{\delta_t}\Gamma(1-\delta_t))}, \quad (6.17)$$

where  $\delta_t = \frac{2}{\nu_t}$ ,  $\Gamma(a, x) = \int_x^\infty t^{a-1} e^{-t} dt$  and  $\Gamma(z) = \int_0^\infty x^{z-1} e^{-x} dx$ .

### 6.3.2 System Throughput

The system throughput is calculated to determine overall system performance by utilizing the outage probability at the DT and at the BU at constant targeted rates [2], and is expressed as

$$T_{sys} = \frac{(1-\beta)}{2} ((1 - P_{out}^{DT})R_{DT} + (1 - P_{out}^{BU})R_{BU}) \quad (6.18)$$

### 6.3.3 System Energy Efficiency

The energy efficiency of the system is determined by dividing the maximum attainable data rate by the total amount of power used by the entire network [169] and is

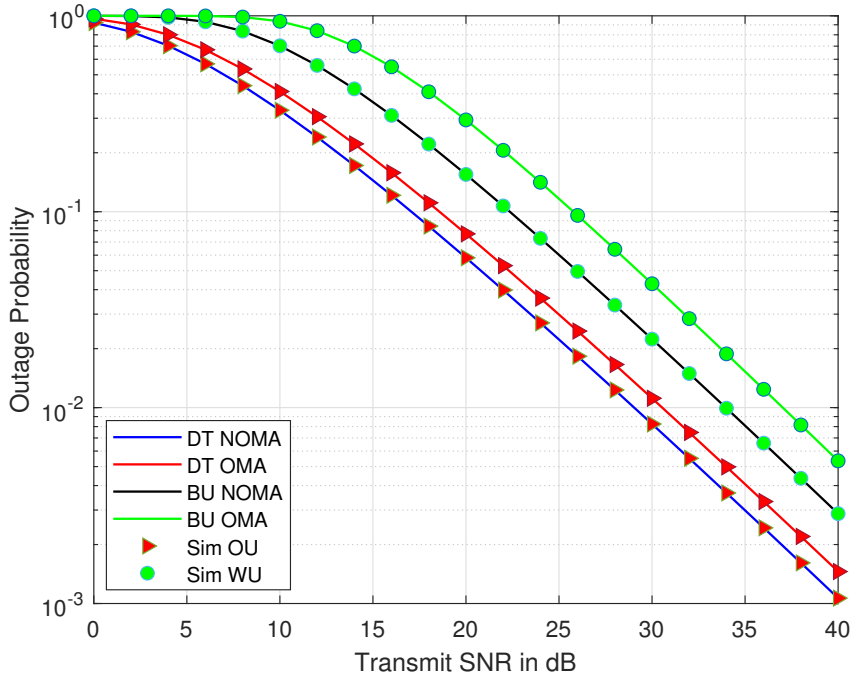


Figure 6.2: Outage probability comparison of NOMA and OMA

defined as

$$\eta_{SEE} = \frac{T_{sys}}{P_b}. \quad (6.19)$$

## 6.4 Results and Discussions

Using Monte-Carlo computer simulations, numerical results are presented in this section to support the theoretical analysis reported in Section 6.3. Hereinafter, unless otherwise mentioned, the simulation parameters are as follows:  $\alpha = 0.2$ ,  $\beta = 0.5$ ,  $r_{id} = 0.7\text{m}$ ,  $r_{ib} = 0.5\text{m}$ ,  $R_{DT} = 0.25$ ,  $R_{BU} = 0.5$ ,  $\nu = 2.7$ ,  $P_b = 1\text{W}$ ,  $\lambda_b = 10^{-3}\text{m}^{-2}$ ,  $\mathcal{Y}_b = 10\text{m}$  [142, 163]. The normalization constants for the non-linear EH model are set at  $a = 2.463$ ,  $b = 1.635$ , and  $c = 0.826$  [158]. For illustration, the proposed system is compared with a OMA based system [124, 156, 157], under the same communication scenario.

In Fig. 6.2, it is observed that the analytical and simulated outage probabilities of both the BU and the DT overlap. It is also observed that the BU with NOMA performs better by 76.92% than the BU with OMA at the transmit SNR of 16dB.

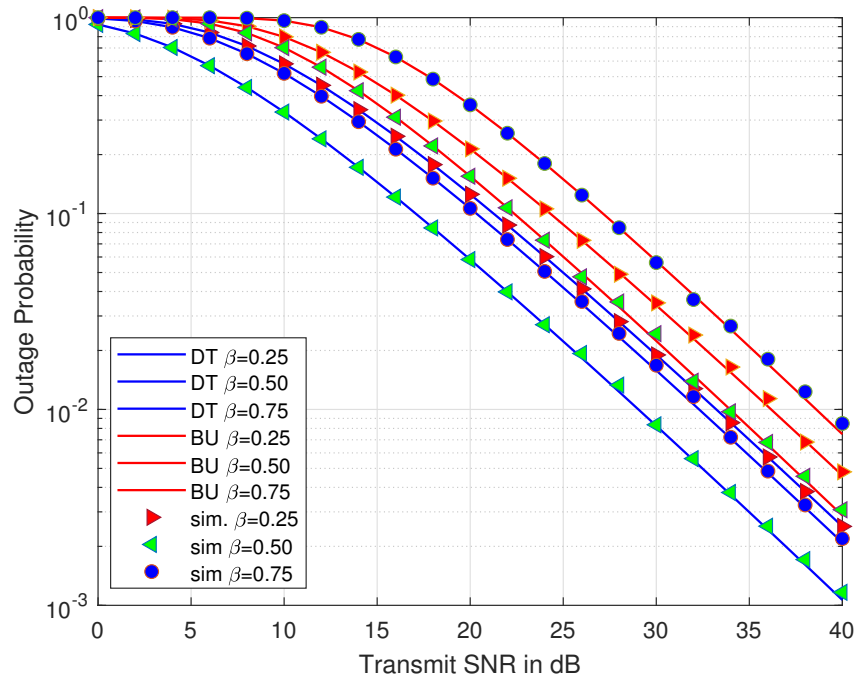


Figure 6.3: Variation of outage probability with transmit SNR for different values of  $\beta$

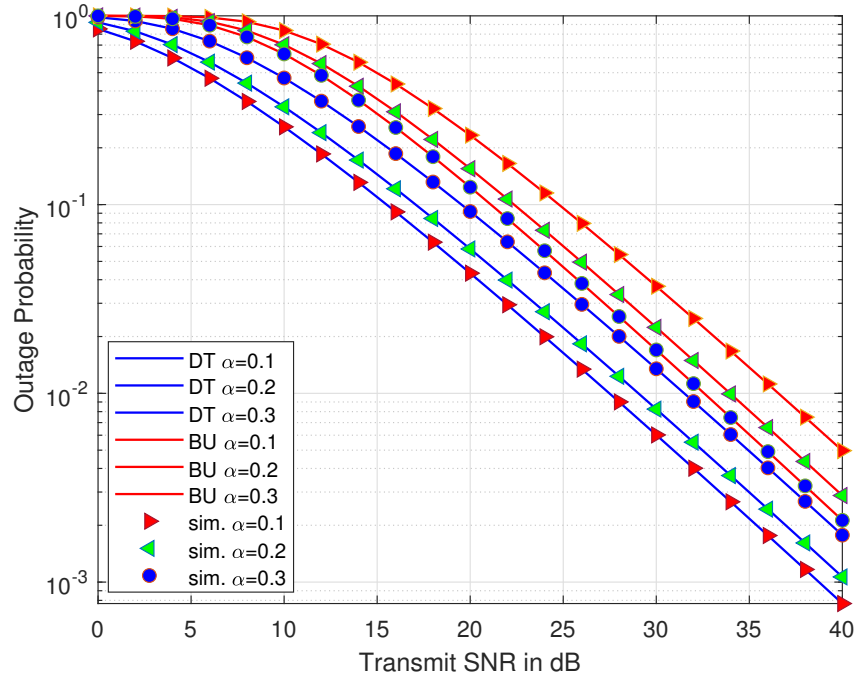


Figure 6.4: Variation of outage probability with transmit SNR for different values of  $\alpha$

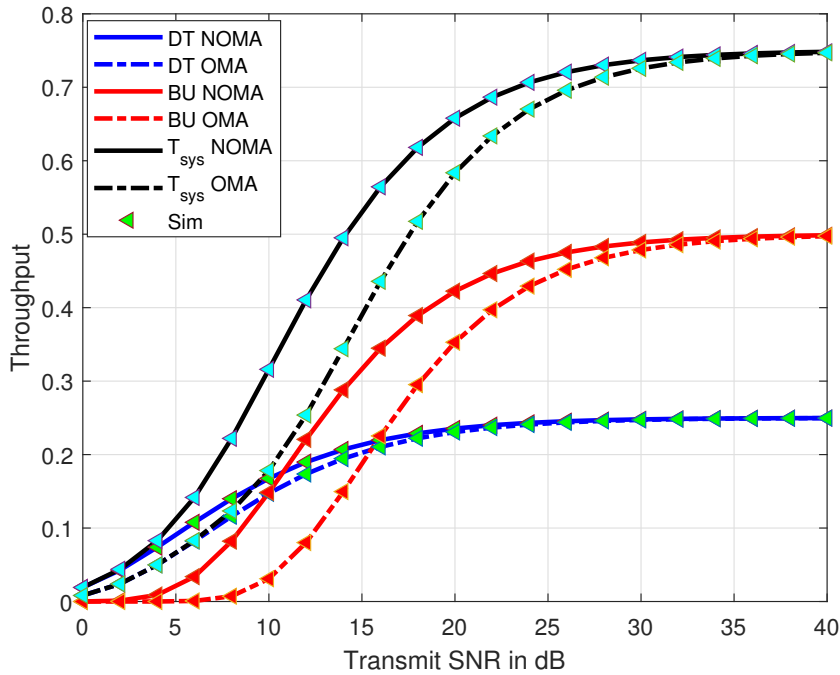


Figure 6.5: System throughput versus transmit SNR

Similarly, the performance of DT with NOMA is better by 30.36% than that with OMA at the transmit SNR of 16dB.

For various values of the TS coefficient  $\beta$ , Fig. 6.3 illustrates the outage probability of BU and DT versus transmit SNR. It can be observed that the performance improves when  $\beta$  increases from 0.25 to 0.5. This is because, with an increase in  $\beta$ , the power needed for cooperative transmission increases as IN harvests energy for  $\beta T$ . However, the performance again drops when  $\beta$  further increases to 0.75. The reason is that increase in  $\beta$  results in a shorter decoding time  $(\frac{1-\beta}{2})T$  for BU as well as for DT.

The outage probabilities of BU and DT are plotted against transmit SNR for various values of the power allocation coefficient  $\alpha$  in Fig. 6.4. It is inferred that the outage performance of BU improves when  $\alpha$  increases from 0.1 to 0.3. This is because with an increase in  $\alpha$  the power allocated to the BU signal increases. However, the power allocated to DT is  $1-\alpha$ , therefore, the performance of DT drops when  $\alpha$  increases from 0.1 to 0.3.

Fig. 6.5 plots the system throughput versus transmit SNR, wherein the solid lines indicate the proposed NOMA system and the dashed lines represent the benchmark OMA system [124, 156, 157]. It is inferred that the system throughput of the

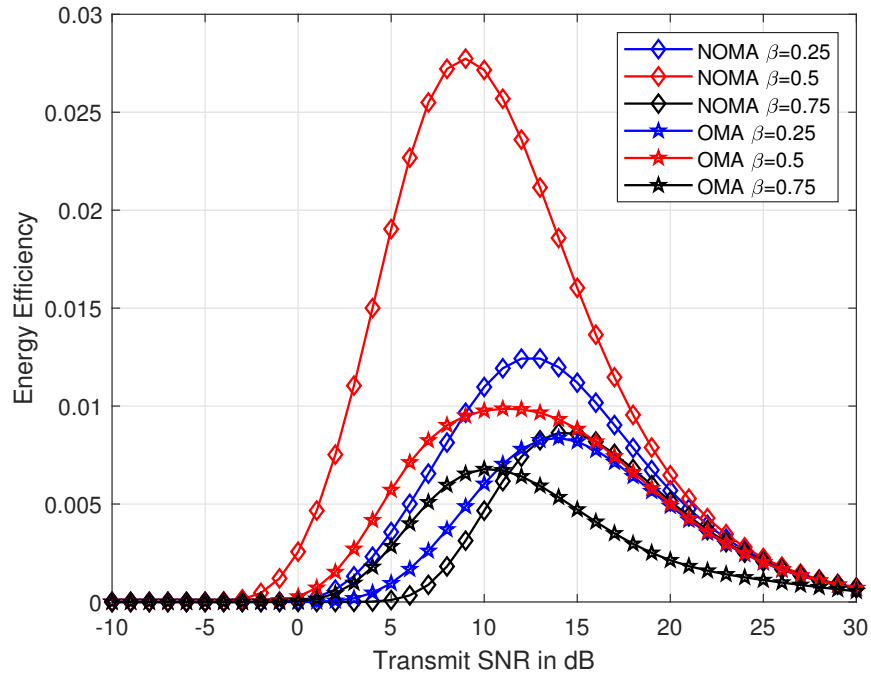


Figure 6.6: System energy efficiency versus transmit SNR

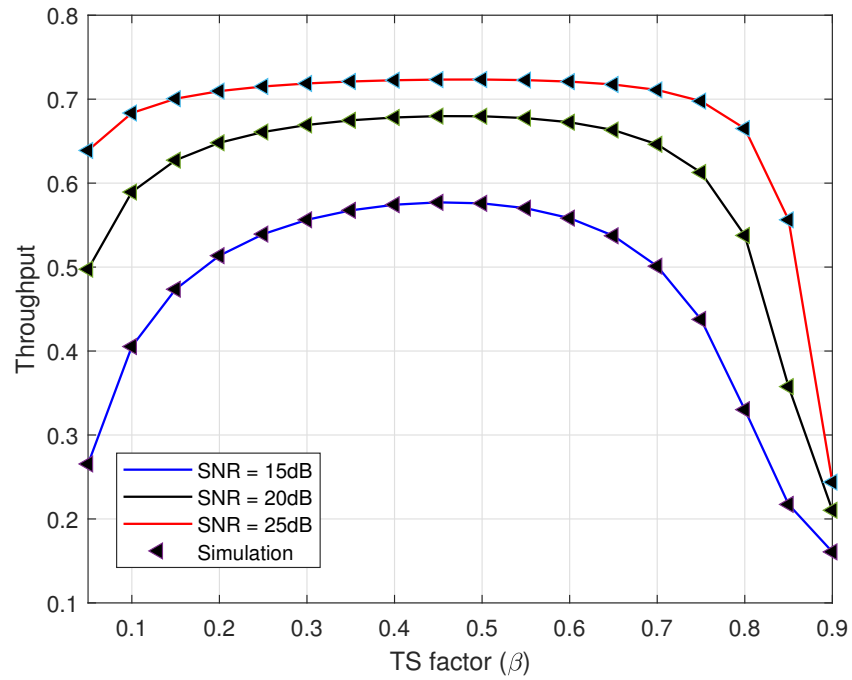


Figure 6.7: System throughput versus TS factor  $\beta$  for different values of transmit SNR

proposed system outperforms the benchmark OMA system. This is because the NOMA is suitable for systems with diverse needs, and in the proposed system, the target rates for DT and BU are different, which makes it suitable for NOMA. Thus, the proposed system model is ideal for scenarios where IoT devices have diverse QoS requirements.

The system energy efficiency is plotted against transmit SNR for various values of the TS coefficient  $\beta$  in Fig. 6.6. It can be observed that the proposed system outperforms the benchmark system for all values of  $\beta$ . Furthermore,  $\beta = 0.5$  achieves the best performance as compared to  $\beta = 0.25, 0.75$ . This is evident from Fig. 6.7 wherein the system throughput is plotted against  $\beta$  for the transmit SNR of 15 dB, 20 dB and 25 dB. The system throughput achieves best performances at  $\beta = 0.5$ .

## 6.5 Summary

In this chapter, the advantage of NOMA in the WPCN with heterogeneous QoS requirements has been investigated, and a practical PB-assisted downlink NOMA scheme has been proposed. First, a PB mounted on the PPP-distributed BS is considered to recharge battery-less IoT devices to enable transmission. Second, in order to make the system practical, a non-linear EH scheme is considered at the PPP distributed IN to assist the BS transmission. Third, in order to achieve higher spectral and energy efficiency, the IN uses NOMA to accommodate IoT devices. Both at the BU and at the DT, the closed-form expression of outage probability is evaluated. The performance at the BU and at the DT is compared with the OMA system. It is shown that the proposed NOMA system outperforms the OMA system in outage probability, system throughput, and energy efficiency. The system throughput achieves best performances at the optimal value of time switching coefficient  $\beta = 0.5$ .

# Chapter 7

## Conclusions and Future Works

### 7.1 Conclusions

This thesis focuses on the system enabled with NOMA in wireless HetNets, which is regarded as one promising technology in future 5G networks. The following aspects are presented in this thesis: 1) The basic principles of NOMA is introduced, including the two key technologies superposition coding and SIC, mathematical demonstration of NOMA and the basic downlink/uplink NOMA transmission model; 2) The potential combination of NOMA with the emerging technologies such as SWIPT and HetNets; and 3) Capturing the topological randomness of the BSs and utilizing stochastic geometric tools to provide tractable analysis. The main contributions and insights are summarized as follows

Initially, the work investigates the application of SWIPT in a PPP-distributed two-tier downlink cooperative NOMA network with imperfect CSI. The FBS tier is enabled with NOMA. A new cooperative NOMA and SWIPT protocol has been proposed, in which near NOMA users that are close to the BS act as energy harvesting relays to help far NOMA users. Stochastic geometry is utilized to model the locations of MBSs, FBSs and users. Closed-form expressions in terms of outage probability and system throughput have been derived at the CCU and the CEU. It is observed that the CCU suffers degradation in outage probability. This highlights the significance of exact channel estimation methods in cooperative NOMA networks, particularly incorporating SWIPT, in order to maintain performance. Further, the outage performance of the CEU experiences significant improvement by employing

cooperation from the CCU. The throughput analysis also highlights that the performance of the proposed system surpasses a cooperative NOMA system without EH. This implies that EH integration at the CCU can lead to enhanced spectral efficiency and overall system throughput in NOMA-enabled HetNets.

Chapter 3 addresses the limitations of using PPP assumption for modeling the SBS tier under realistic assumptions. Since the SBSs are opportunistically deployed by the end users, the interference management becomes challenging, which necessitates the use of appropriate MAC layer protocol, e.g., carrier sensing. Using carrier sensing at the FBS tier renders the BSs to be correlated with each other. The correlated BSs cannot be accurately modeled using the PPP assumption. Therefore, an advanced point process, i.e., RPP is used to model the SBS tier. The retaining model for the SBS tier is discussed, and the analysis at SBS tier is carried out in two phases. In the direct phase transmission, the SBS transmits the superimposed signal to a user pair, comprising of a CCU and a cell-edge user CEU, using NOMA principle. The CCU acts as a cooperative relay to forward information to the CEU in the cooperative phase. Expressions for outage probability and throughput are derived at the user pair served using NOMA. The outage performance of the CEU experiences significant improvement by employing cooperation from the CCU. This implies that the implementation of cooperative strategies helps in improving the performance of users in CNOMA HetNets. Comparison of the proposed EH system with existing solutions are highlighted and useful insights are drawn. The improvement in outage probability observed when EH utilizes RPP as compared to PPP shows the significance of carrier sensing and interference management in enhancing the reliability and efficiency of the system. The optimal value of PS coefficient is also obtained for the proposed system model as  $\beta = 0.5$ .

Chapter 4 investigates the utilization of TS based EH in a cooperative NOMA two-tier HetNet, where the distributions of the BSs are depended upon PPP assumptions. At the SU and the WU, expressions of OP and system throughput have been evaluated. It has been shown that the SU with EH suffers degradation in outage probability. However, SU attains flexibility with regards to energy consumption. Moreover, the outage performance of the WU undergoes notable enhancement by utilizing cooperation from SU. Throughput analysis shows that at high transmit

SNR the considered system with EH achieves better performance than the system without EH. Energy efficiency analysis also illustrates superiority of the proposed system. This implies that EH integration at the CCU can lead to enhanced energy efficiency and overall system throughput in NOMA-enabled HetNets. Finally, the considered system provides better user fairness as compared to the system without EH.

Furthermore, the linear EH model fails to represent the saturation region of practical EH circuits. As most rectennas include non-linear components (e.g., diodes and capacitors), the input/output relationship is non-linear, hence it is necessary to perform analysis with nonlinear harvester models. Therefore, Chapter 5 investigates the utilization of a non-linear EH model in a cooperative NOMA two-tier HetNet. The outage probability at the NOMA users is derived in closed form using stochastic geometry. The performance of the proposed system is compared with the system without EH and the system with linear EH. It is shown that the proposed system attains higher throughput than OMA without EH in the considered scenario.

Finally, in Chapter 6, the advantage of NOMA in the WPCN with heterogeneous QoS requirements has been investigated, and a practical PB-assisted downlink NOMA scheme has been proposed. First, a PB mounted on the PPP-distributed BS is considered to recharge battery-less IoT devices to enable transmission. The chapter address the challenges of EH and transmission in battery-less IoT devices. Second, in order to make the system practical, a non-linear EH scheme is considered at the PPP distributed IN to assist the BS transmission. Third, in order to achieve higher spectral and energy efficiency, the IN uses NOMA to accommodate IoT devices. Both at the BU and at the DT, the closed-form expression of outage probability is evaluated. The performance at the BU and at the DT is compared with the OMA system. It is shown that the proposed NOMA system outperforms the OMA system in outage probability, system throughput, and energy efficiency. The system throughput achieves best performances at the optimal value of time switching coefficient  $\beta = 0.5$ .

## 7.2 Future Works

- The work can be extended to analysis the propagation characteristics, channel models, design considerations, implementation strategies, and exploring potential applications of EH and NOMA enabled HetNet in the 6G wireless networks.
- To develop fundamental limits, performance analysis, network theoretic approaches (e.g., stochastic network calculus, throughput), and theoretical bounds for HetNets in the 6G wireless networks.
- According to the 5G new radio standard, upon reaching out beyond 6 GHz, the coverage area is significantly reduced. Since high-frequency signals are sensitive to blockage effects of trees and buildings the cost-effective technique of intelligent reflective surfaces (IRS) aided networks can be integrated into the present infrastructures. An IRS-aided system relies on many reflective elements, each of which is able to adjust the phase shifts and possibly the amplitude of the incident signals. By aligning the signals reflected by the IRS elements, the received signal of both the BS and of the users can be constructively or destructively superimposed by appropriately adjusting the global CSI. Motivated by the potential benefits, IRS-aided HetNets can be studied for future extension of the work.
- The work in this thesis can also be extended to MIMO systems. Multi-antenna HetNet is another advanced wireless network paradigm relying on spatial multiplexing, which can enhance system capacity and SE by placing a lot of antennas at the BSs. MIMO channels can realize spatial division multiple access for multiple users by using transmit beamforming. As multiple antennas with beamforming is advantageous at FBS tier, this can be explored in the future.
- The MBSs are connected to the network core via high-speed fiber backhaul. However, it is not feasible to provide fiber backhaul to all SBSs. Conversely, wireless backhaul solutions for SBSs have not been widely adopted due to spectrum shortages at sub-6 GHz frequencies. Nevertheless, with the availability of ample spectrum in mm-wave frequencies, achieving fiber-like performance

on the MBS-SBS backhaul links while preserving sufficient bandwidth for BS-user access links becomes feasible. Since both the access and backhaul links are established in mm-wave frequencies, they can share the same network infrastructure and resource pool, facilitating the joint design of the radio access network and backhaul network. In the future, these characteristics can be further studied within a stochastic geometry-based two-tier mmWave HetNets for 6G wireless networks.



# References

- [1] P. Swami, V. Bhatia, S. Vuppala, and T. Ratnarajah, “A cooperation scheme for user fairness and performance enhancement in NOMA-HCN,” *IEEE Trans. Veh. Technol.*, vol. 67, no. 12, pp. 11 965–11 978, 2018.
- [2] Y. Liu, Z. Ding, M. ElKashlan, and H. V. Poor, “Cooperative non-orthogonal multiple access with simultaneous wireless information and power transfer,” *IEEE J. Sel. Areas in Commun.*, vol. 34, no. 4, pp. 938–953, 2016.
- [3] A. Dogra, R. K. Jha, and S. Jain, “A survey on beyond 5G network with the advent of 6G: Architecture and emerging technologies,” *IEEE Access*, vol. 9, pp. 67 512–67 547, 2020.
- [4] P. K. Singya, N. Kumar, and V. Bhatia, “Mitigating NLD for wireless networks: Effect of nonlinear power amplifiers on future wireless communication networks,” *IEEE Microw. Mag.*, vol. 18, no. 5, pp. 73–90, Jun. 2017.
- [5] 3rd Generation Partnership Project (3GPP), “Technical specification group radio access network; evolved universal terrestrial radio access (E-UTRA); physical channels and modulation (Release 15),” Jan. 2019.
- [6] J. M. Meredith, “Study on downlink multiuser superposition transmission for LTE,” in *TSG RAN Meeting*, vol. 67, 2015.
- [7] 3rd Generation Partnership Project (3GPP), “Study on non-orthogonal multiple access (NOMA) for NR (Release 16),” Dec. 2018.
- [8] K. S. Gilhousen, I. M. Jacobs, R. Padovani, A. J. Viterbi, L. A. Weaver, and C. E. Wheatley, “On the capacity of a cellular cdma system,” *IEEE transactions on vehicular technology*, vol. 40, no. 2, pp. 303–312, 1991.

- [9] J. Li, X. Wu, and R. Laroia, *OFDMA mobile broadband communications: A systems approach*. Cambridge University Press, 2013.
- [10] E. Access, “Further advancements for E-UTRA physical layer aspects,” *3GPP Technical Specification TR*, vol. 36, p. V2, 2010.
- [11] Z. Ding, Y. Liu, J. Choi, Q. Sun, M. Elkashlan, I. Chih-Lin, and H. V. Poor, “Application of non-orthogonal multiple access in LTE and 5G networks,” *IEEE Commun. Magazine*, vol. 55, no. 2, pp. 185–191, 2017.
- [12] Y. Saito, A. Benjebbour, Y. Kishiyama, and T. Nakamura, “System-level performance evaluation of downlink non-orthogonal multiple access (NOMA),” in *2013 IEEE 24th annual international symposium on personal, indoor, and mobile radio communications (PIMRC)*, 2013, pp. 611–615.
- [13] R. Hoshyar, F. P. Wathan, and R. Tafazolli, “Novel low-density signature for synchronous CDMA systems over AWGN channel,” *IEEE Trans. Signal Process.*, vol. 56, no. 4, pp. 1616–1626, 2008.
- [14] Y. Du, B. Dong, Z. Chen, J. Fang, and X. Wang, “A fast convergence multiuser detection scheme for uplink SCMA systems,” *IEEE Wireless Commun. Lett.*, vol. 5, no. 4, pp. 388–391, 2016.
- [15] Z. Yuan, G. Yu, W. Li, Y. Yuan, X. Wang, and J. Xu, “Multi-user shared access for internet of things,” in *2016 IEEE 83rd Veh. Technol. Conf. (VTC Spring)*. IEEE, 2016, pp. 1–5.
- [16] X. Dai, S. Chen, S. Sun, S. Kang, Y. Wang, Z. Shen, and J. Xu, “Successive interference cancelation amenable multiple access (SAMA) for future wireless communications,” in *2014 IEEE Int. Conf. Commun. systems*. IEEE, 2014, pp. 222–226.
- [17] M. Vaezi, G. A. A. Baduge, Y. Liu, A. Arafa, F. Fang, and Z. Ding, “Interplay between NOMA and other emerging technologies: A survey,” *IEEE Trans. Cognit. Commun. Netw.*, vol. 5, no. 4, pp. 900–919, 2019.

- [18] Y. Saito, Y. Kishiyama, A. Benjebbour, T. Nakamura, A. Li, and K. Higuchi, “Non-orthogonal multiple access (NOMA) for cellular future radio access,” in *2013 IEEE 77th Veh. Techno. Conf. (VTC Spring)*. IEEE, 2013, pp. 1–5.
- [19] Z. Ding, P. Fan, and H. V. Poor, “Impact of user pairing on 5G nonorthogonal multiple-access downlink transmissions,” *IEEE Trans. Veh. Technol.*, vol. 65, no. 8, pp. 6010–6023, 2015.
- [20] T. Cover, “Broadcast channels,” *IEEE Trans. Inf. Theory*, vol. 18, no. 1, pp. 2–14, 1972.
- [21] T. M. Cover, *Elements of information theory*. John Wiley & Sons, 1999.
- [22] P. Bergmans, “Random coding theorem for broadcast channels with degraded components,” *IEEE Trans. Inf. Theory*, vol. 19, no. 2, pp. 197–207, 1973.
- [23] A. Carleial, “Interference channels,” *IEEE Trans. Inf. Theory*, vol. 24, no. 1, pp. 60–70, 1978.
- [24] T. Cover and A. E. Gamal, “Capacity theorems for the relay channel,” *IEEE Trans. Inf. Theory*, vol. 25, no. 5, pp. 572–584, 1979.
- [25] A. J. Grant, B. Rimoldi, R. L. Urbanke, and P. A. Whiting, “Rate-splitting multiple access for discrete memoryless channels,” *IEEE Trans. Inf. Theory*, vol. 47, no. 3, pp. 873–890, 2001.
- [26] I. Csiszár and J. Körner, “Broadcast channels with confidential messages,” *IEEE transactions on information theory*, vol. 24, no. 3, pp. 339–348, 1978.
- [27] S. Vanka, S. Srinivasa, Z. Gong, P. Vizi, K. Stamatiou, and M. Haenggi, “Superposition coding strategies: Design and experimental evaluation,” *IEEE Trans. Wireless Commun.*, vol. 11, no. 7, pp. 2628–2639, 2012.
- [28] P. Bergmans, “A simple converse for broadcast channels with additive white gaussian noise (corresp.),” *IEEE Trans. Inf. Theory*, vol. 20, no. 2, pp. 279–280, 1974.
- [29] J. G. Andrews, “Interference cancellation for cellular systems: a contemporary overview,” *IEEE Wireless Commun.*, vol. 12, no. 2, pp. 19–29, 2005.

- [30] P. Patel and J. Holtzman, "Analysis of a simple successive interference cancellation scheme in a ds/cdma system," *IEEE J. Sel. Areas Commun.*, vol. 12, no. 5, pp. 796–807, 1994.
- [31] P. W. Wolniansky, G. J. Foschini, G. D. Golden, and R. A. Valenzuela, "V-blast: An architecture for realizing very high data rates over the rich-scattering wireless channel," in *International symposium on signals, systems, and electronics*. IEEE, 1998, pp. 295–300.
- [32] E. Gelal, J. Ning, K. Pelechrinis, T.-S. Kim, I. Broustis, S. V. Krishnamurthy, and B. D. Rao, "Topology control for effective interference cancellation in multiuser mimo networks," *IEEE/ACM Trans. Netw.*, vol. 21, no. 2, pp. 455–468, 2012.
- [33] C. Jiang, Y. Shi, Y. T. Hou, W. Lou, S. Kompella, and S. F. Midkiff, "Squeezing the most out of interference: An optimization framework for joint interference exploitation and avoidance," in *IEEE INFOCOM*. IEEE, 2012, pp. 424–432.
- [34] C. Xu, L. Ping, P. Wang, S. Chan, and X. Lin, "Decentralized power control for random access with successive interference cancellation," *IEEE J. Sel. Areas Commun.*, vol. 31, no. 11, pp. 2387–2396, 2013.
- [35] J. Lee, J. G. Andrews, and D. Hong, "Spectrum-sharing transmission capacity with interference cancellation," *IEEE Trans. Commun.*, vol. 61, no. 1, pp. 76–86, 2012.
- [36] A. Damnjanovic, J. Montojo, Y. Wei, T. Ji, T. Luo, M. Vajapeyam, T. Yoo, O. Song, and D. Malladi, "A survey on 3GPP heterogeneous networks," *IEEE Wireless Commun.*, vol. 18, no. 3, pp. 10–21, 2011.
- [37] H. S. Dhillon, R. K. Ganti, F. Baccelli, and J. G. Andrews, "Modeling and analysis of k-tier downlink heterogeneous cellular networks," *IEEE Journal on Sel. Areas in Commun.*, vol. 30, no. 3, pp. 550–560, 2012.
- [38] W. Bao and B. Liang, "Stochastic analysis of uplink interference in two-tier

- femtocell networks: Open versus closed access,” *IEEE Trans. Wireless Commun.*, vol. 14, no. 11, pp. 6200–6215, 2015.
- [39] D. J. Daley, D. Vere-Jones *et al.*, *An introduction to the theory of point processes: volume I: elementary theory and methods*. Springer, 2003.
- [40] A. Baddeley *et al.*, “Analysing spatial point patterns in r,” Tech. Rep., 2008.
- [41] R. Schneider and W. Weil, *Stochastic and integral geometry*. Springer, 2008, vol. 1.
- [42] S. N. Chiu, D. Stoyan, W. S. Kendall, and J. Mecke, *Stochastic geometry and its applications*. John Wiley & Sons, 2013.
- [43] M. Haenggi, J. G. Andrews, F. Baccelli, O. Dousse, and M. Franceschetti, “Stochastic geometry and random graphs for the analysis and design of wireless networks,” *IEEE J. Sel. Areas Commun.*, vol. 27, no. 7, pp. 1029–1046, 2009.
- [44] S. Weber, J. G. Andrews, and N. Jindal, “An overview of the transmission capacity of wireless networks,” *IEEE Trans. Commun.*, vol. 58, no. 12, pp. 3593–3604, 2010.
- [45] M. Haenggi, R. K. Ganti *et al.*, “Interference in large wireless networks,” *Foundations and Trends® in Networking*, vol. 3, no. 2, pp. 127–248, 2009.
- [46] F. Baccelli and B. Błaszczyszyn, “Stochastic geometry and wireless networks, volume i—theory, volume 3, no 3–4 of foundations and trends in networking,” 2009.
- [47] F. Baccelli and S. Zuyev, “Stochastic geometry models of mobile communication networks,” in *Frontiers in queueing: models and applications in science and engineering*, 1998, pp. 227–243.
- [48] F. Baccelli, M. Klein, M. Lebourges, and S. Zuyev, “Stochastic geometry and architecture of communication networks,” *Telecommunication Systems*, vol. 7, pp. 209–227, 1997.

- [49] J. G. Andrews, F. Baccelli, and R. K. Ganti, “A tractable approach to coverage and rate in cellular networks,” *IEEE Trans. on Commu.*, vol. 59, no. 11, pp. 3122–3134, 2011.
- [50] S. Mukherjee, *Analytical modeling of heterogeneous cellular networks*. Cambridge University Press, 2014.
- [51] S. Singh, H. S. Dhillon, and J. G. Andrews, “Offloading in heterogeneous networks: Modeling, analysis, and design insights,” *IEEE Trans. Wireless Commun.*, vol. 12, no. 5, pp. 2484–2497, 2013.
- [52] H. S. Dhillon, Y. Li, P. Nuggehalli, Z. Pi, and J. G. Andrews, “Fundamentals of heterogeneous cellular networks with energy harvesting,” *IEEE Trans. Wireless Commun.*, vol. 13, no. 5, pp. 2782–2797, 2014.
- [53] Z. Gao, L. Dai, D. Mi, Z. Wang, M. A. Imran, and M. Z. Shakir, “MmWave massive-MIMO-based wireless backhaul for the 5G ultra-dense network,” *IEEE Wireless Commun.*, vol. 22, no. 5, pp. 13–21, 2015.
- [54] J. Schloemann, H. S. Dhillon, and R. M. Buehrer, “A tractable analysis of the improvement in unique localizability through collaboration,” *IEEE Trans. Wireless Commun.*, vol. 15, no. 6, pp. 3934–3948, 2016.
- [55] J. G. Andrews, T. Bai, M. N. Kulkarni, A. Alkhateeb, A. K. Gupta, and R. W. Heath, “Modeling and analyzing millimeter wave cellular systems,” *IEEE Trans. Commun.*, vol. 65, no. 1, pp. 403–430, 2016.
- [56] H. ElSawy, E. Hossain, and M. Haenggi, “Stochastic geometry for modeling, analysis, and design of multi-tier and cognitive cellular wireless networks: A survey,” *IEEE Commun. Surveys & Tuts.*, vol. 15, no. 3, pp. 996–1019, 2013.
- [57] H. ElSawy, A. Sultan-Salem, M.-S. Alouini, and M. Z. Win, “Modeling and analysis of cellular networks using stochastic geometry: A tutorial,” *IEEE Commun. Surveys & Tuts.*, vol. 19, no. 1, pp. 167–203, 2016.
- [58] Y. Liu, Z. Qin, M. ElKashlan, A. Nallanathan, and J. A. McCann, “Non-orthogonal multiple access in large-scale heterogeneous networks,” *IEEE J. Sel. Areas Commun.*, vol. 35, no. 12, pp. 2667–2680, 2017.

- [59] Z. Ding, L. Dai, and H. V. Poor, “MIMO-NOMA design for small packet transmission in the Internet of Things,” *IEEE Access*, vol. 4, pp. 1393–1405, 2016.
- [60] H.-S. Jo, Y. J. Sang, P. Xia, and J. G. Andrews, “Heterogeneous cellular networks with flexible cell association: A comprehensive downlink SINR analysis,” *IEEE Trans. Wireless Commun.*, vol. 11, no. 10, pp. 3484–3495, 2012.
- [61] J. Xu, J. Zhang, and J. G. Andrews, “On the accuracy of the wyner model in cellular networks,” *IEEE Trans. Wireless Commun.*, vol. 10, no. 9, pp. 3098–3109, 2011.
- [62] P. Cardieri, “Modeling interference in wireless ad hoc networks,” *IEEE Commun. Surveys & Tuts.*, vol. 12, no. 4, pp. 551–572, 2010.
- [63] M. Haenggi, *Stochastic geometry for wireless networks*. Cambridge University Press, 2012.
- [64] J. G. Andrews, F. Baccelli, and R. K. Ganti, “A tractable approach to coverage and rate in cellular networks,” *IEEE Trans. Commun.*, vol. 59, no. 11, pp. 3122–3134, 2011.
- [65] H. ElSawy and E. Hossain, “A modified hard-core point process for analysis of random CSMA wireless networks in general fading environments,” *IEEE Trans. Commun.*, vol. 61, no. 4, pp. 1520–1534, 2013.
- [66] G. Alfano, M. Garetto, and E. Leonardi, “New insights into the stochastic geometry analysis of dense CSMA networks,” in *Proc. IEEE INFOCOM*, 2011, pp. 2642–2650.
- [67] H. Q. Nguyen, F. Baccelli, and D. Kofman, “A stochastic geometry analysis of dense IEEE 802.11 networks,” in *Proc. IEEE Int. Conf. Comput. Commun.*, 2007, pp. 1199–1207.
- [68] M. Afshang and H. S. Dhillon, “Fundamentals of modeling finite wireless networks using binomial point process,” *IEEE Trans. Wireless Commun.*, vol. 16, no. 5, pp. 3355–3370, 2017.

- [69] —, “Poisson cluster process based analysis of HetNets with correlated user and base station locations,” *IEEE Trans. Wireless Commun.*, vol. 17, no. 4, pp. 2417–2431, 2018.
- [70] C. Saha, H. S. Dhillon, N. Miyoshi, and J. G. Andrews, “Unified analysis of HetNets using poisson cluster processes under max-power association,” *IEEE Trans. Wireless Commun.*, vol. 18, no. 8, pp. 3797–3812, 2019.
- [71] M.-L. Ku, W. Li, Y. Chen, and K. R. Liu, “Advances in energy harvesting communications: Past, present, and future challenges,” *IEEE Commun. Sur. Tutor.*, vol. 18, no. 2, pp. 1384–1412, 1st Quart. 2016.
- [72] J. Huang, C.-C. Xing, and C. Wang, “Simultaneous wireless information and power transfer: Technologies, applications, and research challenges,” *IEEE Commun. Mag.*, vol. 55, no. 11, pp. 26–32, Nov. 2017.
- [73] T. D. P. Perera, D. N. K. Jayakody, S. K. Sharma, S. Chatzinotas, and J. Li, “Simultaneous wireless information and power transfer (SWIPT): Recent advances and future challenges,” *IEEE Commun. Sur. Tutor.*, vol. 20, no. 1, pp. 264–302, 1st Quart. 2018.
- [74] A. Goldsmith, *Wireless communications*. Cambridge university press, 2005.
- [75] M. K. Simon and M.-S. Alouini, *Digital Communication over Fading Channels*. John Wiley & Sons, 2005, vol. 95.
- [76] Z. Ding, Z. Yang, P. Fan, and H. V. Poor, “On the performance of non-orthogonal multiple access in 5G systems with randomly deployed users,” *IEEE Signal Process. Lett.*, vol. 21, no. 12, pp. 1501–1505, 2014.
- [77] F. Fang, J. Cheng, and Z. Ding, “Joint energy efficient subchannel and power optimization for a downlink NOMA heterogeneous network,” *IEEE Trans. Veh. Technol.*, vol. 68, no. 2, pp. 1351–1364, 2018.
- [78] J. He and Z. Tang, “Low-complexity user pairing and power allocation algorithm for 5G cellular network non-orthogonal multiple access,” *Electron. Lett.*, vol. 53, no. 9, pp. 626–627, 2017.

- [79] Z. Ding, M. Peng, and H. V. Poor, "Cooperative non-orthogonal multiple access in 5G systems," *IEEE Commun. Lett.*, vol. 19, no. 8, pp. 1462–1465, 2015.
- [80] Y. Liu, Z. Ding, M. ElKashlan, and J. Yuan, "Non-orthogonal multiple access in large-scale underlay cognitive radio networks," *IEEE Trans. on Veh. Technol.*, vol. 65, no. 12, pp. 10 152–10 157, 2016.
- [81] V.-D. Nguyen, H. D. Tuan, T. Q. Duong, O.-S. Shin, and H. V. Poor, "Joint fractional time allocation and beamforming for downlink multiuser MISO systems," *IEEE Commun. Lett.*, vol. 21, no. 12, pp. 2650–2653, 2017.
- [82] J. A. Oviedo and H. R. Sadjadpour, "A fair power allocation approach to NOMA in multiuser SISO systems," *IEEE Trans. Veh. Technol.*, vol. 66, no. 9, pp. 7974–7985, 2017.
- [83] J. Choi, "NOMA-based random access with multichannel ALOHA," *IEEE J. on Sel. Areas Commun.*, vol. 35, no. 12, pp. 2736–2743, 2017.
- [84] Y.-G. Lim, C.-B. Chae, and G. Caire, "Performance analysis of massive MIMO for cell-boundary users," *IEEE Trans. Wireless Commun.*, vol. 14, no. 12, pp. 6827–6842, 2015.
- [85] Y. Liu, M. ElKashlan, Z. Ding, and G. K. Karagiannidis, "Fairness of user clustering in MIMO non-orthogonal multiple access systems," *IEEE Commun. Lett.*, vol. 20, no. 7, pp. 1465–1468, 2016.
- [86] Y. Liu, Z. Ding, M. ElKashlan, and H. V. Poor, "Cooperative non-orthogonal multiple access in 5G systems with SWIPT," in *23rd European Signal Process. Conf. (EUSIPCO)*. IEEE, 2015, pp. 1999–2003.
- [87] S. Timotheou and I. Krikidis, "Fairness for non-orthogonal multiple access in 5G systems," *IEEE Signal Process. Lett.*, vol. 22, no. 10, pp. 1647–1651, 2015.
- [88] Z. Yang, Z. Ding, P. Fan, and G. K. Karagiannidis, "On the performance of non-orthogonal multiple access systems with partial channel information," *IEEE Trans. Commun.*, vol. 64, no. 2, pp. 654–667, 2015.

- [89] Z. Zhang, H. Sun, R. Q. Hu, and Y. Qian, "Stochastic geometry based performance study on 5g non-orthogonal multiple access scheme," in *IEEE Global Commun. Conf. (GLOBECOM)*. IEEE, 2016, pp. 1–6.
- [90] J. Men and J. Ge, "Performance analysis of non-orthogonal multiple access in downlink cooperative network," *IET Commun.*, vol. 9, no. 18, pp. 2267–2273, 2015.
- [91] —, "Non-orthogonal multiple access for multiple-antenna relaying networks," *IEEE Commun. Lett.*, vol. 19, no. 10, pp. 1686–1689, 2015.
- [92] Z. Ding, H. Dai, and H. V. Poor, "Relay selection for cooperative noma," *IEEE Wireless Commun. Lett.*, vol. 5, no. 4, pp. 416–419, 2016.
- [93] Y. Tian, A. R. Nix, and M. Beach, "On the performance of opportunistic NOMA in downlink CoMP networks," *IEEE Commun. Lett.*, vol. 20, no. 5, pp. 998–1001, 2016.
- [94] J.-B. Kim and I.-H. Lee, "Non-orthogonal multiple access in coordinated direct and relay transmission," *IEEE Commun. Lett.*, vol. 19, no. 11, pp. 2037–2040, 2015.
- [95] Q.-T. Vien, N. Ogbonna, H. X. Nguyen, R. Trestian, and P. Shah, "Non-orthogonal multiple access for wireless downlink in cloud radio access networks," in *Proc. European Wireless Conference*. VDE, 2015, pp. 1–6.
- [96] N. Shinohara, "Power without wires," *IEEE Microw. Mag.*, vol. 12, no. 7, pp. S64–S73, 2011.
- [97] P. Coporation, "RF energy harvesting and wireless power for low-power applications," *Pittsburgh*, 2011.
- [98] R. Vullers, R. van Schaijk, I. Doms, C. Van Hoof, and R. Mertens, "Micropower energy harvesting," *Solid State Electron.*, vol. 53, no. 7, pp. 684–693, 2009.

- [99] P. Cheng, S. He, F. Jiang, Y. Gu, and J. Chen, "Optimal scheduling for quality of monitoring in wireless rechargeable sensor networks," *IEEE Trans. Wireless Commun.*, vol. 12, no. 6, pp. 3072–3084, 2013.
- [100] S. He, J. Chen, F. Jiang, D. K. Yau, G. Xing, and Y. Sun, "Energy provisioning in wireless rechargeable sensor networks," *IEEE Trans. Mobile Comput.*, vol. 12, no. 10, pp. 1931–1942, 2012.
- [101] L. R. Varshney, "Transporting information and energy simultaneously," in *Proc. IEEE Int. Symp. Inf. Theory (ISIT)*, Toronto, ON, Canada, 2008, pp. 1612–1616.
- [102] R. Zhang and C. K. Ho, "MIMO broadcasting for simultaneous wireless information and power transfer," *IEEE Trans. Wireless Commun.*, vol. 12, no. 5, pp. 1989–2001, 2013.
- [103] A. A. Nasir, X. Zhou, S. Durrani, and R. A. Kennedy, "Relaying protocols for wireless energy harvesting and information processing," *IEEE Trans. Wireless Commun.*, vol. 12, no. 7, pp. 3622–3636, 2013.
- [104] I. Krikidis, S. Sasaki, S. Timotheou, and Z. Ding, "A low complexity antenna switching for joint wireless information and energy transfer in MIMO relay channels," *IEEE Trans. Wireless Commun.*, vol. 62, no. 5, pp. 1577–1587, 2014.
- [105] Y. Liu, S. A. Mousavifar, Y. Deng, C. Leung, and M. ElKashlan, "Wireless energy harvesting in a cognitive relay network," *IEEE Trans. Wireless Commun.*, vol. 15, no. 4, pp. 2498–2508, 2015.
- [106] Z. Ding, I. Krikidis, B. Sharif, and H. V. Poor, "Wireless information and power transfer in cooperative networks with spatially random relays," *IEEE Trans. Wireless Commun.*, vol. 13, no. 8, pp. 4440–4453, 2014.
- [107] P. D. Diamantoulakis, K. N. Pappi, Z. Ding, and G. K. Karagiannidis, "Wireless-powered communications with non-orthogonal multiple access," *IEEE Transactions on Wireless Communications*, vol. 15, no. 12, pp. 8422–8436, 2016.

- [108] Z. Ding, Y. Liu, J. Choi, Q. Sun, M. Elkashlan, I. Chih-Lin, and H. V. Poor, "Application of non-orthogonal multiple access in LTE and 5G networks," *IEEE Commun. Mag.*, vol. 55, no. 2, pp. 185–191, 2017.
- [109] L. Dai, B. Wang, Y. Yuan, S. Han, I. Chih-Lin, and Z. Wang, "Non-orthogonal multiple access for 5G: solutions, challenges, opportunities, and future research trends," *IEEE Commun. Mag.*, vol. 53, no. 9, pp. 74–81, 2015.
- [110] P. Grover and A. Sahai, "Shannon meets Tesla: Wireless information and power transfer," in *Proc. IEEE Int. Symp. Inf. Theory (ISIT)*, 2010, pp. 2363–2367.
- [111] D. W. K. Ng, E. S. Lo, and R. Schober, "Wireless information and power transfer: Energy efficiency optimization in OFDMA systems," *IEEE Trans. Wireless Commun.*, vol. 12, no. 12, pp. 6352–6370, 2013.
- [112] B. Xu, Y. Chen, J. R. Carrión, and T. Zhang, "Resource allocation in energy-cooperation enabled two-tier NOMA HetNets toward green 5G," *IEEE J. Sel. Areas Commun.*, vol. 35, no. 12, pp. 2758–2770, 2017.
- [113] Y. Cao, N. Zhao, G. Pan, Y. Chen, L. Fan, M. Jin, and M.-S. Alouini, "Secrecy analysis for cooperative NOMA networks with multi-antenna full-duplex relay," *IEEE Trans. Commun.*, vol. 67, no. 8, pp. 5574–5587, 2019.
- [114] B. Chen, Y. Chen, Y. Cao, Y. Chen, N. Zhao, Z. Ding, and X. Wang, "Security enhancement using a novel two-slot cooperative NOMA scheme," *IEEE Trans. Veh. Technol.*, vol. 69, no. 3, pp. 3470–3475, 2020.
- [115] J. Tang, J. Luo, M. Liu, D. K. So, E. Alsusa, G. Chen, K.-K. Wong, and J. A. Chambers, "Energy efficiency optimization for NOMA with SWIPT," *IEEE J. Sel. Topics Signal Process.*, vol. 13, no. 3, pp. 452–466, 2019.
- [116] A. Rezaei, P. Azmi, N. M. Yamchi, M. R. Javan, and H. Yanikomeroglu, "Robust resource allocation for cooperative MISO-NOMA-based heterogeneous networks," *IEEE Trans. Commun.*, vol. 69, no. 6, pp. 3864–3878, 2021.

- [117] Y. Liu, Z. Ding, M. ElKashlan, and J. Yuan, “Non-orthogonal multiple access in large-scale underlay cognitive radio networks,” *IEEE Trans. on Veh. Technology*, vol. 65, no. 12, pp. 10 152–10 157, 2016.
- [118] Z. Zhang, H. Sun, and R. Q. Hu, “Downlink and uplink non-orthogonal multiple access in a dense wireless network,” *IEEE J. Sel. Areas Commun.*, vol. 35, no. 12, pp. 2771–2784, 2017.
- [119] J. Wang, B. Xia, K. Xiao, and Z. Chen, “Performance analysis and power allocation strategy for downlink NOMA systems in large-scale cellular networks,” *IEEE Trans. Veh. Technol.*, vol. 69, no. 3, pp. 3459–3464, 2020.
- [120] S. Bisen, P. Shaik, and V. Bhatia, “On performance of energy harvested cooperative noma under imperfect csi and imperfect sic,” *IEEE Trans. Veh. Technol.*, vol. 70, no. 9, pp. 8993–9005, 2021.
- [121] P. Swami, V. Bhatia, S. Vuppala, and T. Ratnarajah, “Performance analysis of offloading in noma-hetnets using imperfect csi,” in *IEEE ANTS*. IEEE, 2018, pp. 1–6.
- [122] P. Shaik, P. K. Singya, N. Kumar, K. K. Garg, and V. Bhatia, “On impact of imperfect CSI over SWIPT device-to-device (D2D) MIMO relay systems,” in *Proc. IEEE Int. Conf. Signal Process. Commun. (SPCOM)*, 2020, pp. 1–5.
- [123] D. Kumar, P. K. Singya, and V. Bhatia, “ASER analysis of hybrid receiver based SWIPT two-way relay network,” *IEEE Trans. Veh. Technol.*, 2021.
- [124] I. Krikidis, “Simultaneous information and energy transfer in large-scale networks with/without relaying,” *IEEE Trans. Commun.*, vol. 62, no. 3, pp. 900–912, 2014.
- [125] Z. Chen, J. Yuan, and B. Vucetic, “Analysis of transmit antenna selection/maximal-ratio combining in Rayleigh fading channels,” *IEEE Trans. Veh. Technol.*, vol. 54, no. 4, pp. 1312–1321, 2005.
- [126] N. Kong, “Performance comparison among conventional selection combining, optimum selection combining and maximal ratio combining,” in *Proc. IEEE Int. Conf. Commun.*, 2009, pp. 1–6.

- [127] P. Swami, M. K. Mishra, V. Bhatia, and T. Ratnarajah, "Performance analysis of NOMA enabled hybrid network with limited feedback," *IEEE Trans. Veh. Technol.*, vol. 69, no. 4, pp. 4516–4521, 2020.
- [128] Z. Ding, P. Fan, and H. V. Poor, "Impact of user pairing on 5G nonorthogonal multiple-access downlink transmissions," *IEEE Trans. Veh. Technol.*, vol. 65, no. 8, pp. 6010–6023, 2016.
- [129] F. Kara and H. Kaya, "Improved user fairness in decode-forward relaying non-orthogonal multiple access schemes with imperfect SIC and CSI," *IEEE Access*, vol. 8, pp. 97 540–97 556, 2020.
- [130] J. G. Andrews, H. Claussen, M. Dohler, S. Rangan, and M. C. Reed, "Femto-cells: Past, present, and future," *IEEE J. Sel. Areas Commun.*, vol. 30, no. 3, pp. 497–508, 2012.
- [131] B. Han, W. Wang, Y. Li, and M. Peng, "Investigation of interference margin for the co-existence of macrocell and femtocell in orthogonal frequency division multiple access systems," *IEEE Syst. J.*, vol. 7, no. 1, pp. 59–67, 2012.
- [132] M. Vaezi, R. Schober, Z. Ding, and H. V. Poor, "Non-orthogonal multiple access: Common myths and critical questions," *IEEE Wireless Commun.*, vol. 26, no. 5, pp. 174–180, 2019.
- [133] S. Abeywickrama, R. Zhang, and C. Yuen, "Refined nonlinear rectenna modeling and optimal waveform design for multi-user multi-antenna wireless power transfer," *IEEE J. Sel. Areas Signal Process.*, 2021.
- [134] J. Venkataraman, M. Haenggi, and O. Collins, "Shot noise models for outage and throughput analyses in wireless ad hoc networks," in *Proc. IEEE Mil. Commun. Conf. (MILCOM)*, 2006, pp. 1–7.
- [135] A. M. Ibrahim, T. ElBatt, and A. El-Keyi, "Coverage probability analysis for wireless networks using repulsive point processes," in *Proc. IEEE 24th Int. Symp. Pers., Indoor, Mobile Radio Commun.*, 2013, pp. 1002–1007.

- [136] D. Wan, M. Wen, F. Ji, Y. Liu, and Y. Huang, "Cooperative noma systems with partial channel state information over nakagami- $m$  fading channels," *IEEE Trans. Commun.*, vol. 66, no. 3, pp. 947–958, 2017.
- [137] Y. Xu, C. Shen, Z. Ding, X. Sun, S. Yan, G. Zhu, and Z. Zhong, "Joint beamforming and power-splitting control in downlink cooperative SWIPT NOMA systems," *IEEE Trans. Sig. Process.*, vol. 65, no. 18, pp. 4874–4886, 2017.
- [138] T. T. H. Ly, H.-S. Nguyen, T.-S. Nguyen, V. V. Huynh, T.-L. Nguyen, and M. Voznak, "Outage probability analysis in relaying cooperative systems with NOMA considering power splitting," *Symmetry*, vol. 11, no. 1, p. 72, 2019.
- [139] Y. Ye, Y. Li, D. Wang, and G. Lu, "Power splitting protocol design for the cooperative NOMA with SWIPT," in *2017 IEEE Int. Conf. Commun. (ICC)*. IEEE, 2017, pp. 1–5.
- [140] A. Salem, L. Musavian, E. A. Jorswieck, and S. Aïssa, "Secrecy outage probability of energy-harvesting cooperative NOMA transmissions with relay selection," *IEEE Trans. Green Commun. Netw.*, vol. 4, no. 4, pp. 1130–1148, 2020.
- [141] A. S. Parihar, P. Swami, V. Bhatia, and Z. Ding, "Performance analysis of SWIPT enabled cooperative-NOMA in heterogeneous networks using carrier sensing," *IEEE Trans. Veh. Technol.*, vol. 70, no. 10, pp. 10 646–10 656, 2021.
- [142] A. S. Parihar, P. Swami, and V. Bhatia, "On performance of SWIPT enabled PPP distributed cooperative NOMA networks using stochastic geometry," *IEEE Trans. Veh. Technol.*, vol. 71, no. 5, pp. 5639–5644, 2022.
- [143] K. Janghel and S. Prakriya, "Throughput of underlay cognitive energy harvesting relay networks with an improved time-switching protocol," *IEEE Trans. Cognitive Commun. Netw.*, vol. 4, no. 1, pp. 66–81, 2018.
- [144] S. Kusaladharma, W.-P. Zhu, W. Ajib, and G. A. A. Baduge, "Rate and energy efficiency improvements of massive MIMO-based stochastic cellular networks with NOMA," *IEEE Trans. Green Commun. Netw.*, vol. 5, no. 3, pp. 1467–1481, 2021.

- [145] H. Xiao, W. Zhang, and A. T. Chronopoulos, “Joint subchannel and power allocation for energy efficiency optimization in NOMA heterogeneous networks with energy harvesting,” *IEEE Systems J.*, vol. 16, no. 3, pp. 4904–4915, 2022.
- [146] M. Moltafet, P. Azmi, N. Mokari, M. R. Javan, and A. Mokdad, “Optimal and fair energy efficient resource allocation for energy harvesting-enabled-PD-NOMA-based HetNets,” *IEEE Trans. Wireless Commun.*, vol. 17, no. 3, pp. 2054–2067, 2018.
- [147] S. Bayat, A. Khalili, and Z. Han, “Resource allocation for MC MISO-NOMA SWIPT-enabled HetNets with non-linear energy harvesting,” *IEEE Access*, vol. 8, pp. 192 270–192 281, 2020.
- [148] T. Han, J. Gong, X. Liu, S. R. Islam, Q. Li, Z. Bai, and K. S. Kwak, “On downlink NOMA in heterogeneous networks with non-uniform small cell deployment,” *IEEE Access*, vol. 6, pp. 31 099–31 109, 2018.
- [149] C.-H. Liu and D.-C. Liang, “Heterogeneous networks with power-domain noma: Coverage, throughput, and power allocation analysis,” *IEEE Trans. Wireless Commun.*, vol. 17, no. 5, pp. 3524–3539, 2018.
- [150] Y. Liu, H. Ding, J. Shen, R. Xiao, and H. Yang, “Outage performance analysis for SWIPT-based cooperative non-orthogonal multiple access systems,” *IEEE Commun. Lett.*, vol. 23, no. 9, pp. 1501–1505, 2019.
- [151] H. Q. Tran, C. V. Phan, and Q.-T. Vien, “Power splitting versus time switching based cooperative relaying protocols for SWIPT in NOMA systems,” *Physical Commun.*, vol. 41, p. 101098, 2020.
- [152] F. Kara and H. Kaya, “Improved user fairness in decode-forward relaying non-orthogonal multiple access schemes with imperfect SIC and CSI,” *IEEE Access*, vol. 8, pp. 97 540–97 556, 2020.
- [153] Z. Ding, “Harvesting devices’ heterogeneous energy profiles and QoS requirements in IoT: WPT-NOMA vs BAC-NOMA,” *IEEE Trans. Commun.*, vol. 69, no. 5, pp. 2837–2850, 2021.

- [154] K. Agrawal, A. Jee, U. Makhanpuri, and S. Prakriya, "Performance of full-duplex cooperative NOMA with mode switching and an EH near user," *IEEE Netw. Lett.*, pp. 1–1, 2022.
- [155] T.-V. Nguyen, V.-D. Nguyen, D. B. da Costa, and B. An, "Hybrid user pairing for spectral and energy efficiencies in multiuser MISO-NOMA networks with SWIPT," *IEEE Trans. Commun.*, vol. 68, no. 8, pp. 4874–4890, 2020.
- [156] T.-T. Nguyen, Q.-V. Pham, V.-D. Nguyen, J.-H. Lee, and Y.-H. Kim, "Resource allocation for energy efficiency in OFDMA-enabled WPCN," *IEEE Wireless Commun. Lett.*, vol. 9, no. 12, pp. 2049–2053, 2020.
- [157] M. Dimitropoulou, C. Psomas, and I. Krikidis, "Generalized selection in wireless powered networks with non-linear energy harvesting," *IEEE Trans. Commun.*, vol. 69, no. 8, pp. 5634–5648, 2021.
- [158] Y. Chen, N. Zhao, and M.-S. Alouini, "Wireless energy harvesting using signals from multiple fading channels," *IEEE Trans. Commun.*, vol. 65, no. 11, pp. 5027–5039, 2017.
- [159] V. Aswathi and A. V. Babu, "Outage and throughput analysis of full-duplex cooperative NOMA system with energy harvesting," *IEEE Trans. Veh. Technol.*, vol. 70, no. 11, pp. 11 648–11 664, 2021.
- [160] D. C. Nguyen, M. Ding, P. N. Pathirana, A. Seneviratne, J. Li, D. Niyato, O. Dobre, and H. V. Poor, "6G internet of things: A comprehensive survey," *IEEE Internet Things J.*, vol. 9, no. 1, pp. 359–383, 2021.
- [161] Y. Liu, S. Zhang, X. Mu, Z. Ding, R. Schober, N. Al-Dhahir, E. Hossain, and X. Shen, "Evolution of NOMA toward next generation multiple access (NGMA) for 6G," *IEEE J. Sel. Areas Commun.*, vol. 40, pp. 1037–1071, 2022.
- [162] Ericsson, "6G—connecting a cyber-physical world," GF'TL-20:001402, 2022. [Online]. Available: <https://www.ericsson.com/4927de/assets/local/reports-papers/white-papers/6g-connecting-a-cyber-physical-world.pdf>

- [163] T.-H. Vu and S. Kim, "Performance evaluation of power-beacon-assisted wireless-powered NOMA IoT-based systems," *IEEE Internet of Things Journal*, vol. 8, no. 14, pp. 11 655–11 665, 2021.
- [164] B. Clerckx, K. Huang, L. R. Varshney, S. Ulukus, and M.-S. Alouini, "Wireless power transfer for future networks: Signal processing, machine learning, computing, and sensing," *IEEE J. Sel. Topics Signal Process.*, vol. 15, no. 5, pp. 1060–1094, 2021.
- [165] T. M. Hoang, N. T. Tan, X. N. Tran *et al.*, "Performance analysis of power beacon-assisted energy harvesting NOMA multi-user relaying system over Nakagami-m fading channels," *AEU Int. J. Electron. Commun.*, vol. 115, p. 153022, 2020.
- [166] D.-T. Do, M.-S. Van Nguyen, T. N. Nguyen, X. Li, and K. Choi, "Enabling multiple power beacons for uplink of NOMA-enabled mobile edge computing in wirelessly powered IoT," *IEEE Access*, vol. 8, pp. 148 892–148 905, 2020.
- [167] A. Jee and S. Prakriya, "Performance of energy and spectrally efficient AF relay-aided incremental CDRT NOMA based IoT network with imperfect SIC for smart cities," *IEEE Internet Things J.*, 2022.
- [168] F. Guo, H. Lu, X. Jiang, M. Zhang, J. Wu, and C. W. Chen, "QoS-aware user grouping strategy for downlink multi-cell NOMA systems," *IEEE Trans. Wireless Commun.*, vol. 20, no. 12, pp. 7871–7887, 2021.
- [169] P. Swami, M. K. Mishra, V. Bhatia, T. Ratnarajah, and A. Trivedi, "Performance analysis of sub-6 GHz/mmWave NOMA hybrid-HetNets using partial CSI," *IEEE Trans. Veh. Technol.*, vol. 71, no. 12, pp. 12 958–12 971, 2022.
- [170] I. S. Gradshteyn and I. M. Ryzhik, *Table of integrals, series, and products*. Academic press, 2014.
- [171] P. Swami, V. Bhatia, S. Vuppala, and T. Ratnarajah, "User fairness in noma-hetnet using optimized power allocation and time slotting," *IEEE Systems J.*, vol. 15, no. 1, pp. 1005–1014, 2020.

## List of Publications

### Journal Papers:

1. **A. S. Parihar**, P. Swami, V. Bhatia and Z. Ding, "Performance analysis of SWIPT enabled cooperative-NOMA in heterogeneous networks using carrier sensing," *IEEE Trans. Veh. Technol.*, vol. 17, no. 10, pp. 10646-10656, Oct. 2021.
2. **A. S. Parihar**, P. Swami and V. Bhatia, "On performance of SWIPT enabled PPP distributed cooperative NOMA networks using stochastic geometry," *IEEE Trans. Veh. Technol.*, vol. 71, no. 5, pp. 5639-5644, May 2022.
3. **A. S. Parihar**, P. Swami, K. Choi, P. Brida, and V. Bhatia, "On performance of NOMA based wireless powered communication networks assisted with power beacons and PPP distributed IN," *IEEE Wireless Commun. Lett.*, vol. 12, no. 7, pp. 1294-1298, July 2023.
4. **A. S. Parihar**, P. Swami, O. Krejcar, K. Choi, and V. Bhatia, "On performance of time switching based energy harvesting enabled cooperative NOMA HetNets," *IEEE Access*, 2023. (Under Review)
5. A. Baghel, **A. S. Parihar**, V. Bhatia, K. Choi, and A. K. Mishra, "On joint impact of HPA non-linearity and imperfect SIC in NOMA enabled HCN using stochastic geometry," *IEEE Trans. Veh. Technol.*, 2023.

### Conference Papers:

1. **A. S. Parihar**, P. Swami and V. Bhatia, "Performance evaluation of energy harvesting aided NOMA-HCN in IoT," in *Proc. Int. Conf. Commun. Syst. Net. Technol. (CSNT)*, pp. 482-489, 2022.

2. **A. S. Parihar**, P. Swami and V. Bhatia, "On performance of IoT devices utilizing energy harvesting and carrier sensing in NOMA-HCN," in *Proc. Nat. Conf. Commun. (NCC)*, pp. 385-390, 2022.
3. **A. S. Parihar**, A. Baghel, P. Swami, and V. Bhatia, "On performance of SWIPT empowered NOMA-HetNet with non-linear energy harvesting," *Proc. Nat. Conf. Commun. (NCC)* pp. 1-6, 2024.
4. A. Baghel, **A. S. Parihar**, V. Bhatia, P. Brida, and M. Augustynek, "Impact of imperfect SIC in NOMA enabled heterogeneous cellular network," in *Proc. Int. Conf. Intelligent Engineering Systems (INES)*, pp. 1-6, 2023.
5. N. Garg, **A. S. Parihar**, and V. Bhatia, "Performance analysis of cache enabled wireless NOMA ultra dense networks using PPP," in *Proc. Int. Conf. Adv. Netw. Telecommun. Sys. (ANTS)*, 2023.